Biomaterials 291 (2022) 121881

Contents lists available at ScienceDirect

Biomaterials

journal homepage: www.elsevier.com/locate/biomaterials

Strategies for 3D bioprinting of spheroids: A comprehensive review

Dishary Banerjee [a,b,c], Yogendra Pratap Singh [a,b], Pallab Datta [d], Veli Ozbolat [e], Aaron O'Donnell [f,g], Miji Yeo [a,b], Ibrahim T. Ozbolat [a,b,f,h,i,j,*]

[a] The Huck Institutes of the Life Sciences, Pennsylvania State University, University Park, PA, USA
[b] Engineering Science and Mechanics Department, Penn State University, University Park, PA, USA
[c] Department of Medicine, Division of Cardiology, University of California, San Diego, La Jolla, CA, 92093, USA
[d] Department of Pharmaceutics, National Institute of Pharmaceutical Education and Research, Kolkata, India
[e] Mechanical Engineering Department, Ceyhan Engineering Faculty, Cukurova University, Adana, Turkey
[f] Department of Biomedical Engineering, Pennsylvania State University, University Park, PA, USA
[g] Department of Biomedical Engineering, Columbia University in the City of New York, New York, NY, USA
[h] Materials Research Institute, Pennsylvania State University, University Park, PA, USA
[i] Department of Neurosurgery, Pennsylvania State College of Medicine, Hershey, PA, USA
[j] Department of Medical Oncology, Cukurova University, Adana, Turkey

ARTICLE INFO

Keywords:
Bioprinting
Biofabrication
Spheroids
Self-assembly
Organoids

ABSTRACT

Biofabricated tissues have found numerous applications in tissue engineering and regenerative medicine in addition to the promotion of disease modeling and drug development and screening. Although three-dimensional (3D) printing strategies for designing and developing customized tissue constructs have made significant progress, the complexity of innate multicellular tissues hinders the accurate evaluation of physiological responses *in vitro*. Cellular aggregates, such as spheroids, are 3D structures where multiple types of cells are co-cultured and organized with endogenously secreted extracellular matrix and are designed to recapitulate the key features of native tissues more realistically. 3D Bioprinting has emerged as a crucial tool for positioning of these spheroids to assemble and organize them into physiologically- and histologically-relevant tissues, mimicking their native counterparts. This has triggered the convergence of spheroid fabrication and bioprinting, leading to the investigation of novel engineering methods for successful assembly of spheroids while simultaneously enhancing tissue repair. This review provides an overview of the current state-of-the-art in spheroid bioprinting methods and elucidates the involved technologies, intensively discusses the recent tissue fabrication applications, outlines the crucial properties that influence the bioprinting of these spheroids and bioprinted tissue characteristics, and finally details the current challenges and future perspectives of spheroid bioprinting efforts in the growing field of biofabrication.

1. Introduction

Biofabrication encompasses designing and fabricating tissue and organ constructs to repair and regenerate defects caused by damage or loss of tissues by infection, trauma, excision, or diseases [1]. In recent years, biofabricated tissue and organ constructs have found prevalent usage in regenerative medicine, particularly in the repair and restoration of damaged tissues, and drug screening and discovery. Ideally, biofabricated constructs should be a custom-fit for each patient – additively manufactured and avoid any concerns related to biocompatibility and innate immune responses, which are crucial for in-vivo success [2]. In such regard, 3D printing technology has evolved from rapid prototyping techniques [3] and was initially used for developing 3D surgical models in the medical industry [4]. Since then, 3D printing has quickly ascended the ladder of the medical industry and found profound use in fabrication of customized patient- and defect-specific prosthesis, like bone implants [5], hearing aids [6], and many more. Until early 2000s, 3D printed constructs did not include any living component and lacked the functionality of human tissues [7], and were mainly used as templates to guide tissue formation [8].

The development of functional human tissues/organs was envisioned in the beginning through early embryonic development [9]. This was changed with the introduction of the concept of 3D printing with cells, referred to as "bioprinting" in 2003, where exposition of cells was

* Corresponding author. The Huck Institutes of the Life Sciences, Pennsylvania State University, University Park, PA, USA.
E-mail address: ito1@psu.edu (I.T. Ozbolat).

https://doi.org/10.1016/j.biomaterials.2022.121881
Received 3 June 2022; Received in revised form 4 October 2022; Accepted 23 October 2022
Available online 28 October 2022

demonstrated using an inkjet printer by Wilson and Boland [10]. Bioprinting can be defined as a computer-aided transfer process for simultaneous writing of living cells and biomaterials for various applications such as tissue engineering, regenerative medicine or other biological studies [11]. To a layman, 3D bioprinting may seem like a conglomeration of futuristic science fiction images; but in reality, it is built on several advancements across several fields of technologies and life sciences. Bioprinted tissue constructs imitate the complexity of natural tissues by providing an artificial microenvironment conducive to cell growth.

To date, two opposing strategies have been investigated to bioprint tissues for different applications: scaffold-based (biomaterials-based) and scaffold-free (cellular-based) methods. Conventionally, exogenous biomaterial matrices, like hydrogels [12], are premixed with appropriate monoculture or coculture of cells and 3D bioprinted to fabricate scaffold-based tissue constructs. These constructs are often supplemented with several biological growth factors [13] to create a 3D environment favorable for tissue growth. Tailored fabrication procedures, with precise control over engineering parameters, offer a wide range of possibilities over conventional tissue scaffold fabrication techniques with desired architecture, geometry, and increased reproducibility. Moreover, control over the composition of bioprinted materials (bioinks) helps achieve optimal structural properties, such as mechanical properties, porosity, and degradation profile alongside geometrical feasibility, leading to the reconstruction of target tissues in a consistent, automized and high-throughput manner [14]. Scaffold-based bioprinting techniques have been widely used due to their ease in tissue fabrication; however, further research needs to be conducted to fabricate suitable robust biomaterials and studying their interactions at the cellular level for functional tissue formation. Scaffold-free bioprinting approach [15], on the other hand, focuses on tissue fabrication using cell aggregates, without the need for scaffold support, triggering cells to secrete their own extracellular matrix (ECM). Cell aggregates can be formed into geometrical configurations, for example, strands, honeycomb, or spheroids, and then allowed to fuse into larger tissues [16–18]. Both approaches have pros and cons, and in cases of 3D bioprinting, they may complement each other in the pursuit of meeting the ever-increasing demand for fabrication of scalable physically-relevant tissues or organs.

In a discussion on bioprinting, it is pertinent to expound the advancements in bioprinting of induced-pluripotent stem cells (iPSCs) to develop tissue constructs, which mimic the function and anatomy of native tissues. Given the extreme sensitivity of iPSCs to stressors during bioprinting– particularly mechanical shear and bioink conditions (pH, viscosity, crosslinking method, etc.), the development of new bioinks for sustaining iPSC viability and differentiation is of utmost importance. Some success has been achieved by bioprinting of iPSC aggregates – also called embryonic bodies embedded in hydrogels [19–21]. The iPSC-laden bioinks undergo mechanical stress, light, ionic and temperature related stress during bioprinting and maintenance of the proliferation and pluripotency of these embryonic bodies after bioprinting is critical. iPSCs or iPSC-derived cells have also been bioprinted to fabricate different tissues – skin [22], bone [23], cartilage [24], cardiac [25] and liver tissues [26]. Although several challenges need to be addressed for iPSC-derived tissue bioprinting – like tendency of the constructs to form tumors after transplantation and low efficiency of their generation and differentiation, yet iPSC-derived transplantation have provided a paradigm shift to how disease treatment have been approached in the current times.

Achieving native-like cell density, complex vascular network and controlling tissue remodeling are some of the major impediments for successful fabrication of tissues – both scaffold-based and scaffold-free [27]. Even if it seems feasible to overcome these elementary concerns, bioprinting strategies are overwhelmed with the conservation of actual size and anatomy of tissues in tandem with their functionalities and shelf-life as well as the cost-effectiveness of the process [28]. Additionally, economic constraints and ethical considerations with engineered tissues make this even more challenging [29]. Towards a more realistic and technologically optimistic approach, vascularized cell aggregates offer a viable alternative for the repair and restoration of damaged tissues. Developmental biology forms the foundation and provides the template on which these engineered cell aggregates are based [30], and consequently assemble to form 3D tissues [31]. Successful integration of tissue engineering and developmental biology is still a work-in-progress; however, this biomimetic approach allows for insightful advancements. The understanding, mimicking and employment of the developmental mechanisms of embryonic histogenesis and organogenesis in tissue engineering serves as a paradigm shift towards scaffold-free applications of bioprinting. Such applications include the fabrication of anatomically-relevant constructs using cellular aggregates (like spheroids, honeycombs or strands) to imitate native tissues. Continuous co-developments in the fields of spheroid fabrication and 3D bioprinting technologies have led to the emergence of novel engineering methods enabling successful bioprinting and fusion of spheroids for tissue repair and regeneration. With the recent developments in several state-of-art strategies, there is a lacuna in available literature wherein no comprehensive review is available focusing on this domain. Towards bridging the gap, this paper reviews the bioprinting strategies involved to form self-assembled tissues from spheroids and highlights the recent progress in tissue fabrication applications using spheroids as building blocks for bioprinting as highlighted in Fig. 1.

2. Limitations of scaffold-based approaches

Scaffold-based approaches involve the fabrication of a porous or non-porous template (out of ceramics, metals, or polymers, depending on their implantation site) conducive to cell attachment and tissue remodeling. The basic criteria for scaffold-based constructs are cell-conductivity, biocompatibility, suitable mechanical properties with tunable biodegradability, porosity to induce vascularization and tissue growth, and maintenance of rigidity and shape *in vitro* and *in vivo* [32]. Despite efforts in the development of effective tissue scaffolds with

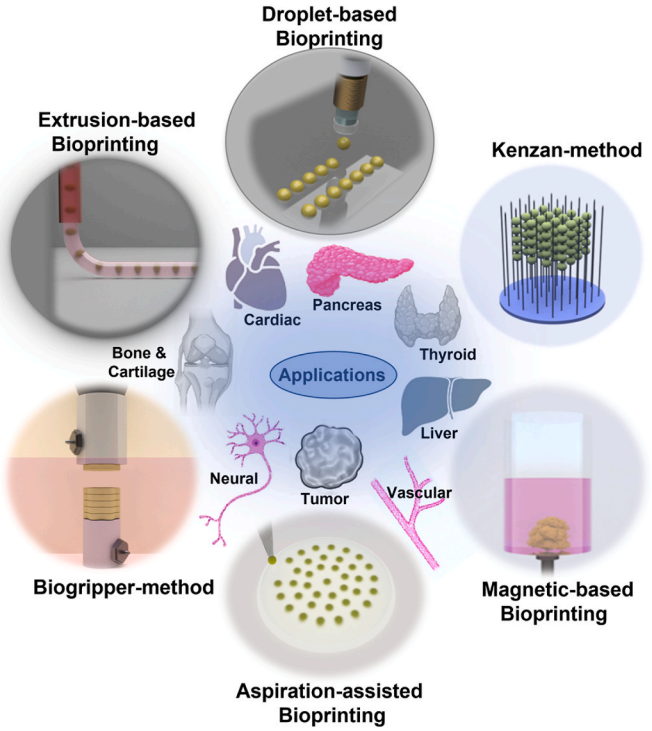

Fig. 1. Different modalities and applications of spheroid-based bioprinting (the images for different tissue types were created using BioRender).

directed cell signaling and tissue morphogenesis, this approach faces some crucial concerns, derived from the inherent disadvantages of scaffold-based approaches. Precise placement and organization of multiple cell types inside scaffolds lead to potential interference with cell interactions or ECM integrity, limiting inter- and intra-cellular interactions. In tandem, the incorporation of tissue-specific cell density pose one of the most salient challenges of the scaffold-based approach, which are yet to be answered [33]. Alongside, most of the scaffold-based approaches expose live cells to shear stress, heat, or other toxic chemicals and hence are intrinsically stressful to cells [34]. Another major elementary hindrance to such an approach is the absence of a biomaterial, robust enough to be used for all tissue engineering applications and conducive enough to support cellular activities of diverse cell types [35]. Most of these biomaterials are proprietary to different companies, allowing limited access for research by end-users, apart from being costly. Thus, many of the recent studies have focused on the biological response with a monotonous geometrical design, which is markedly similar to their native counterparts but neglects the influence of innate structural randomness for diverse applications [7]. These limitations provide significant hurdles for the creation of accurately mimetic 3D tissues. Alongside, the induction of vascularization in engineered scaffolds with a fully-developed vascular network is unsolved hitherto [36], and needs to be addressed for all bioprinted tissues in general, not limited to only scaffold-based approaches. The scaffold-free approach in recent years has witnessed several new emerging technologies, which successfully overcome some of the inherent limitations of the use of scaffold-based approaches while maintaining a high level of precision, high cell density and cellular interactions.

3. Integration of developmental biology approaches to tissue engineering

Most of the above-mentioned concerns are inherent to the scaffold-based approach and can be eliminated for the scaffold-free one, where only cells and self-secreted ECM mimic the formation of innate tissues or organs during embryonic development [37]. Use of sacrificial materials for bioprinting (which are removed after assembly of spheroids) allow sufficient initial inter-and intra-cellular crosstalk, facilitate cellular interactions, improved genotypic and phenotypic functionalities, and pose as a viable alternative to scaffold-based bioprinting [38]. In this regard, developmental biology provides crucial insights into tissue engineering approaches. In a physiological system, the rate of embryonic development is slow whereas tissue engineering demands accelerated tissue growth [39]. Reaching the optimum balance between mimicking essential processes of embryonic development and the development of an accelerated, automated, and commercially scalable technology is still a challenge for the scaffold-free approach. Bioprinting offers a scalable solution, with a high innate tissue-like cell density and absolute precision of 3D organization of multiple cell types while also allowing for vascularization. The concept of the scaffold-free approach relies on an assumption that cells formed of diverse cell types, can undergo self-assembly to form tissue without any external interventions [40]. Thus, using a scaffold-free approach that mimics developmental biology, tissues can be fabricated by guided assembly and re-organization of precise, robotically placed cell aggregates. Apropos, albeit aggregating cells have been formed into spheroids [41–43], honeycombs [44], and strands [45], from a variety of different cell types and their co-cultures, this review only focuses on bioprinting of spheroids and their fusion to form tissues.

4. Spheroids as building blocks

Spheroids pragmatically imitate the functional complexity of natural tissues without the geometrical intricacies and provide an artificial 3D microenvironment conducive to cell growth [46]. Spheroids often are composed of multiple cell types and developed to realistically highlight the critical features of the innate tissue [47]. Generating physiologically- and functionally-relevant tissues by incorporating these building units in ex-vivo cultures, instead of barely mimicking the complexity of the whole organ anatomically, is deemed more informative and pragmatic. The dynamics of spheroid formation can be categorized as (i) binding of integrin proteins to form loose cell aggregates with ECM acting as long-chain linker, (ii) secretion and accumulation of E-cadherins with no significant compaction in cell aggregates, and (iii) compact spheroid formation by hemophilic interactions between E-cadherins [48]. Spheroids offer several advantages, including but not limited to the cellular capability to secrete ECM components with an effective cross-communication between cells in a native-like microenvironment [49] and creating a 3D space favorable for reproducible tissue complexes, such as cartilage [50], pancreas [51], liver [52], and cardiac tissue [53]. Spheroids also have the potential to fuse towards scalable tissue substitutes [54]. Spheroids loaded with endothelial cells (ECs) can facilitate a denser cellular micro-environment, inherent ECM secretion, and a pre-vascularized network [55]. As a result, vascularized tissue complexes can be fabricated with pre-vascularized spheroids [56] allowing more accurate representations of native tissues [57].

The concept of spheroid-based systems leverages the fact that micro tissues can be formed from diverse cell types at high cell density and can undergo relatively complex self-assembly over length scales ranging from 100 to 500 μm [58]. When using human stem cells, spheroids can recapitulate aspects of developmental biology [58] to form organoids that assemble and reorganize into pancreas [59–62], bone and cartilage [17,63–65], brain [66–69], intestine [70,71], kidney [72,73], and eye [74]. While the use of spheroids as building blocks for tissue fabrication shows much promise, many important challenges must be addressed, especially when their bioprinting is not trivial compared to cell-laden hydrogels. Perhaps, the most pragmatic challenge is the unfamiliarity and complexity that creeps in with the use of spheroids and their integration in aseptic culture techniques, making uniformity and reproduction a major concern for all these techniques. Spheroids formed by commercially-available cell repellent culture plates seem more readily adaptable into the regular workflow, with low surface variability and improved consistency. Nutrients and oxygen diffusion into the core of spheroids pose yet another challenge, especially for the ones with larger dimensions. Hence, size uniformity is crucial for consistency in industrial applications, particularly for drug development because of the direct correlation of cellular functions and spheroid size [75]. Moreover, efficient spheroid formation requires segregated groups of cells placed near each other, which becomes more challenging when only a small number of cells are involved. Many researchers have focused on spheroid fabrication from single cells by monoclonal growth, which is a viable alternative for many anchorage-independent cancer cell lines [76,77]. Alongside, mimicking a diverse heterotypic composite tissue microenvironment using spheroids as building blocks still poses a challenge; with limited research performed in such regard [78].

As tissue fabrication methods advance towards the application of spheroids as building blocks, advancements are necessary to overcome these inherent obstacles. Due to the small size (typically ranging from ~100 to 500 μm) of spheroids, fabrication of clinically-relevant volumes of tissues is highly challenging. This could potentially be solved with a robust robotization of fabrication methods; however, further investigations are needed in this aspect [58]. As there is a lack of control over the fusion of spheroids [57], employing techniques to guide the growth of spheroids would allow for enhanced fit and function [79]. As more experimentation is conducted on spheroid fabrication methods, scalability and controlled spheroid assembly should be the key focuses for optimal functionality.

5. Biofabrication of spheroids

Spheroid fabrication is based on the basic principle of cellular self-assembly that occurs during embryonic development [40]. In this

stage, cells are observed to undergo agglomeration without any external forces or chemical agents. This process can be replicated *in vitro*, with the use of a surface that cells cannot adhere to, forcing interaction between the cells [80]. This interaction has been shown to occur in various ways as previously reviewed [81,82]. Commonly used spheroid fabrication methods include but not limited to (a) liquid overlay technique [83]; (b) hanging drop technique [84]; (c) microwell hanging drop technique [85]; (d) microwell arrays [86]; and (e) microfluidic-based technique [87]. Liquid overlay is a method consisting of stirring large volumes of cellular medium (up to 1 L) to generate spheroids [88,89]. Due to the inherent use of large volumes, this method is often used for mass production and only became more popular with the onset of bioreactors. Conversely, a major downside is that the requirement of large cell volumes does not allow for precise control over spheroid size, reducing batch to batch reproducibility [90]. The hanging drop method consists of hanging drops of cell suspension from a surface in which spheroids can form due to gravity [91]. To have better control over the spheroid size and increase spheroid forming efficiency, commercially available platforms have recently made use of 96- (400 μm in size) and 384-well plates. Microwell arrays explore forming spheroids using round-bottom nonadherent 96-well plates [92]. A non-technological approach favors the use of stamps (e.g., elastomeric stamps made via soft lithography) to imprint agarose microwell arrays, which is a cost-effective approach [93]. The inclusion of an additional microfluidic system into the microwell arrays has the potential to scale up this approach with the use of 96-well plates [94]. Microfluidic channels have also been used to facilitate continuous formation of spheroids in a precise manner; however, this approach is technologically intensive (requires rigorous use of sophisticated instruments and techniques), without many advantages over the other techniques.

For tissue engineering applications, hanging drop cultures [95] and microwell arrays [96,97] are commonly used. One of the first studies to show successful spheroid creation in a high-throughput manner was by Tung et al. who developed a robot-assisted hanging-drop culture [84]. Their setup allowed for the fabrication of up to 384 spheroids per array. Neto et al. demonstrated that the use of patterned superhydrophobic biomimetic surfaces, for the generation of high-throughput hanging-drop cultures, can allow for cost efficiency [98]. Using amalgamation of the hanging-drop culture and a sophisticated digital microfluidic platform allowed for the precise regulation of nutrient supply and inter-spheroid metabolic communication, as well as a thorough analysis throughout the process [99]. Non-adhesive hydrogels also provide a means of significant scaling of production, allowing for thousands of spheroids to be generated [82]. This approach also makes the generation of more complex cell aggregate configurations, such as rods, tori, and honeycombs [100]. Further, Fonoudi et al. recently reported a platform that focuses on the large-scale production of clinical-grade human cardiomyocyte spheroids (cardiospheres) derived from iPSCs [101]. The creation of this platform is an innovative step towards the scalable production of cardiospheres required for regenerative applications.

With the advancement of microfabrication and microfluidics, new platforms are being created boosting improvements in spheroid formation efficiency, homogeneity, and precise control over the spheroid size [102,103]. This allows for less labor-intensive and more rapid platforms, equipped for high-throughput screening. Because broad adoption in the medical community is the main goal, platforms like this need to be user-friendly, time-and cost-effective, and compatible with external machines (robotic liquid handling devices and microscopes). This would allow for a system that could be easily adapted for use in laboratories with minimal need for additional amenities ensuring widespread adaptability. Alongside, to be considered as a viable solution for biofabrication, the ideal scenario also necessitates a platform with the capacity for high-throughput spheroid fabrication with controlled size and composition. Within currently available techniques for spheroid fabrication, the use of round bottom low-attachment 96-well plates provide the most consistent way to form spheroids with uniform size and shapes, with low control on spatial distribution of cells inside spheroids, especially in the case of heterocellular spheroids. In this respect, it is also worthy to note that the choice of culture media for culturing a tissue construct formed from heterocellular spheroids, irrespective of their sizes, is application driven. But often, a common choice is the usage of a cocktail of culture media comprising of the individual media of the involved cell types in different ratios (depending on the application of the tissue constructs. However, much improvement is needed for high-throughput fabrication of spheroids for spheroid bioprinting techniques to progress or be embraced for translation purposes. In this regard, single-cell precision bioprinting techniques can be developed and used for fabrication of spheroids. High-throughput bioprinting of single cells may hold the key to consistency and reproducibility of sizes and composition of spheroids, with needs of technological advancement of artificial intelligence with a feedback look to enable the correct parametric choices for spheroid fabrication. With technological advancements, many efforts have been dedicated to the bulk generation of spheroids using bioreactors. Spinner-flask, rotary-shaker and microgravity bioreactors are the three frequently used bioreactor systems for high-throughput generation of spheroids. Theoretically, even though bioreactors are an efficient way for generation of spheroids with minimum requirement of handling, the requirement of adjusting agitation speeds at different time points – initially to induce cell aggregation, then to control spheroid sizes and later to inhibit spheroid merging limit their effective usage [104,105]. Due to the requirement of a diffusive oxygen supply across the entire spheroid domain, the size of spheroids should not exceed a few hundred microns, to prevent necrotic damage to the cells at the core of spheroids. Owing to the smaller size (typically ranging from ~100 to 500 μm) of spheroids, thousands to millions of spheroids are required to generate clinically-relevant volume of tissue substitutes for translation purposes. Hence, the capability to scale up spheroid production and automation are important aspects of efficient future spheroid fabrication techniques [15]. While milestones have been achieved towards the high-throughput production of spheroids, challenges still lay ahead to enable clinical translation of spheroid-based bioprinted tissues. Indeed, the fact that tissues are a complex composition of intricately placed different cell types, and spheroids restrict the resolution of tissue fabrication to about a hundred microns, mimicking the extensive network of vasculature makes the problem ever so intricate. Thus, the need for advancements that allow for more heterogeneity in spheroid formation and controlled fusion, to form macro-tissues with a desired shape and function, is so prevalent in novel biotechnological approaches, to be discussed further in this review.

6. Bioprinting modalities

Until now, bioprinting has been primarily advanced to enable the assembly of cells in a predetermined pattern, mostly within hydrogels, with limited inter- and intra-cell communications, and low cell density [106–109]. Alongside, developments of scaffold-free techniques have been more specialized towards bioprinting of spheroids, which leverages the assembly of spheroids to fuse to form a tissue patch [15]. Extrusion-based bioprinting was adopted early on to deposit spheroids [110]. More recently, technological advances have been towards the direct processing of single spheroids to offer flexibility over patterning into the desired geometry and to resemble the mechanical and biological properties of the native tissue. In the following subsections, we described the modalities explored for bioprinting of spheroids and elucidated their own advantages and disadvantages.

6.1. Extrusion-based bioprinting

Extrusion-based bioprinting is one of the most versatile, convenient bioprinting approaches, and offers the flexibility in terms of operational mechanism to dispense various types of bioinks including hydrogels.

This familiar technique was then extended into the domain of spheroid bioprinting and the very first efforts to bioprint spheroids were introduced by Mironov to investigate their vascularization potential [42,58]. Theoretically, extrusion-based bioprinting extrudes bioink (mixed with cells) through a nozzle using pneumatic or mechanical forces to deposit continuous microfilaments to form the desired geometry. For spheroid bioprinting, the bioink is spheroid-based, which is loaded into a syringe and extruded onto a receiving substrate by depositing one by one to allow fusion forming a tissue patch. Alongside, smaller spheroids can be loaded into a bioink and deposited in a random fashion resulting in limited spheroid density in the bioink.

Jakab et al. used tissue slurry, comprised of ECs and cardiac cells from chicken embryos [111] to study the self-organization of cells into cardiac tissue. The authors used atrio-venticular tissue fragments from 9-day old chicken embryos and dissociated them into single cells. The cells were then cultured and mixed with commercially-obtained human umbilical vein ECs (HUVECs). The mixture was referred to as a cellular slurry and was extruded through an in-house micropipette system to form spheroids. The individual units (spheroids) were incubated and loaded into a straight micropipette, which acted as a cartridge. The bioink was then extruded onto a collagen-based biopaper to form different geometrical configurations. Post bioprinting, assembled tissue patches showed early signs of vascularization with the ECs organized to form vessel-like conduits. Mironov et al. suggested similar methods of

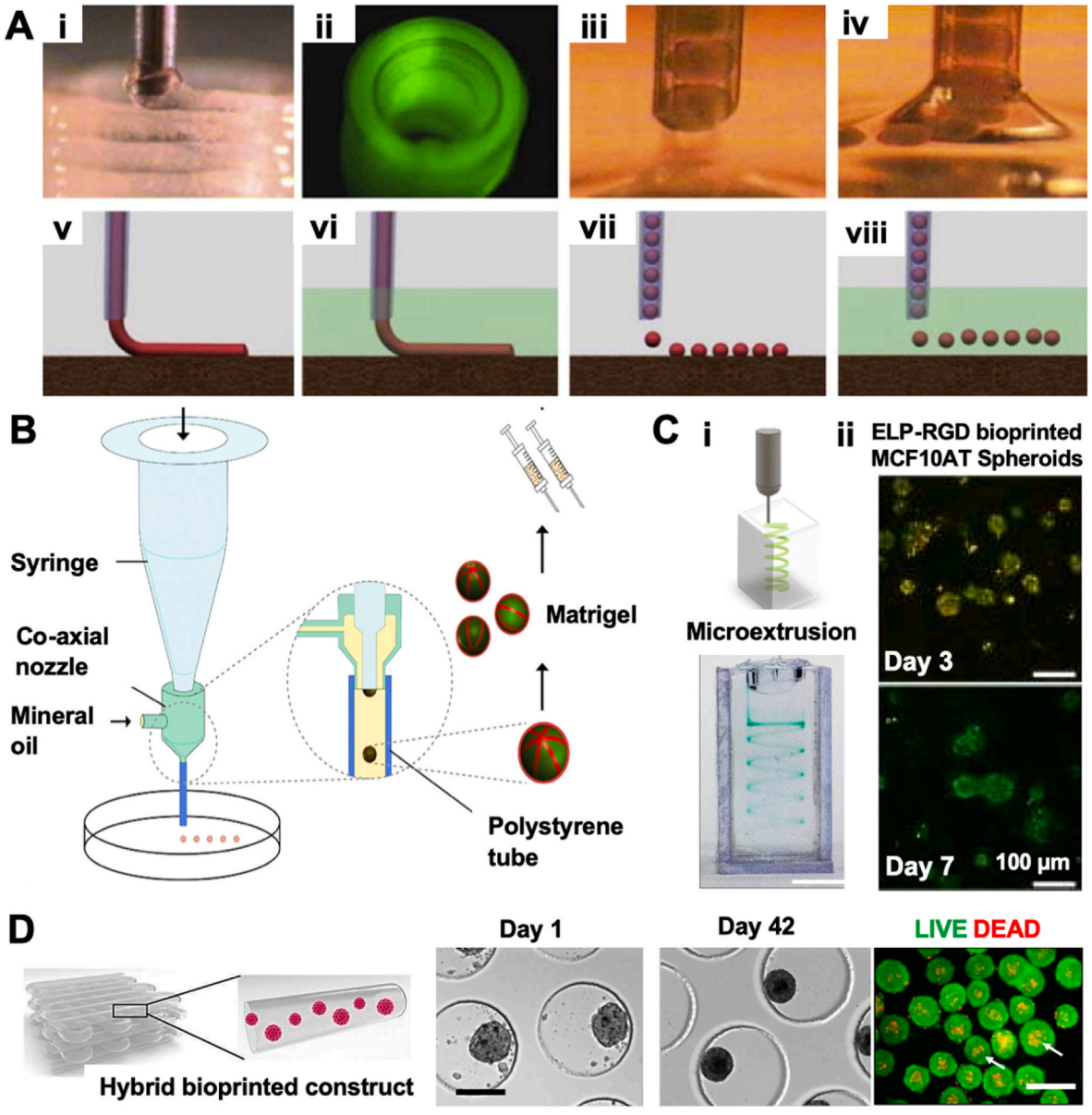

Fig. 2. Extrusion-based bioprinting. (A) Extrusion-based bioprinting of spheroids one by one. (i) Bioprinting in action, (ii) multiple bioprinter nozzles, (iii) tissue spheroids before dispensing, (iv) tissue spheroids during dispensing, (v) continuous dispensing in air, (vi) continuous dispensing in fluid, (vii) spheroid dispensing in air, and (viii) spheroid dispensing in the fluid. Adapted and reproduced with permission from Ref. [58]. (B) Schematic representation of the research strategy showing fabrication of microtissue spheroids by combining preset extrusion-based bioprinting with a microfluidic emulsification system. Spheroids with or without biomimetic structure were used for the in-vivo Matrigel plug assay. Adapted and reproduced with permission from Ref. [112]. (C) Printability and viability of elastin-like protein (ELP) with cell-adhesive RGD amino acid sequence (ELP-RGD) bioink. (i) Qualitative drop-on-demand printability tests of 3 wt% ELP-RGD printed as single drops into circular and S shapes. (ii) LIVE/DEAD staining of human premalignant breast epithelial spheroids (MCF10ATs) in ELP-RGD after bioprinting at Days 3 and 7. Adapted and reproduced from Ref. [115]. (D) (i) Extrusion-based bioprinting and (ii) formation of cartilage microtissues: morphology and viability. Scale bars: 200 μm. Adapted and reproduced with permission from Ref. [121].

directed assembly of spheroids for bioprinting tissue constructs via extrusion of spheroid-based bioink in air or fluid (Fig. 2(A)) [44,58]. Feasibility of fabricating scalable tissues with ease of automation makes special robotic arms (for example in Fabber, a 3D industrial robotic printer Bioassembly Tool) with an extrusion system makes it an attractive candidate allowing directed assembly of spheroids. Bulanova et al. [44] used a multifunctional Fabion 3D bioprinter equipped with a turnstile system, which consisted of three different pistons – a loading piston for holding the spheroid suspension, a trapping piston to hold single spheroids before bioprinting, and a depositing piston to release the spheroid onto a receiving substrate according to a predetermined geometry. In this case, a thyroid lobe and allantoic spheroids were mixed into collagen and bioprinted on a polytetrafluoroethylene (PTFE) membrane generating a vascularized thyroid gland. Hong et al. formed 3D structured microtissue spheroids by combining an extrusion-based bioprinting and microfluidic emulsification system, and developed a liver lobule-like structure, which showed high cell viability and longer structural integrity than that of non-structured spheroids along with the stable in-vivo engraftment of the microtissue (Fig. 2(B)) [112].

Mekhileri et al. integrated 3D bioscaffold fluid-based singularization (to separate individual spheroids) and LabVIEW controlled injection module (to deliver individual spheroids at predetermined spots) into a commercial 3D printer to combine micro-tissue assembly with 3D printing of thermoplastic polymeric frames [113]. The system contains two main regions - upstream and downstream, consisting of four stages –(i) agitation that leads to separation and moving of spheroids towards the upstream region, (ii) capturing of a spheroid on a channel tip, (iii) a secondary agitation while a single spheroid is trapped causing the uncaptured spheroids to go back to the upstream region and (iv) finally releasing the captured spheroid into the desired configuration. The automated bioassembly process was validated by bioprinting chondrogenic microtissues by assembling human articular chondrogenic microtissues along with a thermoplastic frame. In another study, accurate positioning of spheroids was achieved by bioprinting using concentrated solutions of collagen. The high viscosity of bioinks improved the bioprinting fidelity and spheroids could be arranged into patterns with a resolution of 0.5 mm in positioning in the pores of bioprinted collagen meshes. The method was applicable for the fabrication of structurally-stable constructs without the need for external photo-curing, chemical crosslinking, or molding [114].

Hydrogels, engineered from elastin-like protein (ELP), have been developed as bioinks, which could be directly extruded onto an on-chip platform containing vascularized channels. The bioprinting process was demonstrated with both single cells and spheroids taking neural progenitors and breast cancer cells as representative examples in each group (Fig. 2(C)) [115]. Through a computational study, by simulating the cellular rearrangement process after bioprinting, multicellular spheroids were proposed as an attractive sacrificial material (sacrospheres) for fabrication of vascularized constructs. Robu et al. used computer simulations based on Metropolis Monte Carlo algorithm [116] to demonstrate sacrospheres, but other methods derived from synthetic biology [117] or development of a modular library enabling elective cell death [118] can also be used to induce desired cellular behaviors including cell death on command. The authors showed that sacrificial spheroids were able to be bioprinted into a network of complex, branching channels, and post-bioprinting cell-cell adhesion-driven, spontaneous interactions leading to high-resolution tissue microarchitecture, overcoming the resolution of extrusion-based bioprinters employed [119]. Bioprinting of MDA-MB-231 breast cancer cells with gelatin-alginate bioinks has revealed the kinetics of self-assembly of these cells into tumor spheroids. By changing the gelatin to alginate ratio, both the mechanical stiffness of the hydrogel as well as cell-matrix interaction sites were modulated, and shown to have an impact on the viability and size of spheroids thus leading to the formation of a tunable in-vitro model [120].

De Moor et al. have employed extrusion of gelatin methacryloyl (GelMA) loaded with human bone marrow-derived mesenchymal stem cell (MSC) spheroids, which were later successfully differentiated into a chondrogenic lineage. Spheroids fused to form a macrotissue. They observed that a photoinitiator-controlled reduction in stiffness induced increased glycoaminoglycans (GAGs) and collagen II production with decreased collagen I expression (Fig. 2(D)) [121]. In another study, using an extrusion-based bioprinter, Han et al. generated a tumor model by depositing fibroblasts (hDFs) and ECs in gelatin, alginate, and fibrinogen as a blood vessel layer. A U87 glioblastoma multicellular tumor spheroid was then bioprinted on the blood vessel layer. Gradually, blood vessel was observed to sprout out in the vicinity of the spheroid. The model was applied to assess the efficacy of anti-cancer drugs, Temozolomide and Sunitinib [122]. In another study, Colle et al. have employed a high-throughput agarose microwell system to contain bioprinted adipose-derived MSC spheroids in GelMA. Spheroids were viable for up to 2 weeks post bioprinting, demonstrated multilocular microvacuoles, and differentiated to form adipocytes leading to the formation of microtissues [123]. Swaminathan et al. showed that human breast epithelial cells, when bioprinted as spheroids, exhibited higher resistance to Paclitaxel compared to when bioprinted as single cells. On the other hand, when spheroids were co-bioprinted with ECs, the resistance level was lower in heterocellular spheroids compared to homocellular ones [120].

Despite extrusion-based bioprinting has advantages in terms of spheroid bioprinting owing to its versatility, and flexibility of using multiple different hydrogels, its usage is limited due to critical concerns over spheroid fusion, clogging issues, spheroid rupture, and shape deformation when spheroids are deposited one by one. The very first challenge comes from the elaborate process of spheroid loading before bioprinting. To ensure a successful print, spheroids need to be loaded inside a straight syringe, making this process extremely cumbersome for tiny spheroids, particularly when the size of spheroids is not consistent. Owning to self-assembling potencies of spheroids, the time-consuming and laborious process of spheroid loading often leads to aggregation and clogging inside the nozzle, making extrusion very difficult. This necessitates that the spheroid suspension has some delivery medium between them to prevent aggregation issues, further adding to the inefficiencies. Fugitive bioinks with low viscosity to allow extrusion and inert to cell fusion are often the ideal choices. In addition, the diameter of the holding syringe dictates the size of spheroids loaded, leading to less flexibility during bioprinting. For compliance, during pre-bioprinting, spheroids are passed with trapping channels to filter out the size of spheroids according to the desired nozzle diameter. Aside from pre-bioprinting challenges, some inherent challenges occur during and after bioprinting. The low viscosity of the delivery medium often leads to the risk of gaps between spheroids after bioprinting, which deters the entire foundation of assembly of spheroids. Clogging and aggregation of spheroids are quite common during prolonged bioprinting processes - more often using a turnstile method, leading to further time-consuming efforts for cleaning and interfering with the continuity of bioprinting constructs. The choice of the substrate (hydrogels or sacrificial support) used for the extrusion process also limits the cellular interaction among spheroids, often leading to limited fusion. Since extrusion-based bioprinting is often not practiced in cell culture medium, spheroids are exposed to dehydration, often leading to cell necrosis.

Alongside, often only small diameter spheroids (with respect to the nozzle size) are loaded into a bioink for extrusion to reduce clogging related issues. However, this causes random positioning of spheroids in bioprinted constructs, with no precise control over the spheroid location. Increasing spheroid density in the bioink increases the cell-density; however, this can increase the risk of nozzle clogging and induce higher shear stress on spheroids. Unreliability and lack of reproducibility in spheroid formation techniques (leading to wide size distribution) can also induce spheroid clogging and fusion. Despite these challenges, extrusion-based bioprinting is still an exemplary means of fabricating

scalable tissues with decent bioprinting speed facilitating scalability, but the precision is usually insufficient for micro-mimicking structures, for example for organ-on-a-chip applications.

6.2. Droplet-based bioprinting

For bioprinting of cell-laden hydrogels, droplet-based bioprinting comprises inkjet, acoustic, or microvalve bioprinting [124]. The dispensing mechanism uses these modalities along with gravity and the fluid mechanical properties of the bioink to create consistent droplets in a manner that increases the efficiency of ejection compared to extrusion-based bioprinting, by removing the need for a continuous material flow. For bioprinting of spheroids, droplet-based bioprinting involves either (i) the deposition of a single spheroid to pattern droplets of bioink onto a desired surface or (ii) cell bioprinting followed by induction of spheroid formation. In this regard, Gutzweiler et al. [125] used a nano dispenser device (PipeJet P9, BioFluidix GmbH) for forming droplets. This nano dispenser was valve-less, non-contact, and mounted on a 3-axis system of a custom-made droplet-based bioprinter. The nozzle of the nano dispenser was a cylindrical transparent tube with an inner diameter of 200 μm (Fig. 3(A)). To form droplets with 12–13 nL volume, the nano dispenser used a piezo stack actuator with a 10–15 Hz dispensing frequency, with the ability to visualize and analyze ~400 μm droplets from the nozzle tip before bioprinting. Droplets without any spheroids were discarded using a vacuum channel and droplets containing spheroids were deposited onto a substrate, enabling spheroid positioning. The resolution of the camera dictates whether the software could recognize the presence/absence of a spheroid in the droplet, sometimes leading to empty droplets. This method cannot position spheroids tightly in contact with each other to stimulate their assembly.

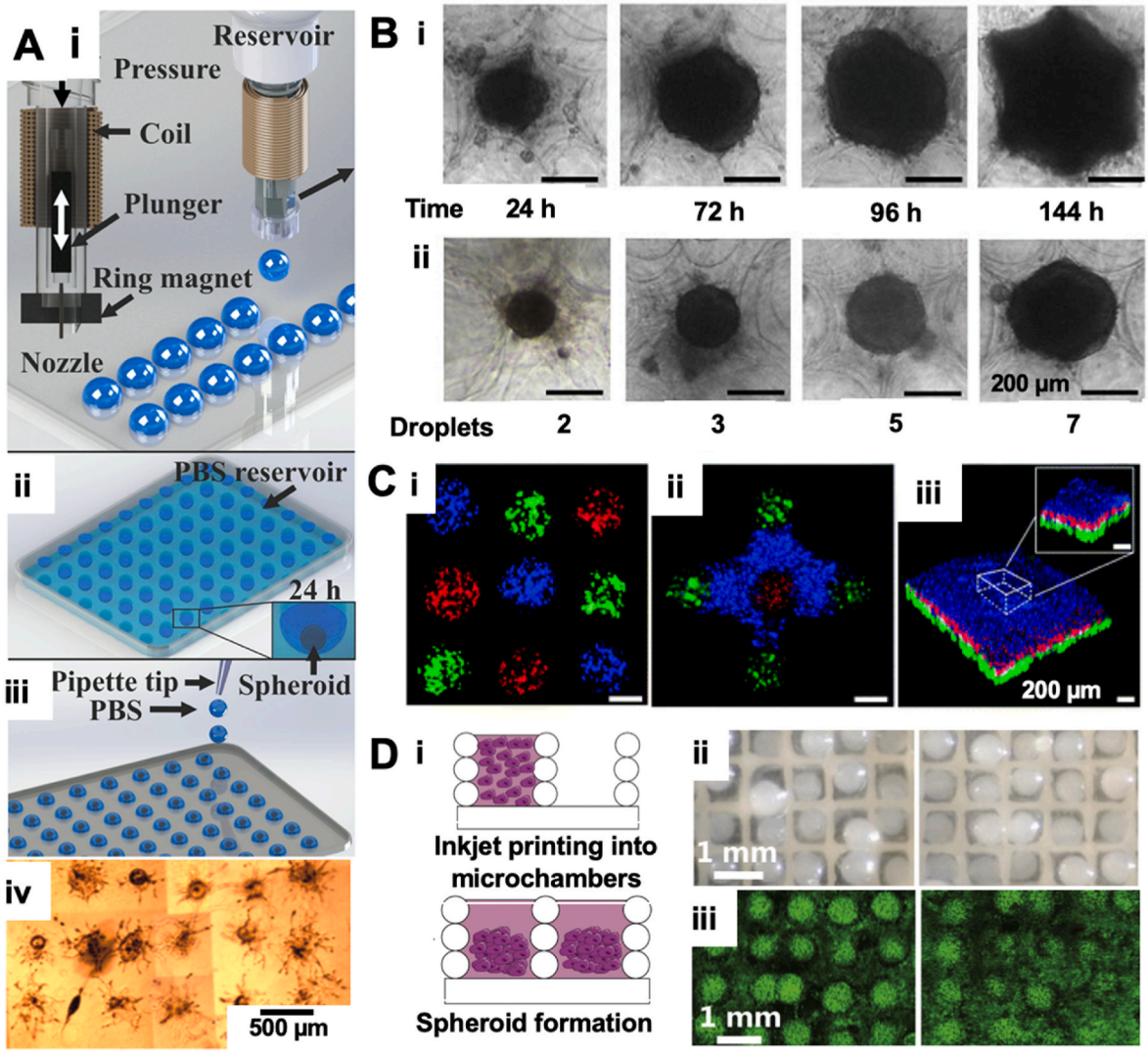

Fig. 3. Droplet-based bioprinting. (A) Droplet array formation. (i) An electromagnetic valve is mounted to a 3-axis system to dispense HUVEC suspensions in array formats onto polydimethylsiloxane (PDMS) coated polystyrene plates for spheroid formation. (ii) Plates are inversely placed above phosphate buffered saline (PBS) reservoirs and incubated for 24 h (iii) After incubation, plates are rinsed with PBS manually by a pipette to wash off droplets containing spheroids from the plate. (iv) Spheroids (each consisting of ~250 HUVECs), 72 h after incubation. Adapted and reproduced with permission from Ref. [125]. (B) 3D Bioprinting of embedded spheroids. (i) Formation and growth of bioprinted neuroblastoma (SK–N-BE(2)) spheroids throughout 144 h. (ii) Size of bioprinted SK-N-BE(2) spheroids after 3 days varied with the number of droplets containing seeded cells (scale bars: 200 μm). Adapted and reproduced with permission from Ref. [14]. (C) Fluorescence and confocal images of 1D (dot arrays (i)), 2D (crossroads (ii)), and 3D (pyramids (iii)) heterogeneous, complex, and diverse hydrogel constructs. The inset shows the distinct layers. Scale bar: 200 μm. Adapted and reproduced with permission from Ref. [128]. (D) (i) Schematic of inkjet bioprinting process, where droplets of cell suspension were deposited in pre-printed PCL microchambers of defined geometry to induce cell condensation and spheroid formation. (ii) Macroscopic and (iii) LIVE/DEAD images (z-stacks) of tissue formation in inkjet seeded samples at Day 28 of culture. Scale bar: 1 mm. Adapted and reproduced with permission from Ref. [221].

Ling et al. developed a more convenient droplet-based bioprinting approach based on MCF-7 cells embedded in hydrogel arrays to guide the formation of concave wells and in-situ formation of spheroids. Fabrication was performed using fugitive gelatin arrays along with in-situ cell seeding for programmed deposition of in-vitro models. This method overcomes the shortcoming of two-stage cell seeding-based spheroid formation techniques, which requires destructive molding and causes significant cell death apart from providing non-homogenous cell distribution [126]. In another study, Utama et al. developed a drop-on-demand bioprinter capable of high-throughput bioprinting of 96-well plate of spheroids for studying cancer models. Spheroids (neuroblastoma and glioblastoma) were embedded in a Ficoll based cell-carrier matrix to control the size and cell number, and then bioprinted. The system was viable for high-throughput screening of drugs, such as Doxorubicin. The half-maximal inhibitory concentration of Doxorubicin was noted to depend on the embedding procedure and spheroid size (Fig. 3(B)) [14].

The standing surface acoustic wave technique has been also used to generate droplets to improve process throughput and culture times. Using this technique, Sriphutkiat et al. showed that excitation at a frequency of 24.9 MHz reduced cell accumulation time compared to excitation at 10.4 MHz while maintaining greater than 90% survival rates for both frequencies [127]. Chen et al. reported an acoustic droplet printing (ADP) method, which was nozzle-free and allowed high-concentration cells, or even spheroids, to be bioprinted without clogging while retaining high cell viability (>94%). The authors developed a tumor microenvironment consisting of a single tumor spheroid surrounded by a high concentration of cancer-associated fibroblasts (CAFs) creating a dynamic tumor invasion function (Fig. 3(C)) [128]. In a further improvisation of this bioprinting modality, microfluidic nozzles were designed and integrated with an airflow spinning device in such a manner that different complex geometries of spheroid constructs, like helical or saddle shapes, can be generated in a single step [129]. Daly et al. reported a strategy where MSCs were inkjetted into 3D printed polycaprolactone (PCL) microchambers to promote initial cellular aggregation into spheroids. Droplets of varying cell densities were used and a single droplet was deposited to fill the microchambers resulting in native-like composition and biomechanical properties of the bioprinted cartilage and osteochondral tissue (Fig. 3(D)).

6.3. Kenzan method

Kenzan method works on the principle of placing spheroids on a needle array for temporary support, called “Kenzan”, to facilitate the fusion of spheroids towards tissue formation and maturation [130]. The name is derived from Japanese words - “Ken” meaning sword and “Zan” meaning mountain. The spheroids are prefabricated, analyzed for proper size distribution and shape, picked up using a robotic arm, and placed on a needle array. Skewered spheroids are incubated to help interact with each other, secrete their ECM, and facilitate fusion to fabricate a scalable tissue. The Kenzan method was developed to circumvent some of the inherent challenges of using spheroids as bioinks – controlling the arbitrary position of spheroids in the bioink. Although much research has suggested the use of prefabricated spheroids arranged in a desired geometry by multiple bioprinting approaches to form a tissue construct, commercialization was first achieved with the intervention of the Kenzan approach in Japan by Cyfuse Biomedical, K·K [130].

The Kenzan method has been employed to fabricate 3D multi-layered constructs with abundant ECM deposition and adequate mechanical properties needed for handle-ability, implantability and clinical translation from assembly of spheroids. LaBarge et al. bioprinted human iPSC-derived spheroids onto a 4 × 4 needle array to form a layer of tissue improving the precision of operation [131]. Extending the Kenzan method, van Pel et al. developed a system to track real-time invasion of human glioma cells into neural progenitor cell-derived spheroids. The authors demonstrated the gradual invasion of glioma cells (stained by a Red CMPTX cell-tracking dye) into the mouse-derived neural spheroids (stained by a CellTracker® Blue CMAC dye) by taking time-lapse confocal images and further validating by cryosectioning. Additionally, different progenitor cells showed marked differences in their responses, thus proving their potential for patient-specific treatment planning [132]. The method was further applied for assembling bone marrow-derived stem cell spheroids and then culturing them under perfusion to reconstruct the bladder tissue in a radiation-induced injury model [133]. Proto vessels were bioprinted from spheroids of hDFs, ECs and smooth muscle cells (SMCs). The vessels were found to retain structural integrity up to five days post in-vivo implantation in immune-deficient rodents. However, while bioprinting, a reduction in the lumen area of the vessel wall was observed, possibly due to compaction, or inadequate matrix organization or amounts of SMCs [130]. In another study, Yurie et al. bioprinted nerve conduits in a tubular arrangement and showed promising outcomes for restoration of sciatic nerve injuries in a rat model [134]. The concept given by Yurie et al. was further explored by another research team for the reconstruction of nerve conduits in canines. A 10-week-long study demonstrated the regeneration of the ulnar nerve in 5 mm defects. This model, for the first time, represented the possibility of functional nerve reconstruction in larger animals from spheroids made from only hDFs [134]. The Kenzan method was also employed for the reconstruction of the diaphragm from spheroids of hDFs and HUVECs [135]. Scaffold-free reconstruction has an advantage of a longer survival rate in animals with the successful reconstruction of target tissues. Similar examples have been demonstrated for bone, cartilage, bladder and cardiac tissue regeneration from spheroids containing a single type of stem cells [133,136,137]. In a recent study, Macino et al. demonstrated the reconstruction of trachea-like tubes using the Kenzan method. Two separate spheroids fabricated from human cartilage cells, hDFs, ECs, and MSCs were stacked alternately for developing the tracheal construct. It is worthy to note that in-depth biological evaluation of such tracheal tubes to reconstruct lost epithelium and capillaries owing to surgical resection in rats is still in progress [138]. Other notable works have been performed towards the reconstruction of the esophagus tissue (Fig. 4(A)) [139], liver [140,141] and tendon/ligament soft tissues [142]. Nakamura et al. used the Kenzan method for fabrication of cartilage for the repair of chondral defects. The authors used iPSC-derived chondrocytes, where post-maturation after self-organization of cells improved tissue mechanical strength and ECM formation (Fig. 4(B)) [143].

In a commercially available Kenzan bioprinter, dome-shaped stainless-steel needles with a diameter of 160 μm are used in the needle array. Arrays are currently available in two formats: 9 × 9 and 26 × 26 needles, with a 500-μm-distance between the needles. The size of spheroids is limited by the distance between each adjacent needle; otherwise, spheroids deform or rupture leading to a damaged tissue construct. This limits the spheroid size variety and flexibility of the cell types that can be utilized. The size of spheroids should range between 400 and 600 μm. It has been stated that the spheroid size distribution should not be more than 50 μm compared to the distance between the needles, which is 450–550 μm (Fig. 4(C)) [144]. Since this method enables bioprinting of individual spheroids into a needle array, the bioprinted tissue can retain the desired geometry, without major compaction. Thus, the spheroid size needs to be optimized according to different cell types by altering the number of cell densities used, especially in cases, where the longer or shorter culture times alter the spheroid dimension, making them unpredictable. Larger spheroids interfere with each other resulting in spheroid rupturing and end-used part errors. Smaller spheroids, on the other hand, do not come in tight contact with each other and consequently, leading to no fusion and hence, no assembly in that area. Hence, during pre-bioprinting, spheroids are required to be filtered for their size distribution, and spheroids falling within a specific size range should be used for bioprinting purposes. Bioprinting using the Kenzan method, theoretically, is an ideal scenario to fabricate tissues using spheroids as

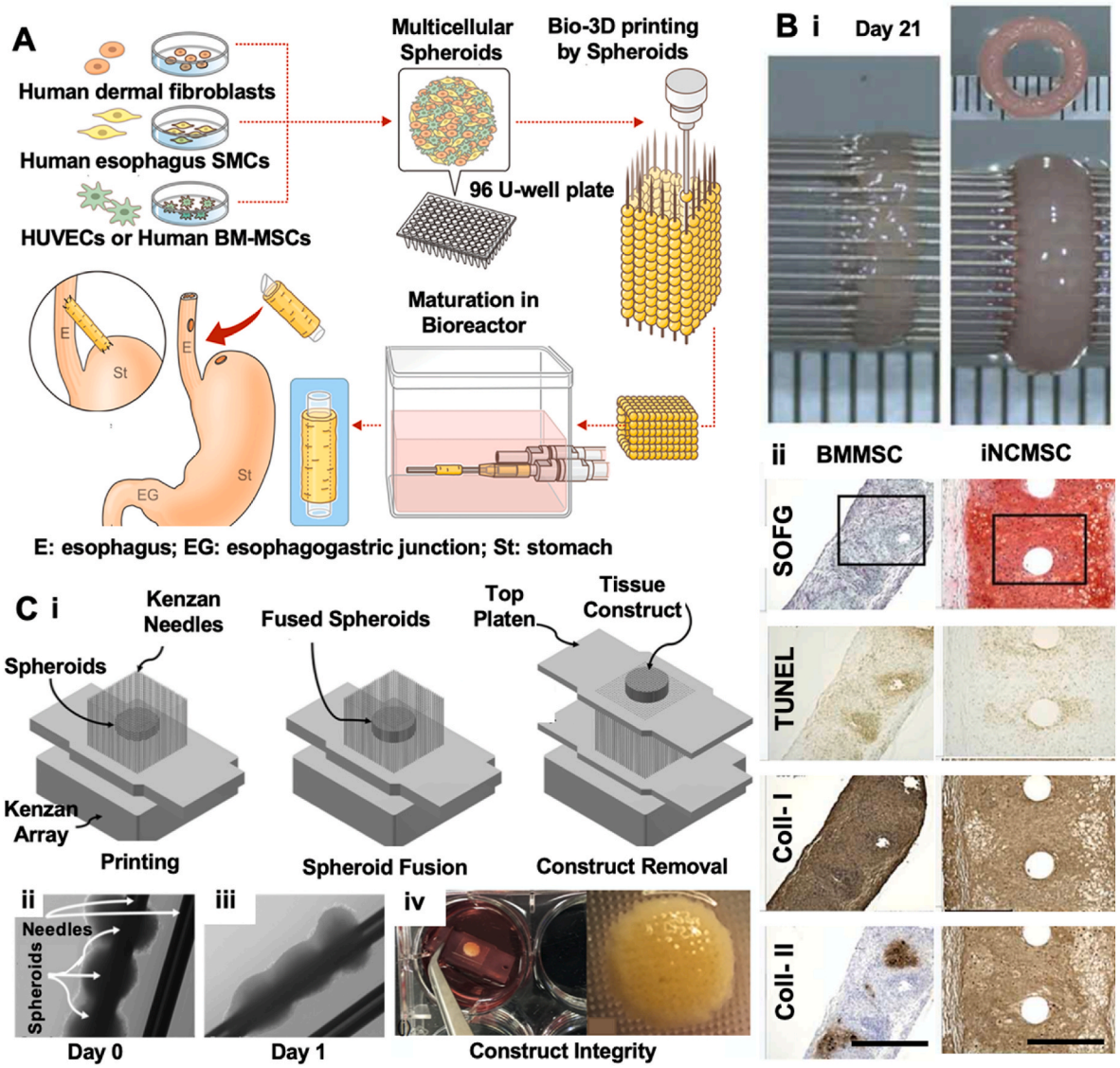

Fig. 4. The Kenzan Method. (A) Multicellular spheroids were created using mixed cell suspensions and an artificial esophagus was then constructed using those spheroids. The artificial esophagus was matured in a bioreactor for a total of 4 weeks. Finally, its transplantation was performed. Adapted and reproduced with permission from Ref. [139]. (B) Comparison of chondrogenesis in iPSC-derived neural crest cells through mesenchymal stem cells induction (iNCMSC) and bone marrow-derived mesenchymal stem cells (BMMSC) constructs. (i) Gross images and (ii) histological evaluations of constructs fabricated using iNCMSCs and BMMSCs. Five layers of spheroids made of same cell numbers were bioprinted on a 7-mm round Kenzan at Day 10 of chondrogenesis. Constructs were cultured on Kenzan for additional 21 days. Images of constructs stained for SOFG, TUNEL, type I and type II collagen. Scale bars: 500 μm. Adapted and reproduced with permission from Ref. [143]. (C) Kenzan platform: (i) the Kenzan needle array is comprised of several needles. Spheroids are impaled onto the Kenzan needles such that spheroids contact one another and fuse. Fused spheroids form a tissue. Tissues constructs can be removed by sliding the top platen from the bottom platen, keeping the tissues intact. (ii) Three spheroids on a Kenzan needle just after bioprinting, and (iii) a day after bioprinting. Needle diameters are 200 μm. (iv) Tissues were removed from Kenzans after 3 weeks. Adapted and reproduced with permission from Ref. [257].

building blocks. However, pragmatically, it is cumbersome and laborious, with sheer precision requirements for successful assembly of spheroids. Alongside, the bioprinting process is not entirely in 3D because end users do not have full control over the vertical axis. The spheroids are skewered between or, sometimes on the microneedles and then repeated with the next layer on top of the previous layer. This method of fabrication, hence, is more like a 2.5D process and brings challenges in the fabrication of structures with curves, geometrical complexities in the Z direction, or even structures with overhangs. Damaged microneedles (due to washing or bioprinting) cause defects during bioprinting and significantly add up to the cost of fabrication. Moreover, exporting the bioprinted structure out of Kenzan is yet another complicated procedure causing defects, such as holes and ruptures, in the final structure. Despite these challenges, the mere commercialization of the Kenzan approach made bioprinters accessible to many researchers, which is a steppingstone for the acceptance of bioprinting approaches for scalability and evolution from bench to bedside.

6.4. *Biogripper method*

The biogripper method utilizes the pick and place principles used in the high-speed electronics assembly, to pick, transport, place and stack microtissues with accuracy. In this regard, Blakley et al. developed a system called Bio-Pick, Place, and Perfuse (Bio-P3) for bioprinting larger size molded cell aggregates (spheroids, toroids, and honeycomb structures) to form tissues construct [145]. This method has three steps - picking a cell aggregate, placing the part on the stack of previous parts,

facilitating cell media perfusion, and allowing fusion to fabricate scalable tissues [146–148]. This method is limited to placing aggregates in the range of 600 μm to millimeters, restricting its usage for microenvironment-related applications. Further, the same group introduced a fluid-driven micro-manipulator and optimized the flexible of the bio-gripper design that maximized the bio-gripper utilities making it capable of picking and placing microtissues 30 times and stacking and aligning 20 microtissues (Fig. 5(A)) [149]. Additionally, they reported a technique, where membrane flow via a gripper was used to create optimum pressure differentials over the top and bottom surfaces of microtissues, allowing the item to be gripped and lifted. A clear syringe-pump-driven device was designed with the etched floor, which grabbed larger tissue aggregates (liver hepatocyte honeycomb structures for a proof of concept) and precisely placed them on a stack [150]. In a recent study, Ip et al. reported the versatility of the Bio-P3 system to be an instrument and bioreactor that can simultaneously assemble and perfuse large physiologically -relevant macrotissues (i.e., 100 million cells per mL within 2 h). The results indicated that the macrotissues built from human hepatocellular microtissues showed stable geometry and function (albumin and urea secretion) over five days (Fig. 5(B)) [151].

Since the gripper head allows precise picking and placing of larger cell aggregates, scalable tissue fabrication seems practical using this approach; however, automation is necessary with significant improvements in precision and resolution of the instrument for high-throughput tissue engineering. The gripper head also uses a commercial cylindrical cell culture insert, which restricts stacking of microtissues larger in size, even up to a centimeter scale. Alongside, the equipment requires an actuating mechanism to manipulate the microtissues of different sizes, and needs them to be in an aqueous media, limiting its usage. Similar to the Kenzan method, Bio-P3 is also a 2.5D approach.

6.5. *Aspiration-assisted bioprinting*

Aspiration-assisted bioprinting (AAB) presents a hybrid mechanism, which leverages the power of aspiration forces to pick up and precisely print/place cell aggregates including spheroids (80–600 μm), tissue strands (~800 μm), and single cells like electrocytes (~400 μm) onto a substrate with minimal cellular damage (Fig. 6(A)) [152]. This approach

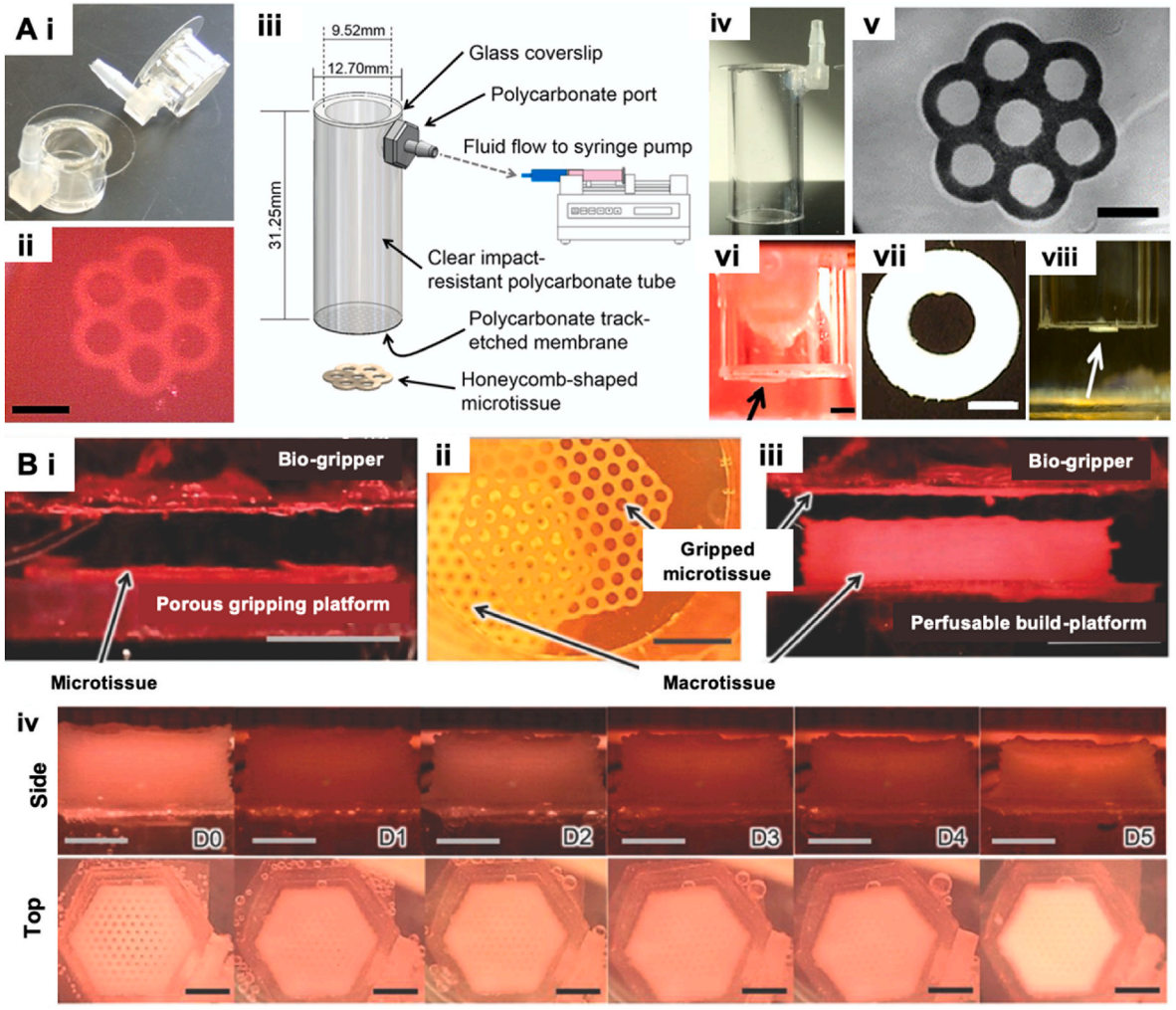

Fig. 5. The Biogripper method. (A) (i) Bio-gripper: (ii) Top view image of a gripped honeycomb microtissue (scale bar: 1 mm). (iii) The schematic and (iv) photograph of a syringe-pump driven bio-gripper. (v) Brightfield image of living honeycomb-shaped microtissue formed in a micro-mold of agarose (scale bar: 1 mm). (vi) Side view image of a gripped honeycomb microtissue (arrow) (scale bar: 2 mm). (vii) Top view image of toroid-shaped polystyrene synthetic part (scale bar: 1 mm). (viii) Side view image of gripped toroid-shaped polystyrene synthetic part (arrow). Adapted and reproduced with permission from Ref. [149]. (B) Building macrotissues: (i) A side-view image of a single six-orbital honeycomb-shaped tissue (4 million HepG2 cells) that has been gripped and moved upward from the gripping platform. (ii) Downward image showing the view through a biogripper of a single six-orbital honeycomb tissue that is gripped and moved above, but not yet aligned with a macrotissue under construction. (iii) A side-view image of a single six-orbital honeycomb tissue that is gripped and in process of being aligned and lowered onto a macrotissue under construction. (iv) Side and top views of a built macrotissue (100 million HepG2 cells, 25 layers) perfused over 5 days. All scale bars: 5 mm. Adapted and reproduced with permission from Ref. [151].

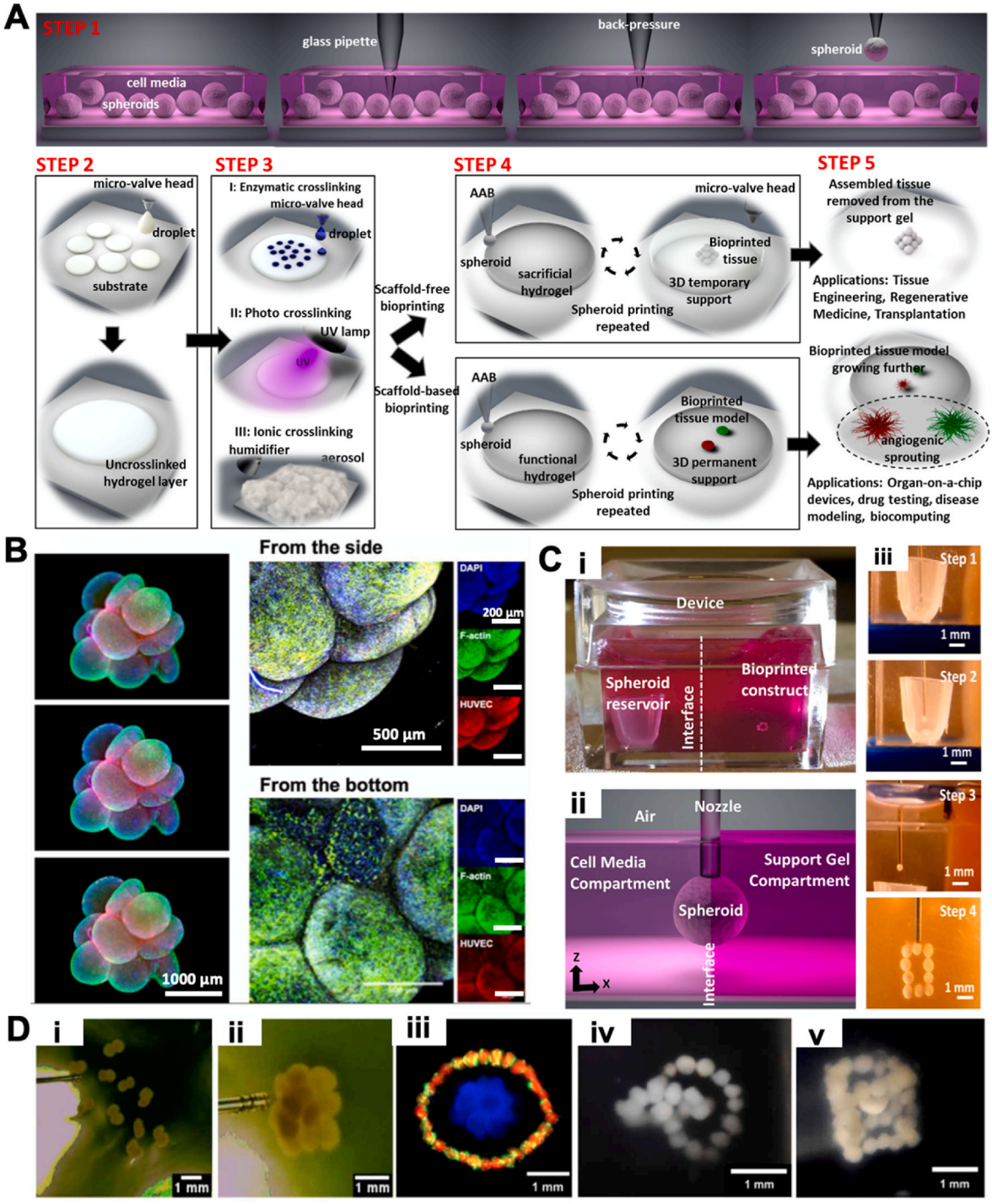

Fig. 6. Aspiration-assisted bioprinting. (A) Step-by-step illustration of picking and bioprinting of spheroids. Adapted and reproduced from Ref. [152]. (B) 3D Bioprinting of MSC/HUVEC spheroids. Fluorescent images of bioprinted pyramid of MSC/tdTomato^{+} HUVEC spheroids at different focal planes highlighting the top, middle and bottom layer (left). Confocal images of the pyramid construct highlight the side and bottom views (right). Adapted and reproduced with permission from Ref. [17]. (C) Aspiration-assisted freeform bioprinting process. (i) The bioprinting setup, where a box was filled with a yield-stress support bath in one compartment and cell media in the other. (ii) A schematic showing the process of spheroid traverse across the support bath and media compartment, and (iii) Images showing a step-by-step illustration of the process. Adapted and reproduced from Ref. [155]. (D) Various configurations with aspiration-assisted freeform bioprinting in alginate microgels with different sizes of spheroids (250–600 µm). Bioprinted spheroids for (i) dumbbell, (ii) pyramid, (iii) Saturn, (iv) linked rings, and (v) spheroid-in-a-box constructs. Adapted and reproduced with permission from Ref. [38].

was developed to improve the positional accuracy and precision (positional precision and accuracy of ~11 and ~15% with respect to the spheroid size) [152] offered by other spheroid bioprinting approaches with reducing the detrimental effects on spheroid viability and tissue damage, with potency to bioprint into a functional gel as a scaffold-based approach or a sacrificial gel as a scaffold-free approach. A minimum aspiration pressure is essential based on a physics-based approach to pick the biologics carefully to prevent damage. Spheroids are then transferred to a deposition area and bioprinted onto or into the receiving substrate, enabling precise placement of a diverse range of

sub-millimetric biological aggregates. Loading a spheroid necessitates a low pressure inside the liquidous media, whilst lifting out of the media, another pressure is exerted on the pipette tip from the liquid media. Therefore, the pressure should be strong enough to overcome this barrier, making optimization of critical lifting pressure very crucial to the success of this approach. For the scaffold-based approach, microvalve bioprinting was employed to generate the functional gel layers (collagen or fibrin), and spheroids were then aspirated, and placed at the desired position to facilitate tissue formation, whereas spheroids were placed onto a sacrificial gel layer (like alginate) for fusion purposes. The support gel is removed upon adequate fusion of spheroids to get an assembled tissue. Along with providing a diverse range of flexibility with spheroid bioprinting, cell aggregates of anisotropic geometry (such as strands) or single cells (like electrocytes) are also able to be bioprinted using AAB, demonstrating the robustness of the system.

Using AAB, Heo et al. demonstrated the bioprinting of bone tissue using this approach by precise bioprinting of prevascularized osteogenically differentiated MSC spheroids incorporated with ECs (Fig. 6 (B)). The bioprinted constructs maintained their geometrical configuration and showed strong expression of both osteogenic and endotheliogenic markers [17]. They also showed the efficacy of the AAB system to bioprint MSC spheroids differentiated into chondrogenic lineage to fabricate a tissue construct to repair osteochondral defects, with retention of phenotypic characteristics [65]. Further, Dey et al. employed aspiration-assisted bioprinting to investigate angiogenesis of tumor spheroids *in vitro*. For bioprinting, this study utilized a spheroid composed of HUVECs and metastatic triple-negative breast cancer cells (MDA-MB-231). Consequently, capillaries in a thick hollow structure (~70 μm) were developed, which successfully reconstructed an in-vivo tumor microenvironment [153]. Efforts have been also invested in achieving a 3D bioprinted cartilage tissue with control over the zonal arrangement of cells and ECM. This heterogeneous zonally-stratified reconstruction of the chondral tissue was made feasible by a hybrid bioprinting mechanism involving both extrusion and aspiration-based bioprinting approaches [65,154].

This approach also offers the flexibility to use cell media, partially crosslinked hydrogel, or sacrificial gel as the receiving substrate to facilitate the fusion of bioprinted spheroids [155]. A support bath or slurry can also be used for bioprinting of spheroids to offer total dimensional freedom for their placement in 3D [155,156]. This leads to the potency of bioprinting spheroids into self-healing yield-stress supporting baths (i.e., Carbopol and alginate microparticles) to pattern high cell-density tissues, like cardiac or bone tissue, with high resolution (Fig. 6(C)) [155,156]. After aspiration, spheroids were transferred directly into the self-healing support bath from the culture media and placed into the desired position allowing assembly, holding the key to enabling a new direction in future freeform bioprinting techniques [38, 155]. Daly et al. utilized this approach and demonstrated bioprinting of spheroids in a hyaluronic acid-based self-healing support gel. This enabled the creation of cardiac rings using iPSCs-derived cardiac microtissues [156].

Despite the success in bioprinting of different tissues using this technique, structurally weak spheroids are seen to rupture because of low cellular cohesivity and dropping of the spheroid at the air-liquid-tissue interface during lifting. An alternative could be the use of self-healing gels next to the spheroid container to avoid exposure of the spheroids at the air-liquid interface, as shown recently (Fig. 6(D)) [38, 155], where the spheroids were held in a cell media container inside a support bath. Alongside, picking and precise placement of spheroids one by one also is a time-extensive procedure, hence, high throughput systems are required to bioprint scalable tissues.

6.6. Magnetic bioprinting

Patterning of spheroids via magnetic forces has emerged as yet another method for the fabrication of larger tissue constructs [157–160]. Magnetic iron oxide microparticles are impregnated into spheroids, which allows the arrangement and clustering of cells into larger tissues under externally applied magnetic stimuli, especially in dynamic suspension culture [157,158]. Although this method boasts a higher level of control, the cell viability, phenotypic expressions, and functionalities are adversely affected by the incorporation of the magnetic particles [161–163], which can be improved by surface coating using oleates, dextran, gold or silica [164–166]. This concern of potential spheroid toxicity was also addressed with the use of biological magnetic nanoparticles, such as magnetoferritin, and the separation of the cellular chamber from the magnetic chamber in a method called Janus magnetic spheroid generation, to reduce the potential toxicity of cells from conventional magnetic particles. This method was deemed successful in the fusion of Janus magnetic spheroids into heterocellular larger constructs [159,160]. Recently, Bowser and Moore leveraged this technique with magnetic nanoparticles to accurately position spinal cord spheroids (formed from spinal cord cells isolated from the spinal cords of the embryonic tissue of Long Evans rats at Day 15 gestation) with high cell viability and no signs of necrosis in 3D biopolymer constructs with the possibility of scaling up and improved shape reproducibility. In vivo-mimetic cell-cell interactions, both at local and long-distance projections, were exhibited by cells after culture (Fig. 7 (A)) [167]. This approach has also shown promise in the treatment of radiotherapy-induced xerostomia by generating functional innervated salivary glands-like organoids derived from human dental pulp stem cells (hDPSCs) [168]. Bioprinted organoids demonstrated high cell viability, stable intracellular adenosine triphosphate, and differentiation into different compartments like ductal, epithelial and neuronal (Fig. 7 (B)) [168]. The modality of magnetic bioprinting also enables real-time monitoring of toxicity by mobile device-based imaging (Fig. 7(C)) [169].

Table 1 demonstrates an overview of spheroid bioprinting techniques. Although a number of research efforts has been dedicated to bioprinting of spheroids, and most of these efforts suffer from (i) poor spatial control in the positioning of spheroids in 3D, (ii) significant cell damage with loss of viability and structural integrity of spheroids, (iii) poor reproducibility of the process when using spheroids that are non-uniform in size (iv) limited ability to form complex 3D shapes, (v) an inability to maintain the designed shape due to cell-mediated contraction of spheroids post-bioprinting, and (vi) lack of scalability for translation into the medical industry. Integration of vascularization is yet another critical aspect, although hardly any of these efforts should successfully incorporate vascularization in any bioprinted tissue constructs. Alternative solutions to circumvent this challenge are to bioprinting the spheroids into functional gels (i.e., fibrin, or collagen) and incorporate them with perfusable vascular networks to facilitate angiogenic sprouting and hence, anastomosis [170]. Alongside, although most of these methods show bioprinting of isotropic tissues, that is hardly the scenario in native tissues. Several tissues, like muscle, cardiac tissue, articular cartilage, demonstrate anisotropic properties, and bioprinting of anisotropic mini-tissue blocks might provide the solution to this long-standing problem.

7. Applications of spheroid bioprinting

Despite the various efforts in bioprinting of spheroids, limited progress has been made towards the fabrication of scalable constructs – at a native-tissue/organ scale relevant for clinical transplantation. Vascularization, scalability, geometrical relevance, and clinical translation are among the major roadblocks to the fabrication of most of the tissue and organ types [171]. In this section, we have expounded the progress in 3D bioprinting of various tissue and organ substitutes using spheroids as building blocks.

7.1. Cardiac tissue

Cardiovascular disorders are responsible for the highest mortality in

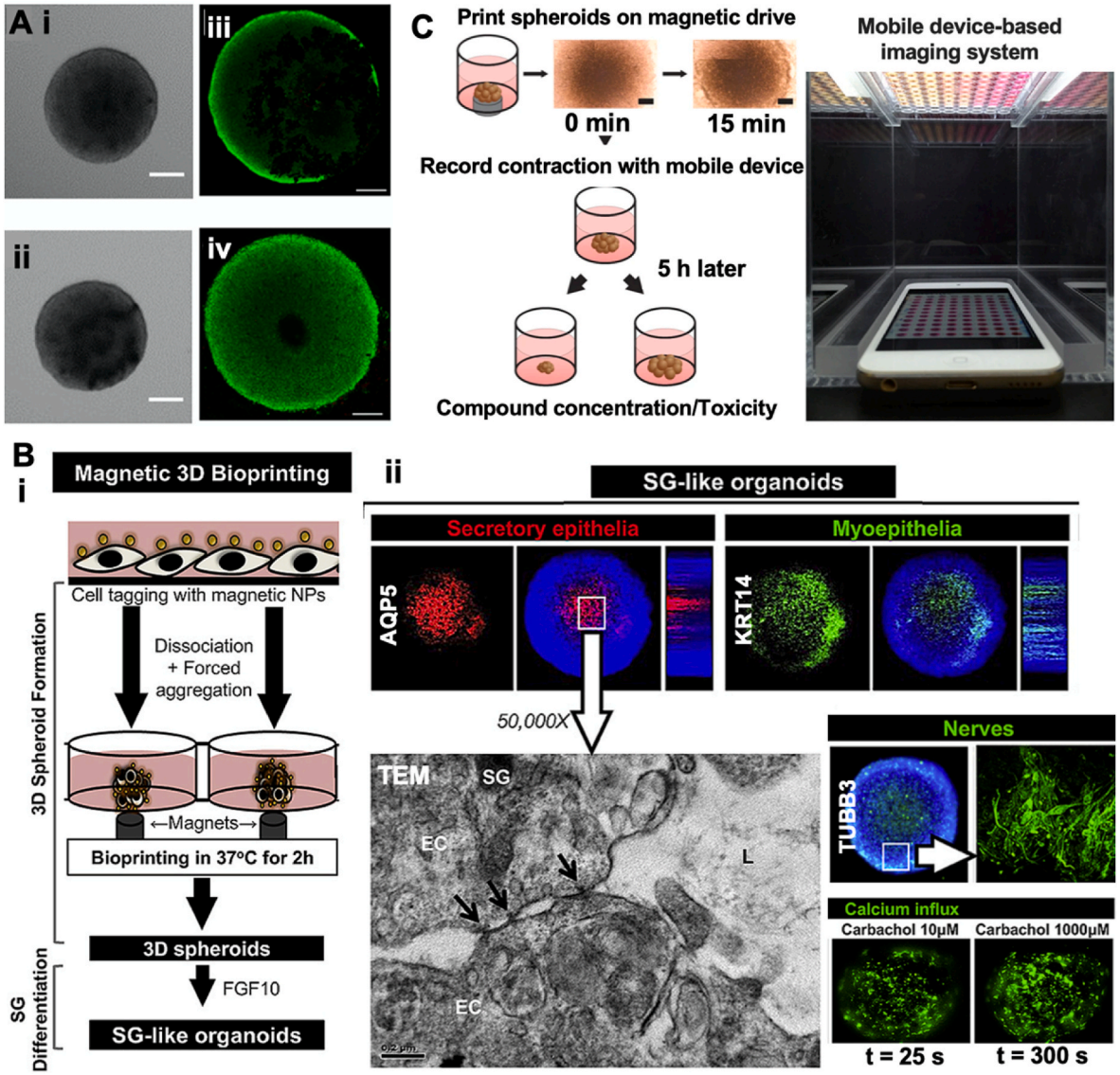

Fig. 7. Magnetic Bioprinting. (A) Characterization of spinal cord spheroids fabricated using magnetic nanoparticles. (i-ii) Representative phase images of spinal cord spheroids. Scale bar: 100 μm. (iii-iv) Viability determination using LIVE/DEAD staining of spinal cord spheroids. Scale bar: 100 μm. Adapted and reproduced with permission from Ref. [167]. (B) (i) Methodological steps required towards the formation and salivary gland (SG) differentiation stages of 3D spheroids towards SG-like organoids. (ii) Representative fluorescent images of differentiated spheroids stained for different SG epithelial markers: acinar secretory epithelial (AQP5), myoepithelial (KRT14), transmission electron microscope micrographs of spheroids, immunostained for nerves (TUBB3), and images showing calcium ion [Ca2+i] mobilization in SG spheroids before and after cholinergic stimulation with Carbachol. Adapted and reproduced with permission from Ref. [168]. (C) Magnetic 3D bioprinting. Cells were incubated overnight with magnetic nanoparticles. After resuspending and levitating the cells, they were then bioprinted for 15 min by putting the plate atop a 96-well magnetic drive. After bioprinting, the magnet was removed and spheroid contracts. The mobile device-based imaging system, with a 96-well plate full of spheroids placed above the mobile device. Adapted and reproduced from Ref. [169].

the United States (US) accounting for about one in every three deaths [172]. To solve this, organ transplantation has been one of the premier research developments for the treatment of cardiovascular disorders, as 2018 marked the 50th anniversary of the first cardiac tissue transplantation performed worldwide in South Africa [173]. With limited donors, site morbidity, and fears of immune rejection being major concerns with transplantation, researchers have found solace in the exploration of cardiac tissue bioprinting – including whole bioengineered hearts [174], cardiac patches [175], biological pumps [176], valves [177], ventricles [178] and blood vessels [179]. 3D Bioprinting of the whole heart refers to the fabrication of the heart [174] consisting of cardiac muscle, endocardium, epicardium, ventricles, atria, and valves, along with a network of blood vessels (from arteries and veins down to capillaries), which has the potential to be translated for clinical heart transplantation. The cardiac patches, on the other hand, are tissue constructs that physiologically or functionally mimic the cardiac muscle and has the potential to augment contractile function in cases of acute myocardial infarction. Thus, depending on the severity of a patient's condition, a cardiac patch may be sufficient to augment lost contractile functions, but a whole bioengineered heart transplantation will be required for chronic heart failure. Yet another crucial aspect within cardiac tissue research is the necessity of creating vascularized tissues [180]. The difficulty in the incorporation of innervation with the development of micro-scale blood vessels (less than 200 μm for free oxygen diffusion) has been the foremost barrier to the successful development of functional organs [181].

Many efforts have been invested into the fabrication and assembly of cardiac spheroids into larger constructs by magnetic bioprinting approach – both by corporate associations and academic settings [159, 182,183]. Kenzan method has been used for cardiac tissue fabrication

Table 1
Bioprinting methods and their comparison.

Bioprinting method	Scaffold-free (SF)/ Scaffold-based (SB)	Spheroid size variety	Spheroid clogging possibility	Spheroid rupture possibility	Scalability	Positioning	Critical Concerns	Parameters to control	References
Extrusion-based	Both	Yes, limited by the nozzle diameter	Yes	Sometimes	Limited if spheroids are bioprinted one by one	Low	Resolution is relatively low (>100 μm); choice of bioink is limited by adequate viscosity requirements; clogging of nozzles is often noticed with high viscosity bioinks or larger spheroids; shear stress exerted on spheroids lowers cell viability	Viscosity of the bioink (with spheroids, bioprinting speed, pressure, nozzle diameter	[44,58, 111,113]
Droplet-based	SF	Yes	Low-Medium	Sometimes	No	Low	Throughput is low; uniform spheroid size is required for droplet formation; clogging issues are noted from non-homogeneous spheroids; Spheroid sizes are limited by the nozzle size.	Viscosity, pressure, surface property of the substrate	[125]
Kenzan	SF	No	No	High	Medium-High	Low	Fixed inter-needle distance limits the size of spheroids and resolution, limited control on the Z-axis, spheroids damaged by skewers leading to lower cell viability	Needle array, inter-needle distance, spheroid size	[130]
Bio-gripper	SF	Yes	No	No	High	Low	The membrane of the building block must be optically transparent; limited to cell aggregates in the range of 600 μm to millimeters; limited control on the Z-axis	The shape of the building block, flow rate, nozzle positioning	[145,149]
AAB	Both	Yes	No	Yes, when spheroids have low surface tension	Low	High	Throughput is low, sometimes spheroid damage is noticed due to low cellular cohesivity and dropping of the spheroid at the air-liquid-tissue interface during lifting	Aspiration force, spheroid diameter and surface tension	[152]
Magnetic-based	Both	Yes	No	No	High	Low	A long-term cell culture period is required; cell viability and phenotypic expressions and functionalities are adversely affected by the incorporation of the magnetic particles	The shape of the magnet, cell density	[168]

with cardiac spheroids. Spheroids were fabricated using a combination of ECs, aortic smooth muscle cells, and hDFs in a 4:1:5 ratio in a cocktail culture medium [184]. Formed spheroids were bioprinted into tubular constructs on a needle array, incubated for fusion and assembly, and then tested in a nude rat model. Polonchuk et al. developed cardiac spheroids using human cardiomyocytes (CMs), hDFs and ECs, in alginate/gelatin hydrogels and then bioprinted them on a microelectrode plate for drug testing. The bioprinted spheroids showed contraction spontaneously and when stimulated, contractile and electrical data could be collected on microelectrode plates (Fig. 8(A)) [185], making it appropriate for industrial applications.

Another study confirmed the use of CMs, ECs, and hDFs in a 70:15:15 ratio to form spheroids and plated them in low attachment Petri dishes in desired predetermined shapes under continuous rotation for 24 h for fusion into cardiac grafts [186]. Arai et al. employed combinations of hDFs, ECs and iPSCs-derived CMs, and confirmed the cellular self-organization in 3D bioprinted cardiac constructs [25]. Human adipose stromal vascular cells were also formed into spheroids and bioprinted into cardiac patches using extrusion-based bioprinting [187]. Daly et al. positioned cardiac spheroids inside a self-healing hyaluronic acid-based granular gel and developed a cardiac infarction model (Fig. 8 (C)) [156] to replicate pathological features and study the repair mechanism, opening yet another avenue for bioprinted cardiac tissues.

Even though recent studies have demonstrated 3D bioprinting of spheroids to form cardiac tissue, the integration of synchronous contractile activity and vascularization (spanning across many orders – from arterial to capillaries) limit their usage. Even then, 3D bioprinting of patient-specific heart tissues holds the key towards an unmet need for clinicians and brings an end to a long-standing problem to promote cardiac regeneration in patients.

7.2. Pancreatic tissue

Diabetes mellitus is one of the most severe health concerns the world is witnessing with an incidence rate of one in every 11 people leaving around 415 million infected worldwide [188]. Allogenic pancreas and Langerhans islets transplantation have been considered as a treatment to restore blood glucose regulation physiologically [189]. However, lack of donors, consequential surgical risks of thrombosis, lifelong immunosuppression therapy, and fear associated with immune rejection have limited their usage to only an insignificant number of patients opting for pancreas transplantation compared to the population of diabetic patients. Various strategies and advancements in recent years towards tissue engineering approaches may offer a viable alternative [190].

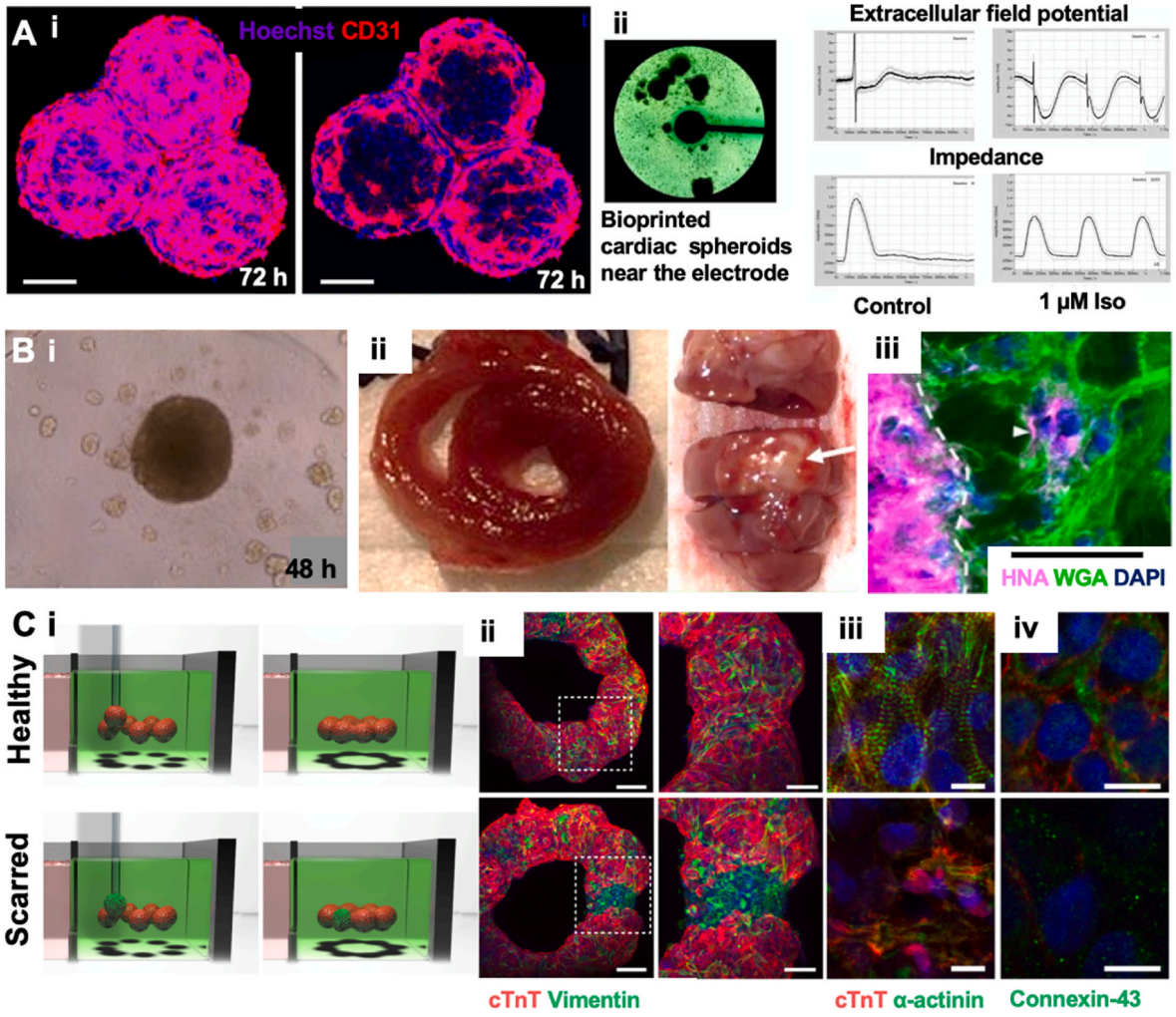

Fig. 8. Bioprinting cardiac tissues. (A) The bioprinting was done using extrusion-based method. (i) VEGF-promoted fusion of three bioprinted cardiac spheroids within 4% alginate-8% gelatin hydrogels. Collapsed z-stacks of fused spheroids 72 h post bioprinting. (ii) Electrical recording from bioprinted cardiac spheroids. Phase-contrast image of bioprinted cardiac spheroids in the proximity of an electrode at the center of a well in a CardioExcyte96 plate (left). Representative measurements of raw mean beat impedance and field potential waveforms shown before and after the addition of 1 μM isoproterenol. Adapted and reproduced from Ref. [185]. (B) The bioprinting was done by Cyfuse Regenova 3D bioprinter using spheroids which were placed on fine needle arrays to create biomaterial-free cardiac patch. (i) Cardiospheres of various cell ratios (iPSC-derived CM:fibroblast:EC ratio 70:15:15) formed in 48 h. (ii) Cross-sections of the explanted heart showing the fibroblast bioprinted cardiac patch. (iii) Human nuclear antigen (HNA) (Magenta), wheat germ agglutinin (WGA) (Green), DAPI (Blue). Scale bar: 40 μm. White arrows indicate the presence of human cells in the native rat myocardium. Adapted and reproduced from Ref. [137]. (C) The bioprinting model was an aspiration-based 3D bioprinting of spheroids. (i) Schematic of 3D bioprinting of healthy and scarred cardiac microtissue rings and (ii) immunofluorescence staining for cTnT and vimentin in healthy and scarred cardiac microtissues after 5 days of fusion within a support. Scale bar: 100 μm (insets: 50 μm). (iii) Immunofluorescence staining for alpha-actinin (green; sarcomeres) and cTnT (red; iPSC-derived CMs) and (iv) connexin-43 (green; gap junctions) and cTnT (red; iPSC-derived CMs), in healthy and scarred regions of microtissues after 5 days of fusion within the support. Scale bar: 10 μm. Adapted and reproduced from Ref. [156]. (For interpretation of the references to color in this figure legend, the reader is referred to the Web version of this article.)

Towards this goal, the presence of ECs has been shown to influence the specific differentiation of pancreatic β-cells and sprouting angiogenesis was reported in these 3D β-cell spheroids [191–193]. These spheroids confirmed neovascularization with improved β-cell viability and functionality over time. Kim et al. [194] explored the development of a pancreatic tissue-derived ECM bioink and combined it with ECs and islets together to characterize their viability, insulin secretion, and bioprintability *in vitro*. Four-layered ~200-μm-thick lattice constructs were generated via extrusion-based bioprinting, which maintained their structural integrity in the physiological conditions for 5 days. Similar cellular viability was observed in bioprinted constructs compared to non-bioprinted constructs five days after incubation (Fig. 9(A)). Recently, Hwang et al. developed a hybrid encapsulation system using a macroporous polymer capsule with a stagger-type membrane and assemblable structure, and nanoporous dECMs hydrogel containing pancreatic islet-like aggregates. The system showed in-vitro and in-vivo biocompatibility in terms of M1 macrophage polarization, and 3D bioprinted pancreatic islet-like aggregates revealed structural maturation and functional improvement along with integrating iPSC-derived insulin-producing cells (Fig. 9(B)) [195]. An exocrine pancreas model was bioprinted using spheroids composed of acinar and ductal cells to study factors contributing to the progression of pancreatic ductal adenocarcinoma, shedding light on future therapeutic strategies (Fig. 9(C)) [196].

One of the major impediments to the bioprinting of pancreatic tissue is the production of functional pancreatic islets itself. Despite the great progress, iPSC-derived pancreatic islets have still limitations; thus, appropriate maturation of these cells *in vitro* after bioprinting with proper 3D microenvironment cues is crucial. In addition, bioprinting of islets into implantable devices in high density has been a challenge,

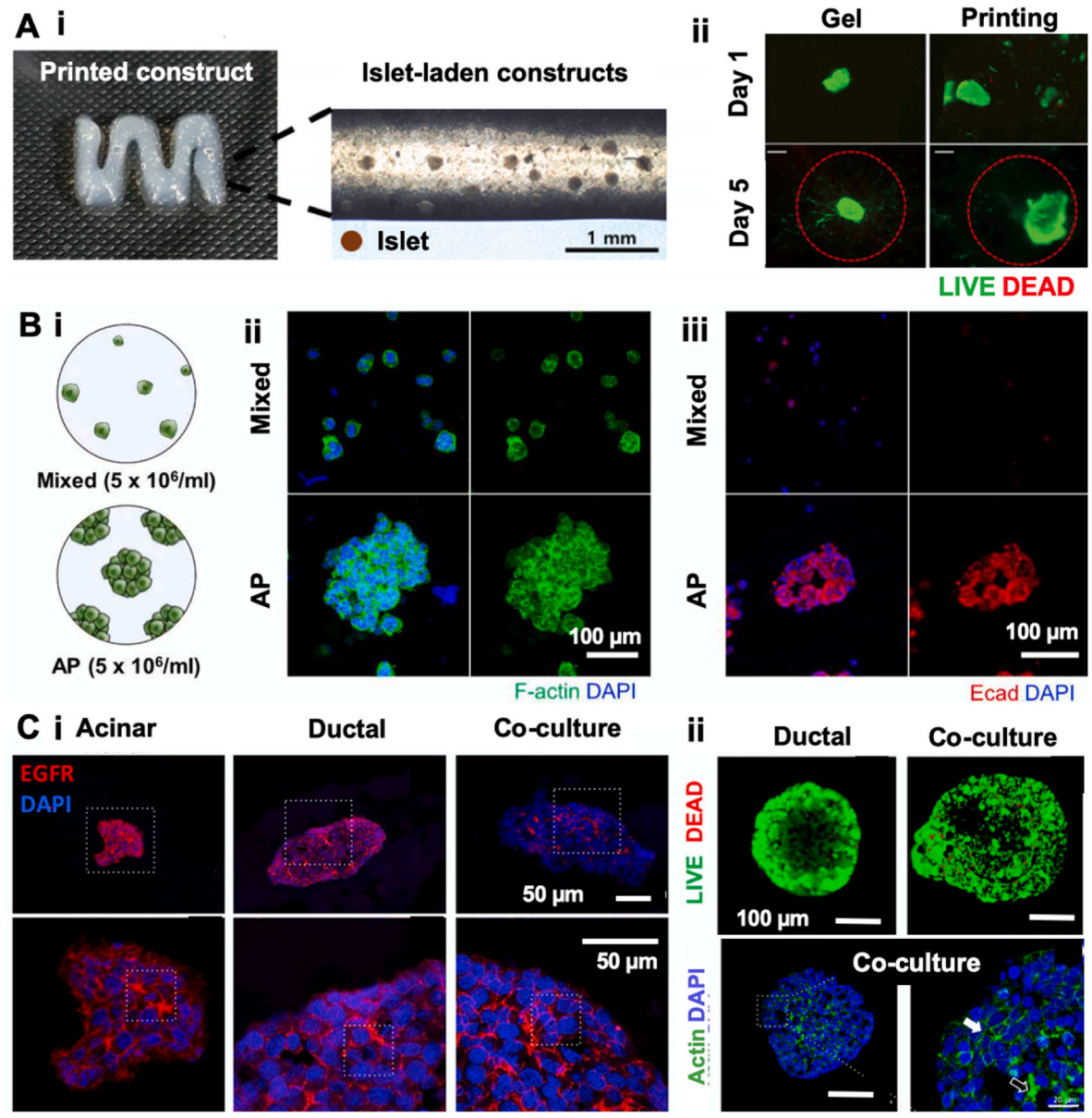

Fig. 9. Bioprinting pancreatic tissues. (A) 3D Bioprinting of islet-laden pancreas-derived ECM bioink for the construction of a pancreatic tissue using microextrusion-based printing technology. (i) Islet-laden bioprinted constructs (ii) and their cell viability over 5 days in culture (scale bar: 100 μm). Adapted and reproduced with permission from Ref. [194]. (B) The macroporous polymer capsule was fabricated using a micro extrusion-based 3D bioprinting system. The figure shows the effects of islet-like aggregate bioprinting (AP) on intercellular behaviors compared with mixed groups after culture for 7 days. (i) Graphical description of mixed and AP groups. (ii-iii) Representative immunofluorescence images of MIN6-m9 cells for F-actin (green), Ecad (red), and DAPI (blue). Adapted and reproduced with permission from Ref. [195]. (C) Laser-assisted 3D bioprinting of exocrine pancreas spheroid models.(i) Immunolabelling of epidermal growth factor receptor (EGFR) in spheroids composed of acinar cells, ductal cells, or acinar and ductal cell co-cultures (1:1 ratio), at Day 14 post bioprinting. (ii) LIVE/DEAD staining of a 20-μm stack at the center of spheroids. Labeling of actin in spheroids composed of acinar and ductal cells in co-culture at Day 14 post bioprinting. Adapted and reproduced with permission from Ref. [196]. (For interpretation of the references to color in this figure legend, the reader is referred to the Web version of this article.)

which restricts the total graft volume with respect to the implanted device volume, which reduces the efficiency of insulin secretion, or the transplant sites cannot carry the required device volume. We believe 3D bioprinting still holds the potential for the coordinated fabrication of pancreatic tissue with precise spatial organization of islets along with the incorporation of vascular networks, leading to enhanced cell viability and hormonal functionalities, crucial for treating diabetic patients. In the meantime, the organ-on-a-chip model might be better suited for the pancreatic islets, with the potential to monitor the dynamic changes in the endocrine hormones and drug modeling in the glucose-dependent environment [190].

7.3. Tumor models

According to the American Cancer Society, in 2019, the number of new cancer cases and deaths were estimated to be over 1.7 million and 660,000 respectively in the US [197]. Being such a prevalent issue, research and drug discovery have been a major focus in the attempt to combat the effects of cancer. The use of tumor models is one main method of research, applied to both developmental studies and drug efficacy, and has seen an increase in efficiency and applicability with the introduction of spheroid bioprinting. These benefits stem from the superior properties of 3D microenvironments over 2D counterparts in mimicking the in-vivo environments [120]. 3D Tissue models using

spheroids are better able to recapitulate the complexity seen in cancerous tissue and combined with the enhanced spatial precision enabled by bioprinting, provide more accurate results in the testing of tumor models [196]. Tumor spheroids recapitulate the genetical and histological morphology of a tumor and retains tumor heterogeneity and help bridge gaps between *in vivo* animal models and *in vitro* 2D culture models [170]. Indeed, they are useful models for avascular tumors, which develop hypoxia [198]. The core of larger spheroids (>500 μm) tend to be hypoxic due to low diffusion of nutrients and media to the center [152].

Tumor organoids have also been demonstrated as outstanding models for understanding the different phases of cancer biology and hence for their potential applications in drug discovery, personalized medicine and disease modeling [199]. In fact, tumor organoids from

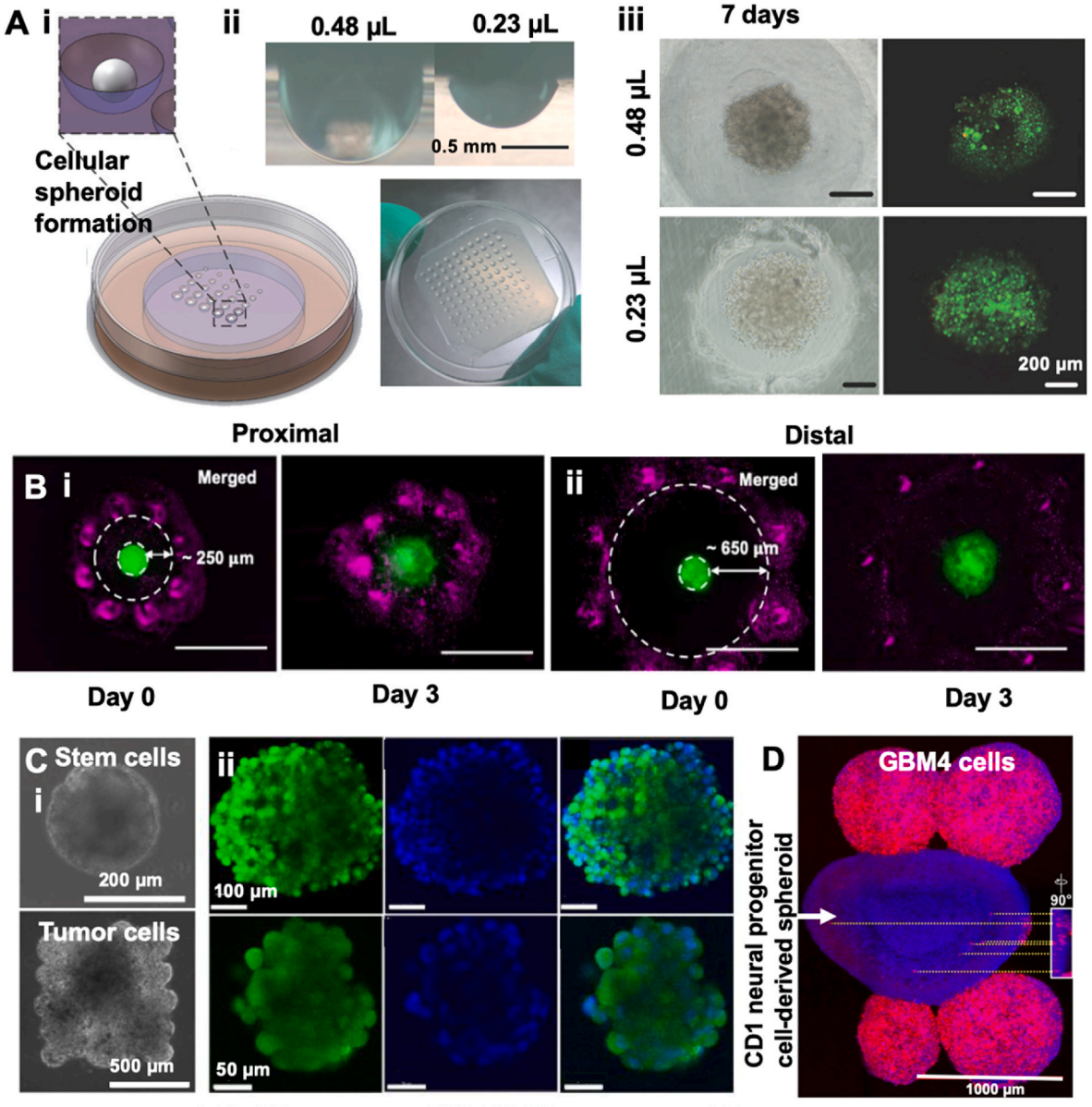

Fig. 10. Bioprinting of tumor models. (A) The bioprinting system used was a custom built, pressure-assisted value-based. (i) A schematic showing spheroid formation in concave wens, (ii) a view of printed gelatin arrays of different sizes on a PTFE-covered Petri dish, and (iii) phase-contrast images of spheroid development and Calcein and ethidium bromide staining of cells after 7 days of culture in wells made of 0.48 μL and 0.23 μL gelatin droplets. Scale bars: 200 μm. Adapted and reproduced from Ref. [126]. (B) A 3D bioprinted immune-cancer model. T cells were labeled with cell tracker violet and bioprinted in a circular pattern into a collagen bath. MDA-MB-231/HDF tumor spheroids were then bioprinted using aspiration-assisted bioprinting at the center of the circle. The distance of T cells from the periphery of the tumor spheroid was maintained at ~250 μm (proximal) or ~650 μm (distal). Fluorescent images of the (i) proximally and (ii) distally bioprinted tumor models right after bioprinting (Day 0), and post T cell treatment (Day 3). Adapted and reproduced with permission from Ref. [203]. (C) (i) Microcapsules created by laser-based bioprinting. Images of various print configurations of microbeads (5 × 5 array and rectangular mat) at Day 14. Both stem cells and tumor cells formed single aggregates. (ii) Confocal images of representative MDA-MB-231 3D aggregates within large (top row) and small (bottom row) microcapsules at Day 14. Aggregates were GFP-transfected and nuclear stained with DAPI (blue). Adapted and reproduced with permission from Ref. [204]. (D) A 3D bioprinter (Regenova; Cyfuse Biomedical K·K., Tokyo, Japan) was used to assemble spheroids. GBM4 cells invading into a CD1 neural progenitor spheroid. Maximum projection of the spheroid. CD1 cells were stained for blue and GBM4 cells were stained for red and blue. The invasion of GBM4 cells into the CD1 spheroid is evident. Scale bar: 1000 μm. Inset: 3D reconstruction of the image stack used to generate b, rotated 90°. The relative locations of six selected cells are indicated with a yellow dashed line. Adapted and reproduced with permission from Ref. [132]. (For interpretation of the references to color in this figure legend, the reader is referred to the Web version of this article.)

living biobanks serve as an oasis for understanding rare cancer and their gradual progression. Even then, 3D cultures of organoids and spheroids fail to recapitulate the entire complex tumor microenvironment (comprising tumor epithelium, stem cells, fibroblasts, and tumor-infiltrating immune cells, along with tumor angiogenesis and relevant cytokines, chemokines, and growth factors). Non-perfused static models, on the other hand, also lack intra- and inter-cellular crosstalk. In such regard, microfluidic devices have the potential to address these concerns and include physiological dosing of therapeutics for drug screening and modeling. Efficient and robust generation of tumor organoids for the generation of clinically-relevant in-vitro platforms [200,201] hold the key for translation of such models from bench to bedside. Duarte Campos et al. employed bioprinting to engineer an on-chip vascular-like conduit for in-vitro modeling using human pre-malignant breast epithelial cell (MCF10AT) spheroids as well as neural progenitor cells. They employed an elastin-like protein with tripeptide Arg-Gly-Asp (RGD) as the hydrogel component. Encouraging viability of MCF10AT spheroids was seen after seven days of culture, whereas their proliferation continued at a rate comparable to the Matrigel control group till 14 days of culture [115]. Using Monte Carlo computational studies, Robu et al. have shown that bioprinting of 3D perfusable constructs using multicellular spheroids as sacrificial bioink can give rise to conduits with more homogenous cell distributions [119]. A custom-made bioprinting system was used to build a concave hydrogel microarray coupled with in-situ seeding of breast cancer cells with high-throughput capacity and high controllability resulting in spheroid formation (Fig. 10(A)) [126,202]. The conclusions drawn from this study reinforce the use of 3D spheroid bioprinting in developing cancer tissue models for long-term study. In a recent work [203], a tumor spheroid was bioprinted at the center of T cells bioprinted in a circular pattern at different proximity to the tumor spheroid in order to develop a mechanistic understanding of immune-cancer interactions, important for cell-based cancer immunotherapies (Fig. 10(B)). Kingsley et al. have shown the application of laser-direct write methodology to fabricate spatially patterned tumor spheroids as well as embryonic bodies (Fig. 10 (C)) [204]. The investigators studied the effect of tumor dimensions for targeted therapy, and found significant spatial variations (increase in Transferrin uptake) indicating the dependence of biological responses on the geometry of spheroids. In another study, Hakobyan et al. developed a bioprinted miniaturized spheroid-based array model and demonstrated that these bioprinted spheroids, composed of both acinar and ductal cells, can imitate the initial stages of pancreatic ductal adenocarcinoma (PDAC) development indicating their potential use in future therapies [196]. In another study, Van Pel et al. attempted to examine the native microenvironment to model glioma cell invasion into neural tissue spheroids using bioprinting (Fig. 10(D)) [132]. The approach allowed for the adequate tracking of tumor invasion enabling understanding of somatic genetic differences of patients and taking a step towards personalized cancer treatments.

Advanced tissue engineering approaches have revolutionized cancer treatment worldwide. Still, further understanding of cancer-immune cell interactions is needed for an appropriate drug modeling and understanding of targeted therapeutics in a dynamic tumor model. Bioprinting of spheroids is still in a nascent stage to fabricate 3D models with adequately positioned cancer cells with stromal cells and ECs and enable a better understanding of the underlying mechanisms controlling immune evasion and reduced anti-tumor response post immunotherapy. We believe further studies improving the resolution of bioprinting with heterotypic spheroids and incorporation of vascularization, and angiogenesis holds the key to advancing in-vitro tumor models for cancer treatment in a dynamic microenvironment with cancer-immune cell interactions.

7.4. Neural tissue

Neuro-pharmaceuticals often exhibit very high attrition rates during drug developments and thus necessitates microphysiological systems for in-vitro screening of leads [205]. For neural systems, considering the complexity and hierarchy of the neural tissue, both spheroid-based biological and conventional microfluidic-based engineering models have limited capacity to recapitulate tissue functions. Human neural stem or neural progenitor cells (NS/PCs) are considered ideal candidates for repairing impaired neural function [206]; however, owing to a gradual reduction in numbers of NS/PCs by age, it is challenging to bioprint neural tissue constructs at the physiologically-relevant cell densities. A potential alternative is enabling self-assembly of cells of neural and endothelial lineage to form cell aggregates and achieve adequate cell density (Fig. 11(A)) [207]. An approach with the combination of fabricating spheroids and bioprinting them precisely to help induce fusion and formation of neural and vascular networks may hold the key to engineering a mimetic-neurophysiological system. Abelseth et al. demonstrated bioprinting of iPSC-derived neural aggregates in a fibrin-based bioink to improve throughputness of traditional neural tissue engineering techniques, especially for drug screening purposes. The authors demonstrated ~94% cell viability 10 days after bioprinting with expression of neuronal markers (neuron specific Class III beta-tubulin (TUJ1)) with neurite extension. Similar conclusion has been demonstrated in a study by Bowser and Moore, who exploited magnetic nanoparticle-based bioprinting with spinal cord spheroids, demonstrating both localized cell-cell cross-talks as well as long-distance neuronal projections. Bioprinted constructs showed consistency and reproducibility proving their potential to provide standardized results (Fig. 11(B)) [167]. Thus, the spheroid bioprinting approach can also be extended to develop a mini-brain model if neuronal- and vascular-associated cells are formed into spheroids and interconnections between them are allowed to grow. The establishment of such neuronal connections can also be helpful for accelerated regeneration [208].

7.5. Thyroid glands

The thyroid gland is an endocrine organ, which is responsible for the secretion of essential hormones for growth, neurological development, and hemostasis. Hypo-functionality of the thyroid gland or even its removal due to cancer or other issues would have a great effect on the body's physiology. In these cases, lifetime hormone therapy is the current method of treatment [209]. One potential avenue of future treatment is autologous tissue replacement, which would eliminate the need for lifetime hormone therapy. In this regard, Bulanova et al. isolated thyroid explants and allantoic tissue from mouse embryos (Fig. 12(A-E)) [44]. These explants were cultured overnight in hanging drops to obtain spheroids for bioprinting. Allantoic spheroids were used to incorporate vascularization by generating a blood vessel capillary network around the thyroid tissue construct. An extrusion-based bioprinting approach with a turnstile functionality and temperature-controlled mechanism was used to bioprint the spheroid-laden collagen gel on a polytetrafluoroethyle membrane. The functionality of the fused tissue was determined by restoration of thyroid homeostasis after implantation in a hypothyroid mouse model. This study, although performed in a mouse model, paved the path for the success of clinical transplantation of a bioprinted vascularized thyroid gland.

Despite the development of a bioprinted thyroid gland, its clinical translation is challenging. For clinical applications, therapeutic-grade thyroid epithelial cells are needed, but receiving such a large number of autologous cells via biopsy is challenging [44]. Even collection of viable thyroid follicles from the human thyroid gland is hardly feasible. In this regard, differentiation of human stem cells into thyroid epithelium is considered a promising technique since it can significantly increase the viability of thyroid follicles [210,211]; however, they demonstrate immature phenotypes. Meanwhile, efforts towards the fabrication of a physiologically-relevant thyroid model from bioprinting of spheroids are still underway for achieving hormonal functionalities.

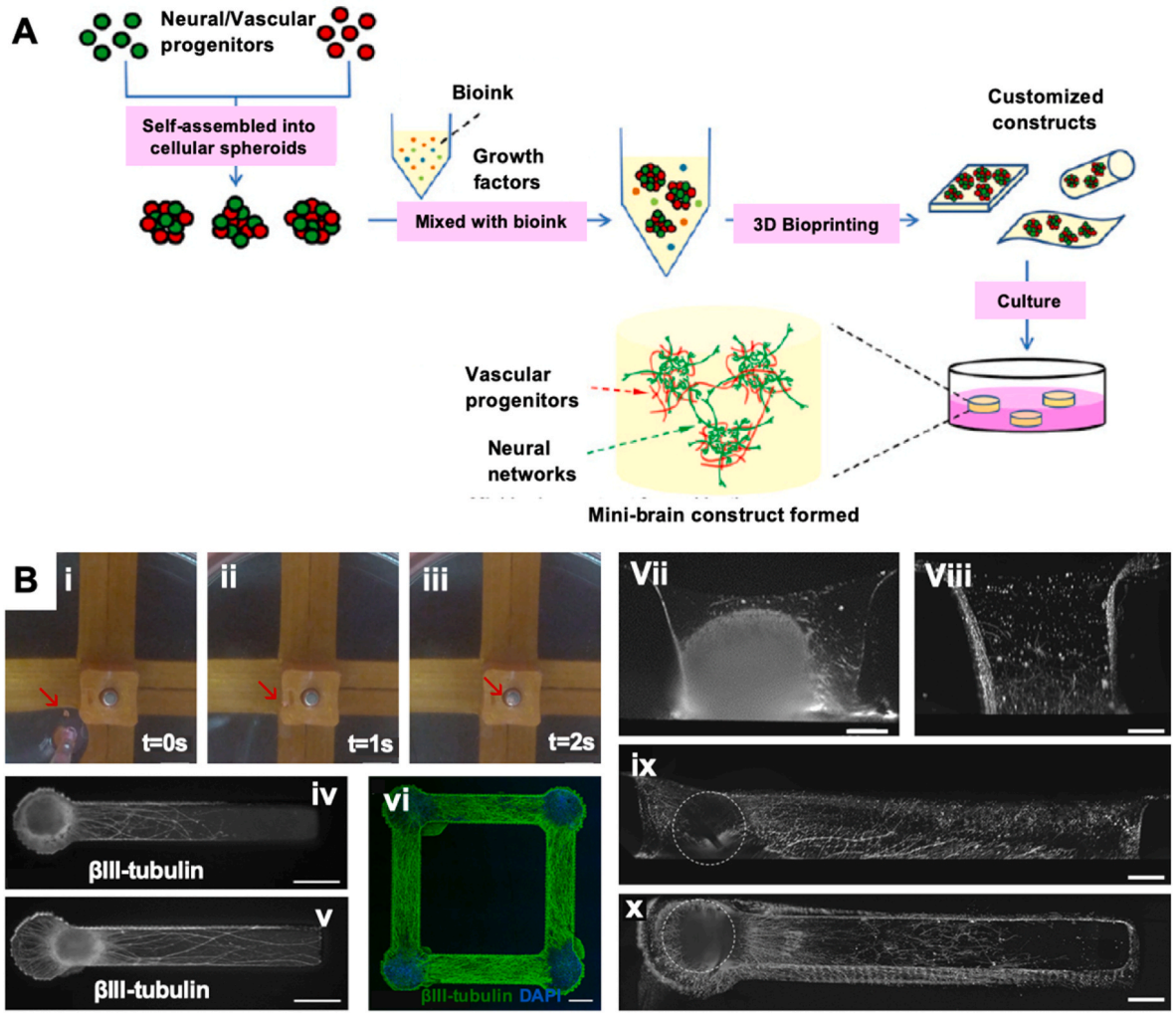

Fig. 11. Bioprinting of neural tissues. (A) A potential strategy to generate mini-brain by extrusion-based bioprinting of spheroids. Adapted and reproduced from Ref. [207]. (B) Using magnetic properties of spheroids for seeding and magnetic bioprinting. (i-iii) The properties of magnetic spheroids enable their translocation. Scale bar: 2 mm. Phase images of neural constructs (βIII-tubulin, white) indicate that the positioning of spheroids in constructs is more accurate (iv) with magnetic bioprinting than (v) manual placement with a pipette alone. Scale bar: 500 μm. (vi) Single plane confocal imaging showing localized cell bodies (DAPI, blue) and extending neurites (βIII-tubulin, green). Scale bar: 200 μm. Dual-view inverted selective plane illumination microscopy (diSPIM) images of hydrogel constructs stained with βIII-tubulin to visualize neurite outgrowth. (vii) An XZ slice through the spinal cord spheroid. (viii) An XZ maximum intensity projection of the neurite growth within the channel, excluding the spheroid. Scale bar: 100 μm. (ix) An YZ maximum intensity projection of the neurite outgrowth through the depth of the hydrogel. (x) An XY maximum intensity projection of the neurite growth occurring within the boundaries of the poly-ethylene glycol (PEG) mold. Scale bar: 200 μm. Adapted and reproduced with permission from Ref. [167]. (For interpretation of the references to color in this figure legend, the reader is referred to the Web version of this article.)

7.6. Bone and cartilage tissue

Musculoskeletal surgeries and orthopedics were the very first fields to incorporate 3D bioprinting technology. Scaffold-based approaches have been more extensively researched for use in bone and cartilage tissue engineering focusing on the use of 3D printed biomaterials [212, 213] owing to the required high mechanical properties for orthopedic and dental applications [214]. Especially, spheroid-based systems prove to be significant for in-vitro cartilage models because the hypoxia gradient evident in spheroids enables mimicking the cartilage micro-environment favoring the differentiation of MSCs into a chondrogenic lineage [215]. However, the long-term stability of 3D bioprinted constructs along with a dearth of in-vivo data on bone regeneration calls into question further use of these constructs in clinical studies [216].

The next major milestone for the successful adoption of orthopedic tissue bioprinting is the ability to bioprint vascularized bone [217]. Microvascular endothelium forms an integral part of the bone tissue, hence the incorporation of ECs in osteogenic spheroids helps mimic the native tissue more closely, and reduced tissue necrosis in the core of spheroids. This can be achieved with bioprinting of human MSCs along with ECs in a complex structure [218]. Recently, Ayan et al. have demonstrated osteochondral tissues using prefabricated spheroids as building blocks (Fig. 13(A)) [65]. In another study, Heo et al. used human MSC and ECs to fabricate heterogeneous spheroids, which were subjected to bioprinting to develop constructs of complex shapes, with demonstration of osteogenic properties [17]. Recently, Celik et al. created a 3D heterotypic pre-vascularized bone tissue model using osteogenic and endotheliogenic progenitor spheroids produced by miR-148 b and miR-210 mimic transfection, respectively. miRNA-transfected spheroids were bioprinted into hollow structures to imitate the Haversian canal as a proof of concept (Fig. 13(B)) [219]. They used the same bioprinting approach to create the osteochondral interfaces with miR-148 b transfected spheroids for the osteogenic zone and miR-140 and -21 transfected spheroids for the chondrogenic zone [220]. Freeform positioning of spheroids with complete 3D bioprinting freedom in Z-axis forms yet another challenge regarding the spheroid

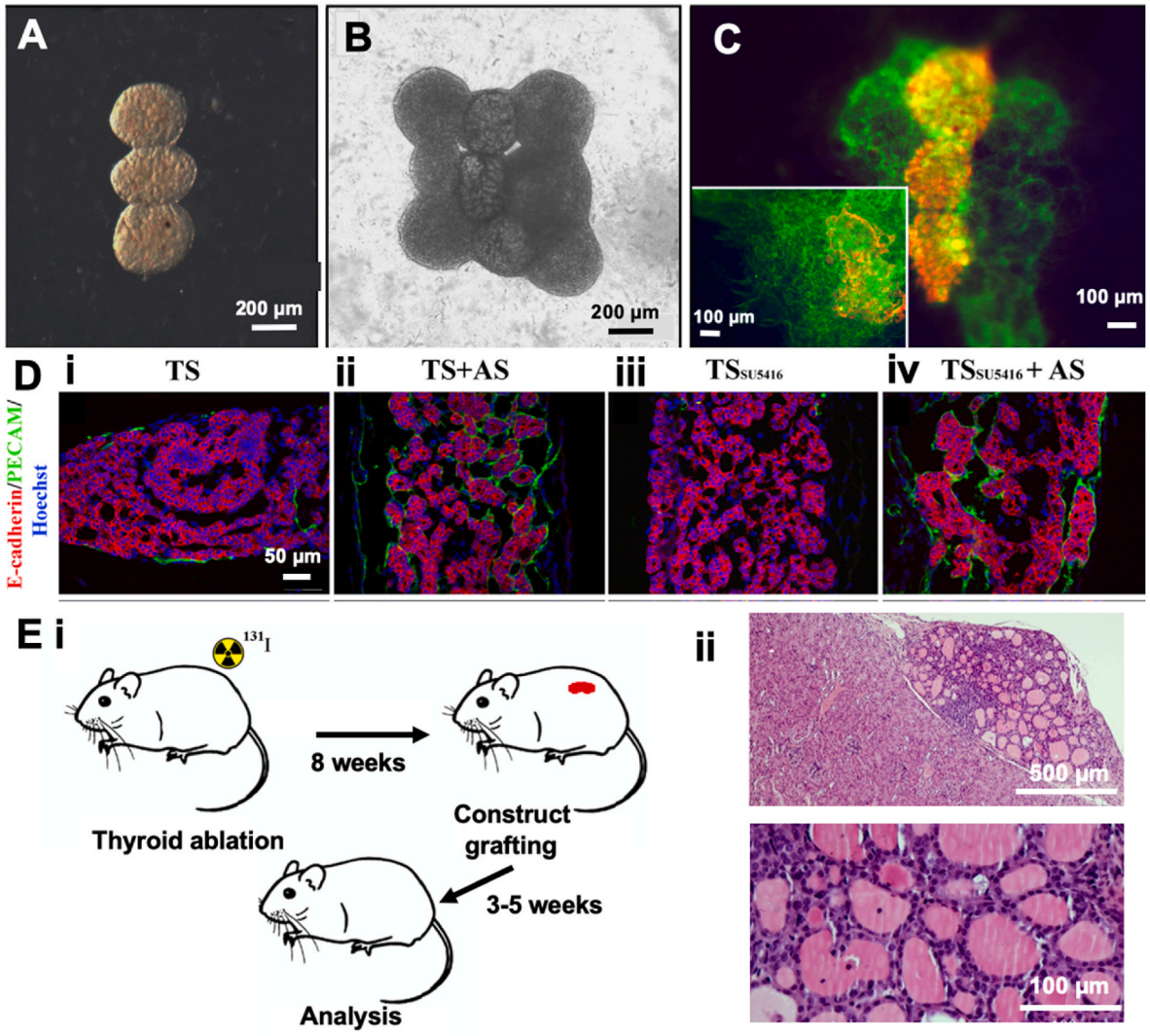

Fig. 12. Bioprinted thyroid glands using the Fabion 3D bioprinter (extrusion-based developed by 3D Bioprinting Solutions. (A) Bioprinted mouse thyroid gland constructs composed of three spheroids from embryonic thyroid explants (3 TS) or (B) composed of three spheroids from embryonic thyroid explants in between six allantoides spheroids (3 TS + 6AS) after a day in culture. (C) Constructs labeled, after a day in culture, with antibodies against platelet and endothelial cell adhesion molecule (PECAM; green) and E-cadherin (red) to visualize endothelial and epithelial cells, respectively. (D) Vascularization of bioprinted mouse thyroid constructs. (i) Bioprinted thyroid spheroids (TS) display only at the periphery of the tissue. (ii) TS bioprinted together with allantoic spheroids (AS) reveal intense PECAM labeling around and inside TS. (iii) TS pretreated with SU5416 (TSSU5416) during hanging drop culture did not show endothelial-specific labeling. (iv) In the presence of AS, TS depleted of EC (TSSU5416) were invaded by EC from AS. (E) Functional rescue of in-vivo thyroid function using bioprinted mouse thyroid constructs. (i) Schematic representation and timeline of mouse 131I-induced thyroid ablation and construct grafting. (ii) Histological analysis of kidneys section. H&E staining on a grafted kidney after five weeks showed follicular organization in grafted tissue and colloid accumulation. Adapted and reproduced with permission from Ref. [44]. (For interpretation of the references to color in this figure legend, the reader is referred to the Web version of this article.)

bioprinting. A very recent effort aimed at the bioprinting of freeform functional cartilage and osteogenic tissues (circular and triangular configurations, respectively) using prefabricated spheroids in yield-stress gels (Fig. 13(C)) [155]. This cost-effective and reproducible methodology offers a viable technology for the fabrication of diverse tissue constructs, which demand precise placement and assembly of spheroids in 3D. Burdis et al. fabricated anatomically accurate stratified articular cartilage using inkjet bioprinting on a microchamber system. Human MSCs and chondrocytes were deposited into these chambers creating organized spheroids to be used. The microchamber strategy enhances the versatility and scalability of spheroid bioprinting allowing for a high level of organization using these cell aggregates [221].

For appropriate bone tissue regeneration, a combination of (1) the natural bone ECM niche, (2) osteogenic and osteoclastogenic cells, (3) topographical cues guiding the cells to the desired type, and (4) vascularization are needed in tandem [222]. The integration of different bioprinting methods and an understanding of an interdisciplinary study regime ranging from tissue engineering, bone biology and mechanical engineering might offer a solution to the fabrication of bone tissue. Cartilage reconstruction is equally challenging owing to its intricate anatomical structure and specific zonal biomechanical properties. In this regard, spatiotemporal cues, formation of hyaline cartilage, zone-specific mechanical and biological properties, and bone-cartilage integration are the unmet requirements for cartilage and osteochondral tissue reconstruction [223–226].

7.7. Liver tissue

The hepatic parenchymal cells in the liver play a critical role in metabolism within the body. Because of this, a large amount of the pharmaceutical industry investment goes towards the development of drugs for treating liver disease, most of which fail in clinical studies.

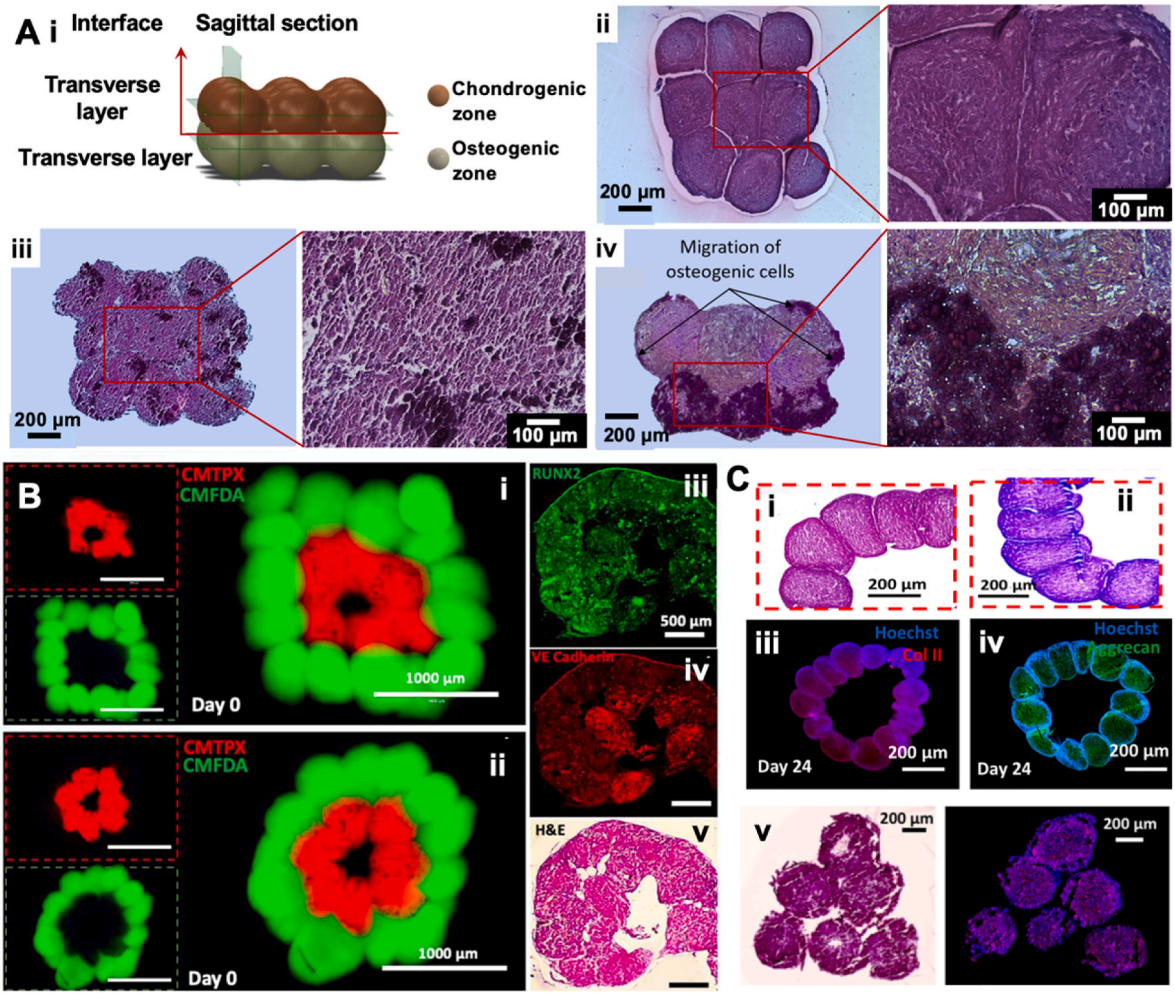

Fig. 13. Bioprinting of bone and cartilage tissues. (A) Aspiration-assisted bioprinting of the osteochondral interface. (i) A schematic diagram showing positions of histological sectioning in the bioprinted interface. (ii-iv) H&E staining of the chondrogenic and osteogenic zones, and the interface. Adapted and reproduced from Ref. [65]. (B) Representation and characterization of the Haversian canal model fabricated using the aspiration-assisted bioprinting technique. (i-ii) Bioprinted structures consisted of adipose-derived stem cell (ADSC) spheroids labeled with CellTracker™ green CMFDA dye and CellTracker™ Red CMTPX dye post bioprinting. Immunoimages, showing (iii) RUNX2 and (iv) VE-cadherin, and (v) a H&E image of a bioprinted structure at Day 14 post bioprinting. Adapted and reproduced with permission from Ref. [219]. (C) Aspiration-assisted freeform bioprinting of cartilage and bone tissues. Histological and immunostaining images of circular cartilage tissues at Day 24 including (i) H&E, (ii) toluidine blue, (iii) Col-II, and (iv) Aggrecan. (v) Bioprinting of triangular-shaped osteogenic tissues in a yield-stress gel. Immunostaining (Hoechst in blue and OSTERIX in red) and H&E staining for bioprinted bone tissue. Adapted and reproduced from Ref. [155]. (For interpretation of the references to color in this figure legend, the reader is referred to the Web version of this article.)

Inadequate preclinical screening is one of the major reasons for such failures and can be addressed by 3D in-vitro tissue models [227,228]. These models are fabricated to recapitulate the in-vivo structure, biology, function and metabolism more realistically in comparison to 2D models. To advance this area of clinical research, Bell et al. aimed to mimic the liver functionalities using spheroids formed from primary human hepatocytes. The spheroids were observed to retain their functionality and morphology *in vitro* for about five weeks of culture with enhanced clinically relevant-sensitivity under chronic exposures of liver pathologies, such as cholestasis, the toxicity of fialuridine, and viral hepatitis [229]. In another study, cryopreserved hepatocytes and mouse fibroblasts were co-cultured to form spheroids in a cell repellent microplate and were used for bioprinting of liver tissue. The Regenova bioprinter was utilized to construct the liver tissue with nine spheroids in each microplate, which was then placed on a needle array, and cultured for four days to allow fusion [141]. The bioprinted tissue demonstrated functional metabolism of lipids, synthesis of bile acid and glucose production for three weeks, showing its potential to be used preclinically for in-vitro hepatotoxicity predictions. Yet another study explored the bioprinting of liver tissue using a spheroid-laden hydrogel. Multicellular spheroids were fabricated using hepatocytes, stellate cells and Kupffer cells (8:1:1), and maintained for three days before bioprinting. The spheroids were then laden in a liver ECM containing hydrogel-based bioink and extruded to fabricate liver constructs (Fig. 14 (A)) [230]. Bhise et al. developed hepatic spheroid-laden GelMA and used liquid droplets to bioprint a 7 × 7 array within a microfluidic bioreactor (Fig. 14(B)) [231]. This liver model was then assembled to form a liver tissue, which was assessed for functionality for 30 days. The microfluidic device was a step forward from the conventional bioreactor organ-on-a-chip devices because it allowed direct access to spheroids throughout experiments and could be used for high-throughput drug-induced liver toxicity studies *in vitro*. Another notable work towards 3D bioprinting of liver spheroids was reported by Goulart et al. by bioprinting of iPSC-derived liver parenchymal cells formed into spheroids in an alginate/Pluronic hydrogel-based bioink using extrusion-based bioprinting (Fig. 14(C)) [232]. The bioprinted constructs demonstrated improved hepatic and metabolic functions for a prolonged culture time, providing insights into the future development of liver tissue using iPSCs.

As many studies have demonstrated, 3D models resembling the

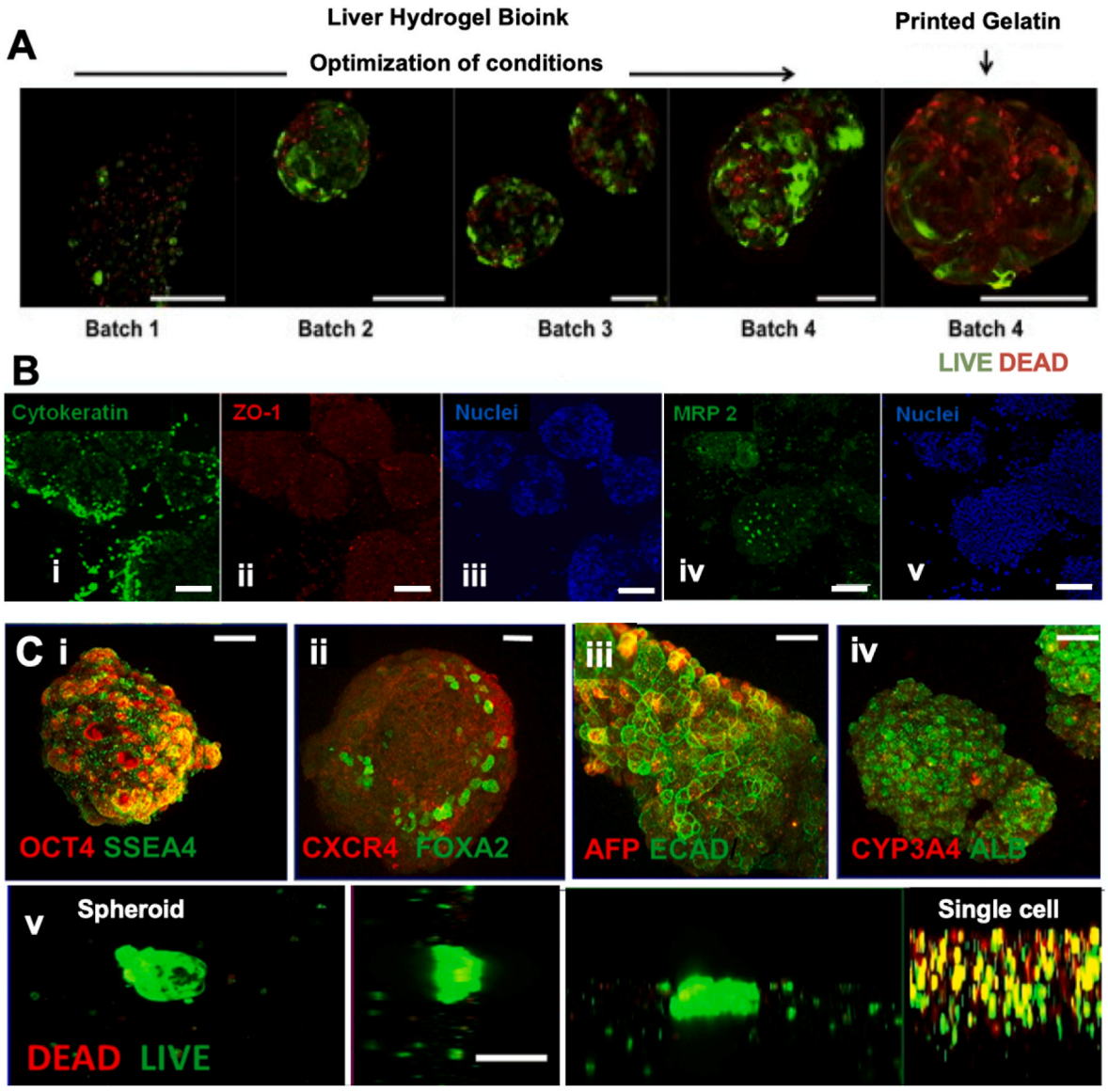

Fig. 14. Extrusion-based bioprinting of liver tissues. (A) Demonstration of parameter optimization of bioprinting and associated viability of liver spheroids bioprinted in a liver-specific bioink. Conditions were optimized over biofabrication batches, resulting in liver constructs with increased viability. Scale bars: 200 μm. Adapted and reproduced with permission from Ref. [230]. (B) Functionality of hepatic spheroids fabricated using direct-write bioprinting and cultured in a bioreactor: confocal microscopy images of cytokeratin 18 (green), ZO-1 tight junction binding protein (red), MRP-2 biliary canalicular transporter (green) and DAPI (blue) immunostained spheroids cultured for 30 days. Scale bar: 100 μm. Adapted and reproduced with permission from Ref. [231]. (C) Hepatic spheroid bioprinting using extrusion-based bioprinting displayed prolonged hepatic and metabolic function. 3D Hepatic differentiation of iPSCs: immunofluorescence staining for (i) OCT4 and SSEA4 at Day 0, (ii) CXCR4 and FOXA2 at Day 3, (iii) ECAD and AFP at Day 9, and (iv) ALB and CYP3A4 at Day 18 (scale bar: 50 μm), (v) Representative image of confocal Microscopy of LIVE/DEAD assay at Day 18 (scale bar: 20 μm). Adapted and reproduced with permission from Ref. [232]. (For interpretation of the references to color in this figure legend, the reader is referred to the Web version of this article.)

complex 3D native microenvironment are essential for liver tissue regeneration [233–235]. Hence, heterotypic liver spheroids have drawn considerable attention to recapitulate the in-vivo tissue architecture and cell-ECM and cell-cell interactions. Yet, the usage of such tissue remains limited owing to low throughput and reproducibility and limited long-term culture (due to rapid loss of functionality within a couple of days) [236]. Besides their limited lifespan, obtaining primary hepatocytes from healthy donors is another challenge [231]. Although reliable commercial cell lines are available as a viable alternative, they do not express necessary metabolic enzymes corresponding to those of native tissues, reflecting the genetic variability of patients [237].

7.8. Vascular tissue

One of the most notable challenges for successful fabrication of scalable tissues and organs is the integration of vascular networks. To obtain clinically-relevant volumes of tissues, vascularization is an integral consideration needed for the transport of nutrients and oxygen to cellular components. To address this issue of complexity, spheroid bioprinting techniques have been utilized to enable the creation of vascular tissues with the necessary structural stability. In an attempt to develop heterocellular vascularized tissues, many researchers have co-cultured spheroids with the addition of ECs to induce vascularization [238]. Norotte et al. bioprinted multicellular vascular spheroids (made from smooth muscle cells, fibroblasts, and Cho hamster ovary cells) concomitantly with agarose rods, to generate a scaffold-free

small-diameter vascular tube (ranging from 0.9 to 2.5 mm) (Fig. 15(A)) [43]. De Moor et al. used a co-culture system, where ECs and hDFs were used for spheroid fabrication and found that the ECs within bioprinted spheroids spontaneously formed capillary-like networks and lumina [239]. This effect was further enhanced with the addition of adipose-derived stem cells (ADSCs) in spheroids, leading to a higher rate of vascularization and fusion of spheroids. These results along with the bioprinted nature of these macro-tissues instill great promise in the scalability of vascularized tissues. Ayan et al. utilized aspiration-assisted bioprinting in a scaffold-based configuration and showed angiogenic sprouting of HUVEC spheroids (Fig. 15(B)). In another study, Tan et al. used 3D bioprinting to robotically place co-cultured spheroids (containing a 1:1 ratio of ECs and smooth muscle cells) into alginate molds to assess tissue proliferation (Fig. 15(C)) [240]. The authors reported that

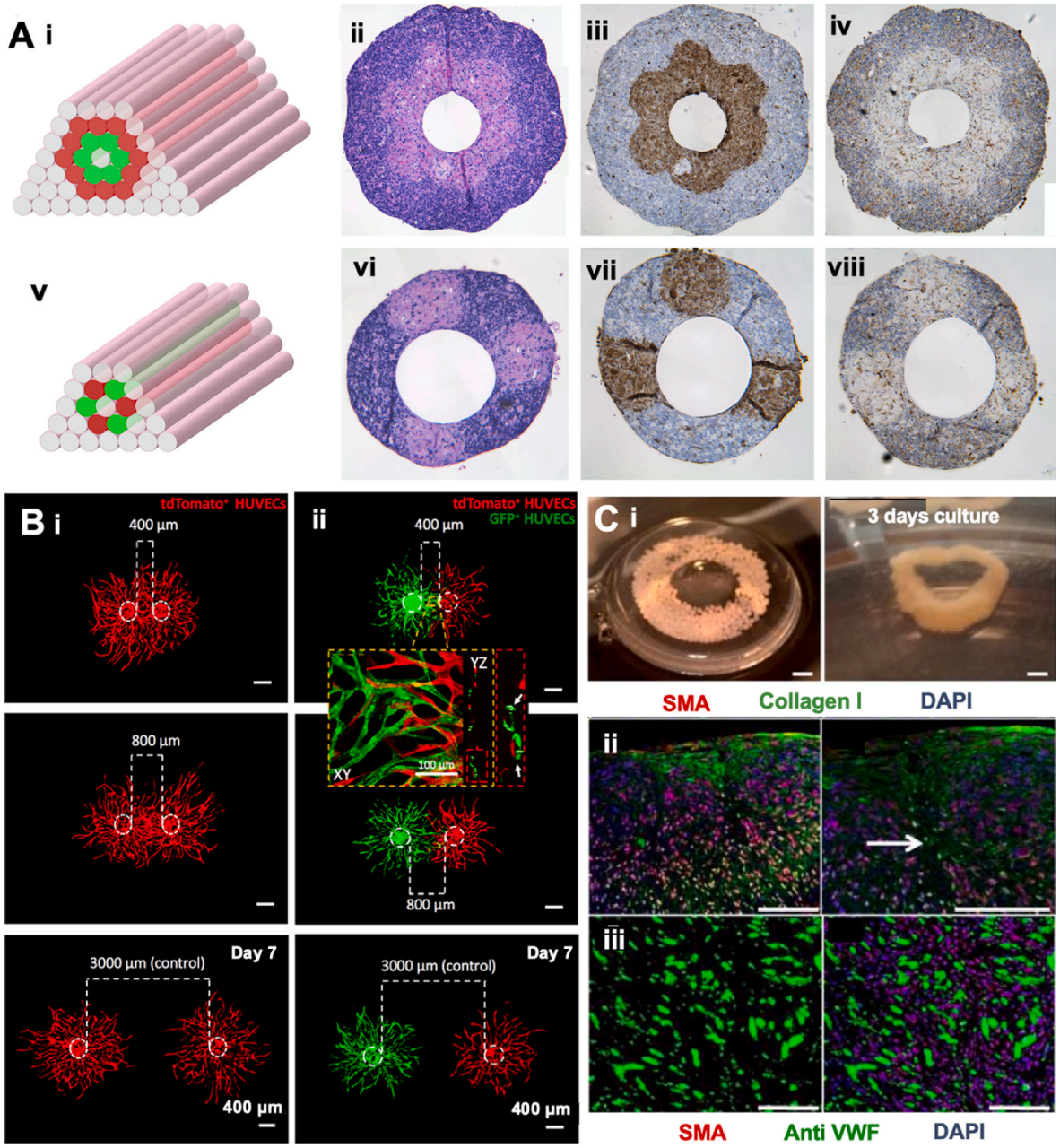

Fig. 15. Bioprinting vascular tissues using specialized extrusion-based bioprinter. (A) Building a double-layered vascular wall. (i, v) Human umbilical vein smooth muscle cells (HUVSMCs) and human skin fibroblast (HSF) multicellular cylinders were assembled according to specific patterns (HUVSMC: green; HSF: red). Panels (ii-iv) and (vi-viii) show the results of histological examination of the respective structures after three days of fusion: H&E (ii, vi), smooth muscle α-actin (brown; iii, vii) and Caspase-3 (brown; iv, viii) stainings are shown. Adapted and reproduced with permission from Ref. [43]. (B) Aspiration-assisted bioprinting of physiologically-relevant culture environments to study the angiogenic sprouting behavior of HUVEC spheroids. (i) Epifluorescent images of bioprinted tdTomato^{+} HUVEC spheroids with varying distances (400–3000 μm) apart on Day 7. (ii) Epifluorescent images of bioprinted GFP^{+} and tdTomato^{+} HUVEC spheroids with varying distances (400–3000 μm) apart on Day 7 along with higher-magnification confocal images of the interface region in XY and YZ planes showing capillaries formed by both GFP^{+} and tdTomato^{+} HUVECs (indicated by white arrows). Adapted and reproduced with permission from Ref. [152]. (C) A droplet-based bioprinted (Palmetto 3D Printer) was used for bioprinting. (i) 3D Alginate molds for seeding vascular spheroids (i.e., made of smooth muscle cells and endothelial cells). Scale bar: 1 mm. Immunofluorescence analysis of tissue units cultured for 16 days at 40X and 63X magnification for (ii) smooth muscle actin (SMA), and collagen I; (iii) anti VWF and merge picture. Scale bar: 100 μm. Adapted and reproduced with permission from Ref. [240]. (For interpretation of the references to color in this figure legend, the reader is referred to the Web version of this article.)

spheroids were able to fuse into a toroid shape provided by the mold and secreted collagen type 1, indicating proper cell-cell adhesion and maturation [17]. These studies, among others, represent a major milestone in the advancement of spheroid bioprinting technologies towards the successful fabrication of vascularized tissues.

As vascular networks, from arteries (~500 μm diameter) down to capillaries (~10 μm diameter), are necessary for the reconstruction of scalable tissues, improvement of bioprinting resolution using spheroids is a major roadblock [239]. Also, further advancement is required for fabrication of smaller spheroids, necessary for the fabrication of such smaller blood vessels. Furthermore, vascularized spheroids often are heterotypic and cocultured with a variety of other cell types, such as cardiac muscle, liver, bone, and others, as appropriate for the required tissue fabrication purposes. For each specific cell type, an extensive

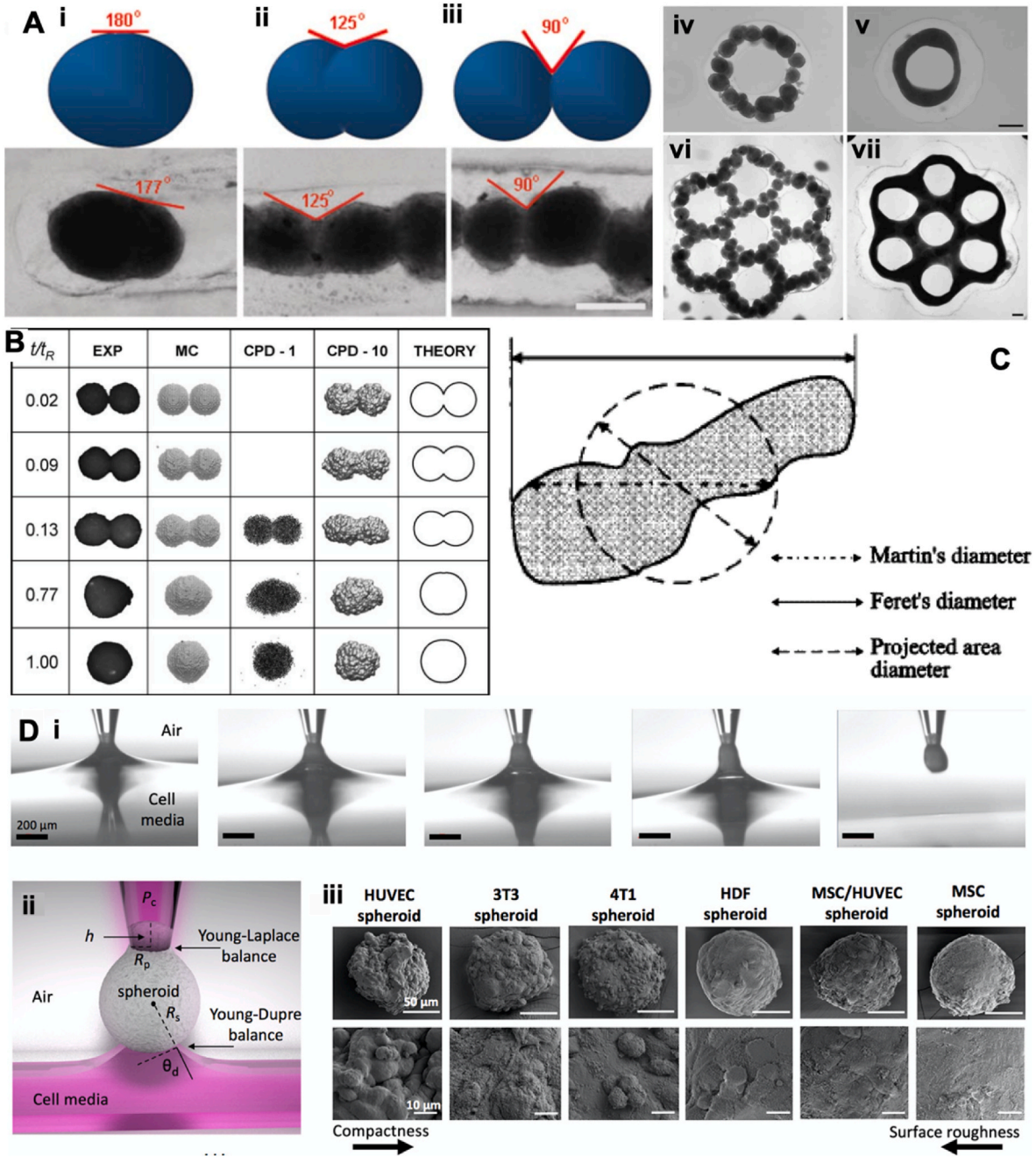

Fig. 16. (A) The extent of microtissue fusion is less complete with increasing pre-culture time. The average angle between fused spheroids within rod microtissues was measured as shown (i-iii), with a 180° angle indicating a microtissue with no obvious fusion point. Complex shapes can be assembled using spheroids as building units. Human fibroblast spheroids, approximately 300 μm in diameter, were generated and cultured for a day, then harvested and seeded into molds with toroid (iv and v) and honeycomb (vi and vii) features. Representative images of fusion are shown at the initial time point (iv and vi) and at a steady-state time point 24 h after assembly (v and vii). Scale bar: 200 μm. Adapted and reproduced with permission from Ref. [243]. (B) Snapshots of the fusion of spheroids obtained from experiments, Monte Carlo simulations, and Cellular Particle Dynamics model simulations (CPD-1 and CPD-10), and from theoretical modeling. Adapted and reproduced with permission from Ref. [247]. (C) Schematic illustration of different particle diameters (Martin's diameter, Feret's diameter, and projected area diameter) based on projected images. Adapted and reproduced with permission from Ref. [258]. (D) Picking and lifting spheroids. (i) Time-lapse images during the spheroid lifting process at the interface of cell media and air. (ii) A schematic showing physical parameters involved in the lifting of a spheroid from the cell media. (iii) SEM images of HUVEC, 3T3, 4T1, HDF, MSC/HUVEC, and MSC spheroids (compared to HUVEC spheroids) at Day 2. Adapted and reproduced with permission from Ref. [152].

effort is also required to optimize cell-cell ratio, viability, EC migration, and capillary tube formation making a time-consuming and laborious procedure [241,242].

8. Tissue properties influenced by spheroid bioprinting

8.1. Shape fidelity

For optimal bioprinting and biological outcomes, often soft and printable bioinks are the choice for bioprinting, despite the fact they undergo significant deformation during and post bioprinting, impairing shape fidelity. Although printability is only a qualitative measurement and may seem rather intuitive, shape fidelity measurements lack consensus in the scientific community and hugely depends on the utilized bioprinting technique. It is worthy to note that tremendous progress in the fabrication of spheroids is needed to improve size control and reproducibility of spheroids for their widespread use in bioprinting. The resolution offered by bioprinting techniques involving spheroids is directly influenced by the spheroid size and is rather important for many tissues' reconstruction purposes, especially vasculature. Alongside, one of the major challenges for the clinical application of spheroid bioprinting happens to be concerned regarding the shape fidelity of fabricated tissues. Using spheroids as building blocks, as discussed before, scientists showed tremendous progress for a variety of tissue engineering applications, yet the bioprinted final geometry and configuration of final tissue product is observed to undergo substantial changes in the days following bioprinting. With a gradual fusion of spheroids, bioprinted constructs experience shrinkage and compaction. This compaction leads to the most significant shape changes that bioprinted tissues undergo and has been a huge consideration of the design parameters before bioprinting. Indeed, many individual spheroid parameters, such as sphericity, inherent cellular properties, etc., contribute to the spheroid fusion process, influencing the overall assembly of tissue constructs.

8.2. Micro-tissue fusion

As discussed before, the fundamental aspect of using spheroids as tissue building blocks is their inherent fusion potency. Spheroids, when in direct contact, act like two viscous liquid drops and merge forming one single spheroid if no hindering obstruction, such as mold or substrate, is present. For example, Rago et al. used PDMS molds to fabricate spheroids of HDFs using micro-molded cell-repellent hydrogels, following which the fused spheroids were cultured and further cast into a secondary agarose gel-based micro-mold to generate trough shaped recesses (Fig. 16(A)) [243]. The authors demonstrated the role of pre-culture time of spheroids and their fusion rate on the fusion angle and steady-state length of the fused tissue constructs. Molded tissue usually assembles and eventually shrinks forming a variety of different shapes influenced by inter-or intra-cellular interactions, cell types, cellular fates, cellular positions, and the deposited ECM (such as elastin and collagen), whilst shrinkage can be controlled using molds. An important aspect worth mentioning in such a discussion is that the fusion of spheroids made of different cell types are usually not similar, becoming a crucial problem in cases of heterotypic microtissue fabrication. Shahin-Shamsabadi et al. showed that fusion of adipose and C2C12 mouse myoblasts occurs more in direct comparison to 3T3-L1 adipose-like tissue derived from mouse 3T3 fibroblasts [244,245]. In addition, when using collagen and Geltrex as substrates, spheroid formation and shrinkage showed different behavior, leading to a smaller diameter of the spheroid in a collagen substrate after 6 h of culture.

The fusion process of spheroids has been quantified using theoretical and computational models to understand the nature and type of involved parameters as described below. For a homocellular spheroid, the fusion occurs in almost a symmetrical manner, while for heterocellular spheroids, the spheroid with higher cohesiveness is enveloped by the lower cohesive one [58].

8.2.1. Theoretical models

In theory, the fusion of two cell aggregates, such as spheroids, is similar to the coalescence of two viscous liquid drops touching each other. The most important factors involved in the calculation of this phenomenon are surface tension and viscosity of spheroids. Theoretical calculation of this shape evolution, assuming that spheroids act the same as viscous liquid drops and other approximations, could be derived using hydrodynamic laws [246]. Flenner et al. on the other hand, established a more accurate calculation validated by computational simulation (Fig. 16(B)) [247]. Assuming these fusing drops as spherical caps, while the drops fuse, the diameter of the fused tissue increases, with their centers coming closer to each other. The process continues until a single spherical drop is formed with a larger diameter size than its smaller predecessors. The radius of the final spherical drop is approximately $2^{1/3}$ times the initial radius of the smaller creator drops, assuming the two forming drops are similar in size.

8.2.2. Computational models

Monte Carlo Method: Monte Carlo (MC) computational simulation is used for solving a variety of problems ranging from molecular dynamics to materials science and biology, especially in cases involving a huge degree of freedom [248]. The Potts model utilizes statistical physics describing the liquidity of tissue [249,250]. In this model, tissue is considered to be made of lattice structure and each cell of several lattice regions or sites is labeled with assigned identification numbers. The average number of sites per cell is kept approximately near a determined target value. Deviation from the target value is constrained by the elastic term in the overall energy. As the cells interact with each other, the evolution is described by the Metropolis algorithm and change in cell migration and morphology is calculated accordingly [249,250]. Flenner et al. uses a similar method, which is developed into a 3D lattice model for larger quantities of cellular interaction [247]. This enables the stimulation of the tissue liquidity for spheroids. ECM and cells are designed as particles on sites, gathered in a 3D manner in a cubic lattice structure. This model could be further improved to account for other parameters, such as cell differentiation and proliferation and even, ECM remodeling. Fleming et al. [251] studied the spheroid fusion using the same liquidity-based MC method. Three different sites - external medium/culture, smooth muscle cells, and ECs were identified, and the outer and inner layers of spheroid fusion were investigated using this method. After 5×10^4 MC steps, partial diffusion was observed, after 45×10^4 MC steps, the luminal fusion was observed, and after 2×10^6 MC steps, the minimal adhesive energy was reached when the spheroids were assumed combined.

Cellular Particle Dynamic Method: Flenner et al. considered cell aggregates as cellular particles to have a more realistic model for their assembly (Fig. 16(B)), and aimed to develop a correlation between tissue level properties and cellular/subcellular properties [247]. They used different molecular dynamics packages, such as Nanoscale Molecular Dynamics (NAMD) and Large-scale Atomic/Molecular Massively Parallel Simulator (LAMMPS), for molecular simulation of spheroids.

8.3. Co-culture

An approach that holds the key to the development of complex, heterocellular tissues, is the successful bioprinting of co-cultures containing multiple cell types. The use of co-culture systems has witnessed profound applications in modeling of cancerous tissues and in studies pertaining interactions of heterocellular tissues. This process, however, requires extremely high attention to detail as different cell types necessitate unique parameters for their growth. Cell viability, printability, structural stability, and interaction with the base hydrogel are key considerations for creation of co-cultured bioinks (Fig. 17(A)) [252]. Successful research into bioprinting of multicellular spheroids has

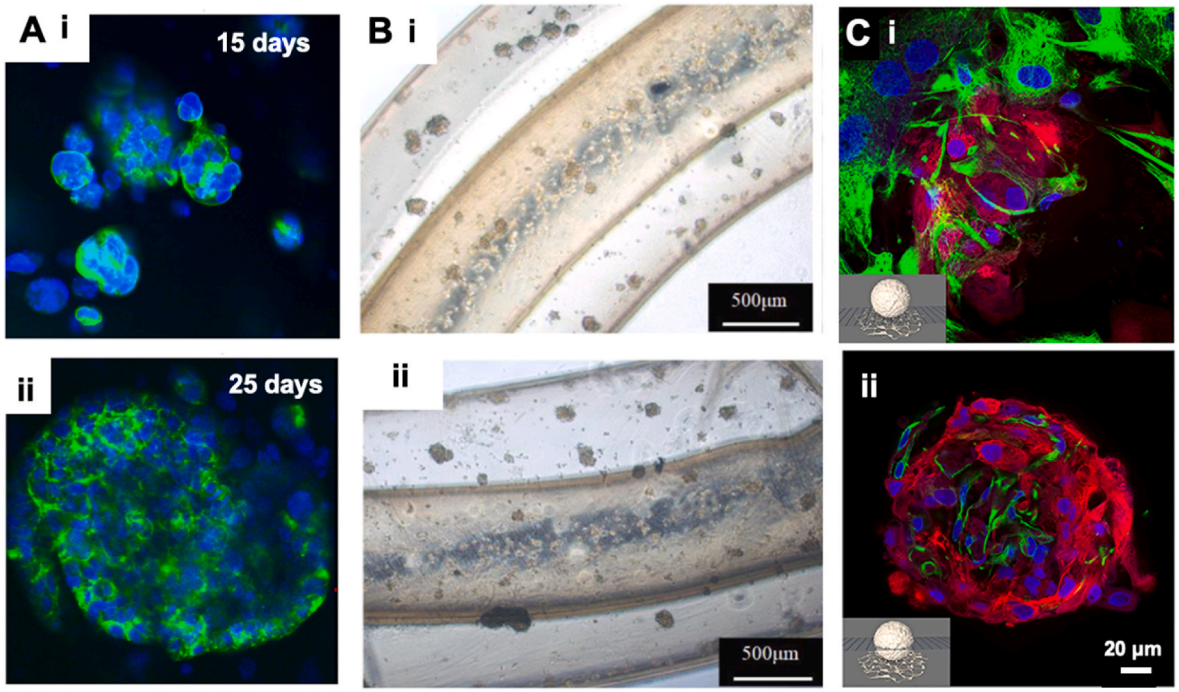

Fig. 17. (A) Patient-derived xenograft and cancer-associated fibroblast (PDX-CAF) spheroid formation. Cytoskeleton distribution of co-culture spheroids in bioprinted scaffolds after staining with actin (green) and nucleus (blue) on Days 15 and 25. An increase in spheroid size with time was observed. Adapted and reproduced with permission from Ref. [252]. (B) Coaxial bioprinting of multicellular structures. Images of morphological changes in multicellular structures for a (i) 5-day or (ii) 7-day cultures. Adapted and reproduced with permission from Ref. [253]. (C) Immunohistochemical characterization of co-cultured of iPSC-derived cardiomyocytes with cardiac fibroblasts. Nuclei are labeled with DAPI (blue). (i) Confocal optical section on the substrate level of a spheroid cultured for a month. Immunostaining for myosin heavy chain (red) and vimentin (green). (ii) Confocal optical section above the substrate level of the same spheroid as shown in (i). Adapted and reproduced with permission from Ref. [255]. (For interpretation of the references to color in this figure legend, the reader is referred to the Web version of this article.)

shown the ability to maintain high cell viability and proliferation (Fig. 17(B)) [253]. Co-culturing of different cell types also influences individual spheroid characteristics, such as shape and integrity. A study performed on the co-culture of human chondrocytes and MSCs showed how different ratios of cell types within the culture changed the shape and size of resulting spheroids [254]. Decreasing the amount of chondrocytes relative to MSCs in the matrix, from 50:50 to 25:75, yielded spheroids with more roundness and smaller size. Other studies also noted the effects of co-cultures on tissue features and characteristics including function and fidelity. A 3D co-culture of cardiomyocytes with cardiac fibroblasts was found to improve the features of cardiac spheroids, namely cell morphology and gene expression (Fig. 17(C)) [255]. Similarly, in a liver model co-culture, the function, integrity, and viability of hepatocytes were markedly increased in co-culture in comparison to pure cultures [256]. For use in bioprinting with multiple cell types, co-culture systems must be precisely tuned to express the desired qualities.

9. Spheroid properties influencing bioprinting

9.1. Spheroid sphericity

Sphericity (roundness) of a spheroid is an important parameter for bioprinting. Sphericity of a spheroid has been observed to be directly influenced by the spheroid culture time [257]. Different cell types demonstrate different sphericity with respect to time. In droplet-based bioprinting, the sphericity of spheroid is not a concern but with more precise devices and image analysis tools, diagnosing more spherical spheroids could lower the chance of drops containing multiple spheroids. For extrusion-based bioprinting, on the other hand, sphericity is a key feature when spheroids are deposited one by one, and low sphericity may result in bioprinting failure. In Kenzan and aspiration-assisted bioprinting, sphericity is just as important, dictating the print quality. Especially, in the Kenzan method, bioprinting non-spherical spheroid hampers skewered down into Kenzan and cause a structural issue. Although irregular-shaped spheroids cause bioprinting concerns and should be avoided, these spheroids can be characterized using Martin's diameter, Feret's diameter, and projected area diameter (Fig. 16(C)) [258].

9.2. Spheroid compactness

The compactness of spheroids is yet another important parameter, especially while considering different bioprinting processes. The longer time the fabricated spheroids maintained in culture media, the higher their compactness. Currently, no definition or relationship is demonstrating the compactness of spheroids. However, for aspiration-assisted bioprinting, the compactness was measured with consecutive aspiration and flushing every 4 h [152]. Different types of spheroids were monitored every 4 h up to 24 h with aspiration and flushing once. If spheroid were intact with no breakage, they were considered to have sufficient compactness. Compactness is shown to increase with the increase in cell density of spheroids. The density of spheroids increases when the cells and components of spheroids are formed tightly together leading to a smooth surface. The ratio between the average minimum and maximum contour of a spheroid to the spheroid area was used in determining the smoothness of the spheroid. Noticeably, smoother surfaces in a single type of spheroid showed higher compactness (Fig. 16(D)) [152]. It is pertinent to note that longer culture yields compact spheroids, which are resilient against mechanical stresses during bioprinting, but they lose their fusion capabilities.

9.3. Spheroid size

Another important factor influencing bioprinting for scalable tissue fabrication (in centimeter scales) is the spheroid size. The spheroid size could be customized as per the application tailoring factors such as cell types, seeding density, and culture period. Additionally, the spheroid size directly influences its oxygen microenvironment. Large spheroids (>500 μm) often develop necrotic cores due to lack of sufficient oxygen transport. Consistent spheroid size is very importance because it determines the therapeutic efficacy and clinical reproducibility, and recent advances in spheroid fabrication techniques offer favorable solution to address these limitations, where techniques, such as microwell arrays, can produce uniform-sized spheroids in a high-throughput manner [259, 260]. The spheroid size depends on the resolution and other capabilities of the spheroid bioprinting technique (such as the minimum size spheroid that is bioprintable), and the resilience of spheroids against hypoxia as they are usually avascular. Several bioprinting strategies have been explored for their potentiality in spheroid assembly, each influencing the spheroid size. In case of direct extrusion-based bioprinting, the process is needle size dependent, thus limiting the size and density of spheroids. Kenzan method requires uniform specific size spheroids depending on the fixed distance between needles, which restrains size variation [257]. The suitability of spheroids used in the bio-gripper method is dependent on the size of the grippe [145]. Concurrently, certain applications may require assembling spheroids of different sizes into specific architectures. Towards this, aspiration-assisted bioprinting method allows the use of broader range of sizes from 80 to 600 μm without any restriction on the size uniformity in the same bioprinted structure [152].

10. Scaffold-based and scaffold-free bioprinting

Bioprinting of spheroids can generally be divided into two subcategories, scaffold-based and scaffold-free, based on the framework used for tissue growth. Tissue scaffolds are external structures that support the growth of cells around them, allowing the formation of tissues in desired complex geometries [261]. An ideal scaffold needs to have certain characteristics such as allowing cell growth and adhesion and supporting spheroid growth and fusion, high porosity, ideal mechanical properties, biocompatibility, and tunable biodegradation [262]. The critical aspect of the scaffold-based design is the temporary nature of the scaffold material - the ideal goal is for the scaffold to act as a foundation for tissue growth and biodegrade into non-toxic components at a determined rate tunable to the tissue growth rate [263]. This enables the newly grown tissues to retain proper function and occupy the designed biological architecture. In this regard, Efimov et al. tested the cellular interactions of HDF spheroids on an electrospun polyurethane scaffold [264]. The group observed that the microenvironment of the cell-scaffold interface might significantly improve the regenerative capabilities of HDF spheroids *in vivo*. Other studies also pointed toward the ability of scaffolds to better direct spatial organization of cells for fabrication of more complex tissues [265]. An alternative method of scaffold-based spheroid bioprinting focused on the use of a multi-head deposition system that systematically prints a PCL scaffold along with a chondrocyte cell-encapsulated alginate hydrogel, in a layer-by-layer fashion [266]. This method enabled the fabrication of well-defined tissue constructs with negligible effects on cell viability, by exploiting the ability of additive manufacturing to fine-tune the biochemical makeup of each layer. While scaffold-based approaches have benefits like improved spheroid orientation and structural stability, they also present several shortcomings such as degradation associated complications, limited in-vivo integrity, immunological response, and limited cell density.

To avoid such limitations, many researchers have transitioned to scaffold-free methods. Scaffold-free methods remove the dependency on the external scaffolding structure, relying only on the endogenously produced ECM to provide its mechanical stability [267]. Scaffold-free methods often utilize tissue spheroids as building blocks. Though still in the early phases of research, many groups have done tremendous progress such as Ong et al. using heterocellular spheroids, comprised of iPSC-derived CMs, ECs, and HDFs, to fabricate cardiac tissue patches [137]. While scaffold-free constructs eliminate many of the concerns posed by scaffold-based constructs, they introduce their vital limitations. Mainly, scaffold-free constructs cannot form highly complex geometries, without the mechanical stability and organization augmented by an external support. Looking ahead, especially concerning in-vivo applications, scaffold-free methods offer beneficial capabilities, as long as scalability and stability issues can be overcome. Regardless, the future of successful spheroid bioprinting may seek to employ a synergistic approach in which the two methodologies can be used in a complementing manner [15].

11. Challenges and limitations in bioprinting of spheroids

Bioprinting of spheroids can be broadly categorized into three phases – (i) pre-bioprinting, where spheroids are fabricated, and made ready for a bioprinting process, (ii) bioprinting, and (iii) post bioprinting, where the bioprinted tissues are cultured long-time enabling spheroid fusion and tissue maturation. In this section, we will discuss the challenges and concerns, yet to be addressed in each of these phases for successful fabrication of tissues.

11.1. Pre-bioprinting

Amidst several advantages of spheroid bioprinting, there are certain inherent limitations while trying to utilize bioprinters and spheroids for bioprinting. These limitations branch from the spheroid fabrication process and extend to even bioprinter device functionality and mechanism. The very first step towards successful spheroid bioprinting methods stems from successful fabrication and harvesting of spheroids. The most efficient and user-friendly method is the use of cell-repellent U-bottom 96 well-plates. Depending on the opted spheroid fabrication choices, collection of spheroids can be sometimes challenging. For example, the use of agarose mold can be cumbersome while collecting the spheroids as they get mechanically disturbed, leading to impaired cell viability along with the presence of agarose particles partly inside or stacked to spheroids. Along with fabrication approaches, the size of spheroids also plays a major role in spheroid viability. Larger spheroids possess more dead cells in their core due to hypoxia and insufficient nutrients infusion. In addition, percent live cells often cannot be quantified with a non-destructive measurement assay easily [16]. This heterogeneous makeup of dead and live cells in the core and shell, respectively, affects the properties of spheroids. Controlling the size of spheroids is thus yet another important parameter to consider before bioprinting. Controlling the cell density in a spheroid is just as important to demonstrate a native-like cell density in bioprinted tissues. However, some fabrication methods pose limitations regarding the size and density of spheroids. Thus, an optimized combination of spheroid fabrication approach with cell density and size of spheroids is crucial to their successful bioprinting.

In most cases, spheroids fabricated for bioprinting must demonstrate size uniformity. Especially, spheroid size distribution plays an important role in extrusion-based and Kenzan bioprinting methods. Researchers have recently investigated the optimization of spheroid sphericity and size distribution for the Kenzan method [123]. A specific diameter range is obtained by analyzing the size distribution using an integrated automated camera-based detector for both Kenzan and droplet-based bioprinting. Non-uniform size distribution of spheroids causes spheroid rupture, low accuracy, and failure in tissue formation. In an extrusion-based setup, the spheroid size distribution is problematic since larger spheroids are prone to get stuck in nozzles, whereas smaller spheroids are difficult to bioprint in the desired order. Some methods,

however, offer more size distribution versatility such as aspiration-assisted and droplet-based bioprinting. However, the droplet-based approach suffers from low resolution. On the other hand, for using different sizes of spheroids, different back pressure should be estimated while using aspiration-assisted bioprinting.

Morphology of spheroids is another important factor contributing to the bioprinting process. Except for droplet-based and aspiration-assisted bioprinting, all other methods need a well-defined spherical shape, which can be manipulated using different ratios of cell types and an optimized spheroid culture time. Longer spheroid culture period leads to more sphericity, with an increase in surface tension, which in turn reduces cohesiveness of spheroids and alters their potency to assemble. In general, spheroids demonstrate viscoelastic behavior. After initial fabrication, spheroids show more viscous behavior, with higher cohesiveness and lower surface tension. Depending on the size and type of spheroids, gradually with an increased culture time due to abundant ECM deposition, spheroids demonstrate more and more elastic behavior, with higher surface tension and lower adhesiveness.

Surface tension of spheroids is another vital consideration for bioprinting. In an extrusion-based setup, the surface tension is optimized for higher cell viability and to prevent spheroid aggregation and nozzle clogging. In droplet-based bioprinting, spheroid aggregation leads to droplets containing more than a single spheroid as discussed before. In Kenzan and aspiration-assisted bioprinting, spheroids are picked up one-by-one leading to no such clogging issues; however, it is worthy to note that spheroids get stuck in a nozzle tip if too much back pressure is applied. Yet, in every scaffold-free bioprinting method, enough cohesiveness of spheroids is necessary to enable their fusion into tissue patches, along with optimized viscoelasticity to maintain structural integrity and avoid getting ruptured. Therefore, it may be concluded that higher surface tension would be more appropriate for droplet-based bioprinting, while optimization of surface tension should be more critical for extrusion-based, Kenzan, biogripper, and aspiration-assisted bioprinting approaches. The compactness of spheroids also increases with longer spheroid culture time and influences mechanical properties of spheroids. Choice of cell types, in particular, alters the compactness of spheroids, especially for bioprinting applications requiring fusion of heterocellular spheroids.

11.2. During bioprinting

For initiating any bioprinting process, first and foremost, parameters such as bioprinting resolution, precision, reproducibility, cost-effectiveness, and versatility, should be well-thought-out and selected according to the target application. Alongside, flexibility with regards to spheroid size distribution, mechanical properties, surface tension, morphology, and compactness need to be considered whilst making a decision with the choice of the bioprinting process and need to be maintained consistent throughout the entire process. Some of the spheroid properties, like sphericity and size distribution, however, take more importance in certain bioprinting modalities, such as extrusion-based bioprinting. Several concerns arise during the bioprinting process, which stem from the inherent design of the process or the variation in spheroid properties. In extrusion-based bioprinting, spheroid lineup, clogging, and aggregation are some of the most commonly occurring problems during bioprinting. Even near-perfect characteristics – adequate spheroid size, perfect sphericity, proper compactness, and low cohesiveness does not ease the difficulties. Bioprinting process time also plays a very crucial role for a successful print. Longer bioprinting times lead the spheroids to start self-assembling inside nozzles leading to further clogging issues and structural deformity in the finished product. In droplet-based bioprinting, however, the presence of multiple spheroids in a single droplet is the most common issue, often caused by adhesiveness, spheroid aggregation, or even longer bioprinting times. Longer spheroid culture time leading to low cohesiveness with lower aggregation potency is thus helpful for droplet-based bioprinting. Increased cohesiveness of spheroids, whereas is crucial for the Kenzan method to facilitate fusion. Sufficient mechanical properties of spheroids are also important, especially for Kenzan and aspiration-assisted bioprinting to allow sufficient handleability for bioprinting. The duration of spheroids in air also influences the viability of tissues. This necessitates improving processing time for both of these approaches to fabricate any tissue size of clinical relevance.

The most accurate method in terms of positional precision of spheroids is aspiration-assisted bioprinting. Extrusion-based bioprinting (when spheroids are extruded one by one) also provide high precision with regards to the spheroid placement depending on the spheroid size. In Kenzan, the distance between needles dictates the positional precision. All of the presented approaches also have been hindered by a lack of control over the positional precision in Z direction. This challenge was recently circumvented by enabling freeform bioprinting in self-healing yield-stress gels by fabricating complex geometries [152].

Scalability and throughput of the process are yet other crucial factors to consider for applications relevant to clinical translation. The throughput ability of all available bioprinting modalities is low limiting their use to mainly research purposes. To provide a relevant number to the understanding of the scalability for clinical transplantation purposes, the age-adjusted mean cell density in human central lens epithelium is 5008.6 cells per mm^2 (in males) and 5780.6 cells per mm^2 (in females) [268] but the average cell density in human organs ranges from 1 to 3 billion cells per ml [269]. Even with the most scalable spheroid bioprinting technique available, we have been to generate only a couple centimeter long tissue constructs. For a scaffold-free 1 cm^2 construct (with 1 mm in thickness), we can theoretically bioprint more than 100 k spheroids (considering a spheroid size of 400 μm in size). It is worthy to note than cells vary significantly in size and hence number of cells required to make a spheroid of 400 μm may change with the type of spheroid required for a specific application, but it can be estimates to range from 10 k to 15 k cells per spheroid for a 400 μm spheroid size [152]. However, with advances in biofabrication strategies, clinical translation of engineered tissues is becoming more feasible. For example, researchers from Kyoto University in Japan created tubular conduits using a Regenova 3D bioprinter from Cyfuse Biomedical [270, 271]. These conduits can regenerate the damaged nerves in rats and are currently undergoing clinical trial in humans. In general, the throughput of these processes can be improved with the flexibility of using bigger or non-uniform spheroid/microtissue sizes or reducing the bioprinting process time. At the current stage, most processes have limitations with the size of spheroids that can be desired, except aspiration-assisted bioprinting, which could be optimized and altered quite easily to accommodate a range of spheroid sizes. However, for other methods, spheroid size poses a major limitation towards scalability. Although aspiration-assisted bioprinting approach offers many flexibilities of a wide range of spheroid size, size distribution, or cell types, scalability of the tissue construct is still an issue, yet to be solved. The lack of a rapid spheroid bioprinting modality is one of the major impediments to the widespread embracement in the field of tissue engineering.

In a similar line, automation and commercial availability of these methods is also crucial for their widespread acceptability and accessibility. Kenzan method is the only system that has been fully automated and commercialized until now for spheroid bioprinting. Yet, this process is pretty inflexible in terms of the spheroid parameters, and optimization of all pre-bioprinting aspects like size distribution, spheroid size, sphericity, and compactness are laborious. The aspiration-assisted bioprinting approach is a semi-automated system [152]. In addition, it should be noted that user-friendliness, cost-effectiveness, and versatility are also crucial for increased use of spheroid bioprinting processes.

11.3. Post-bioprinting

Bioprinting spheroids as building blocks at desired configurations ultimately enable spheroid fusion and lead to the formation of tissues.

This assembly of spheroids to form tissues often results in shrinkage and hole filling, deforming the desired bioprinted structure. Several groups have investigated multiple molds to allow constructs to retain the shape of final structures or have considered such shrinkage and shape alterations in their design parameters or even modulated the culture time of spheroids for shape preservation. Restrains, such as pillars, temporary supports, or scaffold-based substrates, are ideal for maintaining the final architecture. For example, Mekhileri et al. [113] designed a scaffold with a defined shape, where micro-tissues, such as spheroids could be positioned and confined to generate the desired structure for chondrogenic applications. In general, it might be worth mentioning that molding and confinement generate finer details in the final structure. However, sometimes shrinkage of cell aggregates still occurs within the confinement or the molding leading to structural failure with no sufficient effects on shrinkage from the molds [244,245]. Sometimes, the mold or the substrate is not hydrophilic and needs to be hydrated to make them more stable and less contractive allowing better spheroid attachment to the substrate while increasing hydrophilicity.

Shrinkage and compactness of spheroids are influenced by a variety of factors – cell types, culture times, spheroid size, or the potency of cells to aggregate. Excessive contraction of spheroids after bioprinting puts the individual spheroids not in direct contact with their adjacent spheroid and deters the entire foundation of assembly to form tissues. A recent effort demonstrated the retainment of shape after the bioprinting of cartilage using MSC spheroids in a self-healing yield stress gel [155]. Bioprinting was done in two different ways – (i) bioprinting of pre-differentiated chondrogenic spheroids to form a tissue patch and (ii) bioprinting of MSC spheroids to form the tissue patch and then differentiating them into a chondrogenic lineage. Higher shrinkage and loss of shape was observed while differentiating the already assembled tissue patch, compared to the other strategy. This may be due to the higher self-assembling potency of MSC spheroids compared to the already differentiated chondrogenic counterparts. This study paved the path to demonstrating yet another way to enable tissue fabrication from spheroids at desired configurations.

After allowing sufficient time to enable fusion of spheroids into a tissue construct, a temporary support substrate is removed to further culture it. Substrate removal is another laborious and time-consuming concern to be considered post-bioprinting. For the scaffold-free method, bioprinting is usually performed on a substrate – a biocompatible sacrificial gel or Kenzan, to support spheroid fusion. The sacrificial gel is chosen to keep in mind the post-processing and gel removal steps. Common choices of sacrificial gels include gelatin, agarose, alginate, or Carbopol. Although agarose and Carbopol offer excellent support for spheroid fusion, both of these gels deem cumbersome and difficult to remove, often leading to the breaking of assembled tissue constructs. Alginate and alginate-based sacrificial gels are hence of particular interest in partially and fully-crosslinked mode as they can be dissolved by alginate lyase and easily removed. Biologically functional gels, such as fibrin generated from fibrinogen and thrombin layers, are also used as a substrate in a scaffold-based approach and are not removed post-bioprinting.

Substrate removal for the Kenzan method has been done very delicately after the fusion of spheroids as there are ample chances of breakage of the tissue. The formed tissue has permanent holes that are remnants from the needles in Kenzan, which often hampers the viability of the tissue. Depending on the cell type and spheroid culture time, the holes repair over time. Often, the fused tissue fabricated in a Kenzan is observed to demonstrate higher compactness and density, which makes the removal process very difficult and more prone to tissue breakage and structural deformity [137]. When the fabricated tissue is not compact, on the other hand, removal from the Kenzan is easier, but the holes are not properly repaired with higher amount of damaged tissue around them [143]. Thus, the Kenzan process is a tradeoff between the structural accuracy of fabricated tissue constructs and the effort- and time-demanding removal process from the Kenzan.

12. Clinical applications

3D Bioprinting has been increasingly used in a wide range of healthcare settings. Although it is not a new technology, its clinical use in medicine is entering a dynamic period marked by a broad range of clinical applications, and ongoing technological advancements including tissues for transplantation [272] and analogues for toxicity testing, disease modeling, and for patient-specific drug screening, with the potential to eliminate the use of animal models in preclinical research as per 3Rs approach (Replace, Reduce and Refine). The clinical translation of bioprinting requires addressing some of the existing issues to ultimately scale-up to affordable and clinically-relevant volume of tissues along with efficient vascularization for ready implantation. We reviewed the entire procedure of bioprinting discusses these issues in detail elsewhere [273]. Furthermore, 3D bioprinting for organoids or cellular aggregates has potential to address the problem of obtaining large tissue constructs to fabricate biomimetic complex tissues and organs. Organoids or spheroids derived from patient-derived iPSCs are suitable to be developed as preclinical models for testing drugs. Many drugs fail when they go to human clinical trials from preclinical models mainly because they are tested on models that do not physiologically mimic humans. Organoid-based drug testing is thus a valuable strategy for investigating repurposed drugs and new drug discovery following preclinical trials [274].

Currently, less than 10% of new anticancer drug candidates entering Phase I trials are eventually approved by the Food and Drug Administration (FDA) [275]. The transition of preclinical breakthroughs from “bench to bedside” is one of the major challenges. The improved ability to recapitulate organogenesis cues *in vitro* has led to the development of the organoid model [276]. The tumor organoids reflect the genetic and phenotypic characteristics of tumor epithelium, such as heterogeneity and 3D spatial organization facilitating their increased use to study cancer. The ability of patient-derived organoids (PDOs) to predict responses to chemotherapy for cancer patients has gained significant interest lately [199,200,277]. In an ongoing clinical trial (NCT03890614), the inventors aim to compare chemosensitivity between chemotherapy combinations in bone marrow aspirates using 3D organoid models. For automated organoid biofabrication using 3D bioprinting (hyaluronic acid and gelatin-based hydrogel), bone marrow aspirates (around 3–7 ml) are collected from participants with hematologic malignancy being evaluated for relapsed disease to generate 3D constructs followed by viability assessment of myeloma cells. In another recent ongoing clinical trial (NCT04755907), the inventors aim to validate the potential of 3D bioprinted tumor models and organoids in predicting the response to chemotherapy in colorectal cancer (CRC). 3D bioprinted CRC models and organoids will be developed from surgically resected tumor tissues of CRC patients with or without liver metastases. The predictive ability of 3D models for chemotherapy sensitivity in CRC patients will be compared with that of the organoids.

Overall, efficient, and cost-effective organization of organoids in a clinically relevant timeframe would enable drug screening for individual patients. Optimization of procedures for robustness and sensitivity in drug screening paired with validation of drug response predictions from clinical studies would further allow the implementation of organoid-based personalized medicine in clinical settings. Organoids generated from both healthy and diseased tissues holds great promise for drug discovery and development.

13. Future outlook

In this review, we describe the current state-of-the-art in spheroid bioprinting techniques and discuss the involved technologies. Despite advancements in bioprinting of spheroid-based building blocks within scaffolds or without scaffolds, there are still significant challenges ahead. For instance, the integration of a vascular network remains a critical challenge, as in other bioprinting and biofabrication approaches.

Without vascularization, scalability of bioprinted tissues is limited, and mainly tubular- and flat-shaped tissues could be achieved using spheroids. As bioprinting of multi-scale vascular network is not trivial with the use of spheroids due to their intrinsic minimum size, such vascular networks can be built using other means, e.g., scaffold-based bioprinting methods detailed in our earlier review [278], and spheroids can be positioned around the bioprinted vascular networks. Despite endothelial cells have been incorporated into spheroids [64] and the use of pre-vascularized spheroids in microphysiological systems have been demonstrated, robust generation of perfusable vascular networks within spheroid bodies is still a major roadblock towards the use of spheroids in scalable tissue biofabrication. Use of spheroids for scalable tissues with functional and anatomical complexity requires fabrication of these spheroids with controlled size in a high-throughput manner. A step towards robotic scalable fabrication of uniform sized spheroids was performed by creation of microrecessions in a non-adherent hydrogel in a 96-well plate [82], making the process more robust, and eliminate the need for human interference and laborious cell seeding processes. These high-throughput fabrication platforms hold the key for significant advances in bioprinting modalities involving spheroids, especially in a scenario where both academia and industries are readily searching for reproducible and robust techniques for scalable fabrication of tissues for regenerative medicine.

Most of the existing tissue engineering methods are either scaffold-based and scaffold-free. Recently a third strategy involving the possibility of a synergistic, convergence approach has been proposed that could alleviate bottlenecks of the two previous options. This method can be realized in multiple ways such as but not limited to the bioprinting of spheroids into functional hydrogels or creation of highly porous microscaffolds with the spheroids bioprinted into pores. In a recent study, achieved via two-photon polymerization [279], single spheroids were grown within porous cages. Through bottom-up assembly, these cages can be joined and employed as modular building blocks for generating scalable tissues.

Despite spheroids constitutes a microenvironment mimicking cell density in native tissues, their morphology, anatomy and physiology may not closely recapitulate such of native tissues. In this regard, use of organoids, which are self-organizing, self-renewing stem-cell based structures resembling organs, can be considered repetitive building blocks, even with void features, such as kidney organoids (i.e., tubuloids [280]), for implantable organs. Hollow organoids, on the other hand, needs delicate bioprinting technologies as their mechanical and structural properties are highly weak and prone to break apart during bioprinting. Such organoids can also be accompanied by vascular organoids [281] or both vascularization and functional organoid formation can be realized in coculture systems simultaneously.

Another implication of the biophysical nature of factors at work during scaffold-free bioprinting depends on types of possible applications as well as the required training, competencies, and mindset of users and operators as spheroid bioprinting processes are not as straightforward as typical bioprinting processes, such as extrusion-based bioprinting of hydrogels. Nevertheless, as a branch of bioprinting, bioprinting of spheroids remains a quantitative discipline, with the potential to benefit from advanced analytics and biosensors, molecular-level optimization, and computer modeling.

Declaration of competing interest

I.T.O. serves as a scientific advisor for Biolife4D and Brinter and owns stock in Biolife4D. The other authors declare that they have no known competing financial interests or personal relationships that could have appeared to influence the work reported in this paper.

Data availability

This is a review paper and no new data have been presented.

Acknowledgements

This work has been supported by National Science Foundation Award 1914885, National Institute of Dental and Craniofacial Research Award R01DE028614, National Institute of Allergy and Infectious Diseases Award U19AI142733, 2236 CoCirculation2 of TUBITAK award 121C359, and a contract from The Lysosomal and Rare Disorders Research and Treatment Center Inc. (I.T.O.). We thank Prof. Seda Tigli Aydin (Bulent Ecevit University) and Zaman Ataie (Penn State) for useful discussions and their help with editorial corrections, and Mustafa Ayhan (Cukurova University) for his help with the creation of 3D design models for the bioprinting techniques. The opinions, interpretations, conclusions, and recommendations are those of the authors and are not necessarily endorsed by National Science Foundation, National Institute of Dental and Craniofacial Research, National Institute of Allergy and Infectious Diseases Award and TUBITAK.

References

[1] J.S. Temenoff, A.G. Mikos, Review: tissue engineering for regeneration of articular cartilage, Biomaterials 21 (2000) 431–440, https://doi.org/10.1016/S0142-9612(99)00213-6.
[2] J. Saroia, W. Yanen, Q. Wei, K. Zhang, T. Lu, B. Zhang, A review on biocompatibility nature of hydrogels with 3D printing techniques, tissue engineering application and its future prospective, Bio-Design Manuf. 1 (2018) 265–279, https://doi.org/10.1007/s42242-018-0029-7.
[3] K. Torres, G. Staśkiewicz, M. Śnieżyński, A. Drop, R. Maciejewski, Application of rapid prototyping techniques for modelling of anatomical structures in medical training and education, Folia Morphol. (Wars.) 70 (2011) 1–4.
[4] A. Tejo-Otero, I. Buj-Corral, F. Fenollosa-Artés, 3D printing in medicine for preoperative surgical planning: a review, Ann. Biomed. Eng. 48 (2020) 536–555, https://doi.org/10.1007/s10439-019-02411-0.
[5] K.C. Wong, 3D-printed patient-specific applications in orthopedics, Orthop. Res. Rev. 8 (2016) 57–66, https://doi.org/10.2147/ORR.S99614.
[6] C.G. Sandström, The non-disruptive emergence of an ecosystem for 3D Printing — insights from the hearing aid industry's transition 1989–2008, Technol. Forecast, Soc. Change 102 (2016) 160–168, https://doi.org/10.1016/j.techfore.2015.09.006.
[7] S.V. Murphy, A. Atala, 3D bioprinting of tissues and organs, Nat. Biotechnol. 32 (2014) 773–785, https://doi.org/10.1038/nbt.2958.
[8] S.C. Cox, J.A. Thornby, G.J. Gibbons, M.A. Williams, K.K. Mallick, 3D printing of porous hydroxyapatite scaffolds intended for use in bone tissue engineering applications, Mater. Sci. Eng., C 47 (2015) 237–247, https://doi.org/10.1016/j.msec.2014.11.024.
[9] A.D. Metcalfe, M.W.J. Ferguson, Tissue engineering of replacement skin: the crossroads of biomaterials, wound healing, embryonic development, stem cells and regeneration, J. R. Soc. Interface 4 (2007) 413–437, https://doi.org/10.1098/rsif.2006.0179.
[10] W.C.J. Wilson, T. Boland, Cell and organ printing 1: protein and cell printers, Anat. Rec. Part A, Discov. Mol. Cell. Evol. Biol. 272 (2003) 491–496, https://doi.org/10.1002/ar.a.10057.
[11] I.T. Ozbolat, 3D Bioprinting, Fundamentals, Principles and Applications, Elsevier, Oxford, 2016, https://doi.org/10.1016/C2014-0-02349-0.
[12] J.L. Drury, D.J. Mooney, Hydrogels for tissue engineering: scaffold design variables and applications, Biomaterials 24 (2003) 4337–4351, https://doi.org/10.1016/S0142-9612(03)00340-5.
[13] M.E. Oest, K.M. Dupont, H.-J. Kong, D.J. Mooney, R.E. Guldberg, Quantitative assessment of scaffold and growth factor-mediated repair of critically sized bone defects, J. Orthop. Res. 25 (2007) 941–950, https://doi.org/10.1002/jor.20372.
[14] R.H. Utama, L. Atapattu, A.P. O'Mahony, C.M. Fife, J. Baek, T. Allard, K. J. O'Mahony, J.C.C. Ribeiro, K. Gaus, M. Kavallaris, J.J. Gooding, A 3D bioprinter specifically designed for the high-throughput production of matrix-embedded multicellular spheroids, iScience 23 (2020), 101621, https://doi.org/10.1016/j.isci.2020.101621.
[15] I.T. Ozbolat, Scaffold-based or scaffold-free bioprinting: competing or complementing approaches? J. Nanotechnol. Eng. Med. 6 (2015) https://doi.org/10.1115/1.4030414.
[16] Y. Wu, M. Hospodiuk, W. Peng, H. Gudapati, T. Neuberger, S. Koduru, D. J. Ravnic, I.T. Ozbolat, Porous tissue strands: avascular building blocks for scalable tissue fabrication, Biofabrication 11 (2018), 015009, https://doi.org/10.1088/1758-5090/aaec22.
[17] D.N. Heo, B. Ayan, M. Dey, D. Banerjee, H. Wee, G.S. Lewis, I.T. Ozbolat, Aspiration-assisted bioprinting of co-cultured osteogenic spheroids for bone tissue engineering, Biofabrication 13 (2021), 015013, https://doi.org/10.1088/1758-5090/abc1bf.
[18] S. Xin, D. Chimene, J.E. Garza, A.K. Gaharwar, D.L. Alge, Clickable PEG hydrogel microspheres as building blocks for 3D bioprinting, Biomater. Sci. 7 (2019) 1179–1187, https://doi.org/10.1039/C8BM01286E.
[19] A. Faulkner-Jones, C. Fyfe, D.-J. Cornelissen, J. Gardner, J. King, A. Courtney, W. Shu, Bioprinting of human pluripotent stem cells and their directed

differentiation into hepatocyte-like cells for the generation of mini-livers in 3D, Biofabrication 7 (2015), 044102, https://doi.org/10.1088/1758-5090/7/4/044102.
[20] L. Koch, A. Deiwick, A. Franke, K. Schwanke, A. Haverich, R. Zweigerdt, B. Chichkov, Laser bioprinting of human induced pluripotent stem cells—the effect of printing and biomaterials on cell survival, pluripotency, and differentiation, Biofabrication 10 (2018), 035005, https://doi.org/10.1088/1758-5090/aab981.
[21] Q. Gu, E. Tomaskovic-Crook, G.G. Wallace, J.M. Crook, 3D bioprinting human induced pluripotent stem cell constructs for in situ cell proliferation and successive multilineage differentiation, Adv. Healthc. Mater. 6 (2017), 1700175, https://doi.org/10.1002/adhm.201700175.
[22] Y. Kim, N. Park, Y.A. Rim, Y. Nam, H. Jung, K. Lee, J.H. Ju, Establishment of a complex skin structure via layered co-culture of keratinocytes and fibroblasts derived from induced pluripotent stem cells, Stem Cell Res. Ther. 9 (2018) 217, https://doi.org/10.1186/s13287-018-0958-2.
[23] G. Gao, A.F. Schilling, K. Hubbell, T. Yonezawa, D. Truong, Y. Hong, G. Dai, X. Cui, Improved properties of bone and cartilage tissue from 3D inkjet-bioprinted human mesenchymal stem cells by simultaneous deposition and photocrosslinking in PEG-GelMA, Biotechnol. Lett. 37 (2015) 2349–2355, https://doi.org/10.1007/s10529-015-1921-2.
[24] D. Nguyen, D.A. Hägg, A. Forsman, J. Ekholm, P. Nimkingratana, C. Brantsing, T. Kalogeropoulos, S. Zaunz, S. Concaro, M. Brittberg, A. Lindahl, P. Gatenholm, A. Enejder, S. Simonsson, Cartilage tissue engineering by the 3D bioprinting of iPS cells in a nanocellulose/alginate bioink, Sci. Rep. 7 (2017) 658, https://doi.org/10.1038/s41598-017-00690-y.
[25] K. Arai, D. Murata, A.R. Verissimo, Y. Mukae, M. Itoh, A. Nakamura, S. Morita, K. Nakayama, Fabrication of scaffold-free tubular cardiac constructs using a Bio-3D printer, PLoS One 13 (2018), e0209162, https://doi.org/10.1371/journal.pone.0209162.
[26] X. Ma, X. Qu, W. Zhu, Y.-S. Li, S. Yuan, H. Zhang, J. Liu, P. Wang, C.S.E. Lai, F. Zanella, G.-S. Feng, F. Sheikh, S. Chien, S. Chen, Deterministically patterned biomimetic human iPSC-derived hepatic model via rapid 3D bioprinting, Proc. Natl. Acad. Sci. USA 113 (2016) 2206–2211, https://doi.org/10.1073/pnas.1524510113.
[27] V. Mironov, V. Kasyanov, C. Drake, R.R. Markwald, Organ printing: promises and challenges, Regen. Med. 3 (2008) 93–103, https://doi.org/10.2217/17460751.3.1.93.
[28] I.T. Ozbolat, Yu Yin, Bioprinting toward organ fabrication: challenges and future trends, IEEE Trans. Biomed. Eng. 60 (2013) 691–699, https://doi.org/10.1109/TBME.2013.2243912.
[29] G. Gao, Y. Huang, A.F. Schilling, K. Hubbell, X. Cui, Organ bioprinting: are we there yet? Adv. Healthc. Mater. 7 (2018), 1701018 https://doi.org/10.1002/adhm.201701018.
[30] F. Marga, A. Neagu, I. Kosztin, G. Forgacs, Developmental biology and tissue engineering, Birth Defects Res. Part C Embryo Today - Rev. 81 (2007) 320–328, https://doi.org/10.1002/bdrc.20109.
[31] H.A. McCauley, J.M. Wells, Pluripotent stem cell-derived organoids: using principles of developmental biology to grow human tissues in a dish, Development 144 (2017) 958–962, https://doi.org/10.1242/dev.140731.
[32] S.J. Hollister, R.D. Maddox, J.M. Taboas, Optimal design and fabrication of scaffolds to mimic tissue properties and satisfy biological constraints, Biomaterials 23 (2002) 4095–4103, https://doi.org/10.1016/S0142-9612(02)00148-5.
[33] S. Talukdar, Q.T. Nguyen, A.C. Chen, R.L. Sah, S.C. Kundu, Effect of initial cell seeding density on 3D-engineered silk fibroin scaffolds for articular cartilage tissue engineering, Biomaterials 32 (2011) 8927–8937, https://doi.org/10.1016/j.biomaterials.2011.08.027.
[34] C. Jungreuthmayer, S.W. Donahue, M.J. Jaasma, A.A. Al-Munajjed, J. Zanghellini, D.J. Kelly, F.J. O'Brien, A comparative study of shear stresses in collagen-glycosaminoglycan and calcium phosphate scaffolds in bone tissue-engineering bioreactors, Tissue Eng. 15 (2009) 1141–1149, https://doi.org/10.1089/ten.tea.2008.0204.
[35] Y. Shin, S. Han, J.S. Jeon, K. Yamamoto, I.K. Zervantonakis, R. Sudo, R.D. Kamm, S. Chung, Microfluidic assay for simultaneous culture of multiple cell types on surfaces or within hydrogels, Nat. Protoc. 7 (2012) 1247–1259, https://doi.org/10.1038/nprot.2012.051.
[36] S. Yin, W. Zhang, Z. Zhang, X. Jiang, Recent advances in scaffold design and material for vascularized tissue-engineered bone regeneration, Adv. Healthc. Mater. 8 (2019), 1801433, https://doi.org/10.1002/adhm.201801433.
[37] U. Blache, M.M. Stevens, E. Gentleman, Harnessing the secreted extracellular matrix to engineer tissues, Nat. Biomed. Eng. 4 (2020) 357–363, https://doi.org/10.1038/s41551-019-0500-6.
[38] M.H. Kim, D. Banerjee, N. Celik, I.T. Ozbolat, Aspiration-assisted freeform bioprinting of mesenchymal stem cell spheroids within alginate microgels, Biofabrication 14 (2022), 024103, https://doi.org/10.1088/1758-5090/ac4dd8.
[39] A. Akkouch, Y. Yu, I.T. Ozbolat, Microfabrication of scaffold-free tissue strands for three-dimensional tissue engineering, Biofabrication 7 (2015), 031002, https://doi.org/10.1088/1758-5090/7/3/031002.
[40] K. Jakab, C. Norotte, F. Marga, K. Murphy, G. Vunjak-Novakovic, G. Forgacs, Tissue engineering by self-assembly and bio-printing of living cells, Biofabrication 2 (2010), 022001, https://doi.org/10.1088/1758-5082/2/2/022001.
[41] X. Ma, J. Liu, W. Zhu, M. Tang, N. Lawrence, C. Yu, M. Gou, S. Chen, 3D bioprinting of functional tissue models for personalized drug screening and in vitro disease modeling, Adv. Drug Deliv. Rev. 132 (2018) 235–251, https://doi.org/10.1016/j.addr.2018.06.011.
[42] K. Jakab, A. Neagu, V. Mironov, R.R. Markwald, G. Forgacs, Engineering biological structures of prescribed shape using self-assembling multicellular systems, Proc. Natl. Acad. Sci. USA 101 (2004) 2864–2869, https://doi.org/10.1073/pnas.0400164101.
[43] C. Norotte, F.S. Marga, L.E. Niklason, G. Forgacs, Scaffold-free vascular tissue engineering using bioprinting, Biomaterials 30 (2009) 5910–5917, https://doi.org/10.1016/j.biomaterials.2009.06.034.
[44] E.A. Bulanova, E. V Koudan, J. Degosserie, C. Heymans, F. Das Pereira, V. A. Parfenov, Y. Sun, Q. Wang, S.A. Akhmedova, I.K. Sviridova, N.S. Sergeeva, G. A. Frank, Y.D. Khesuani, C.E. Pierreux, V.A. Mironov, Bioprinting of a functional vascularized mouse thyroid gland construct, Biofabrication 9 (2017), 034105, https://doi.org/10.1088/1758-5090/aa7fdd.
[45] J. Groll, J.A. Burdick, D.-W. Cho, B. Derby, M. Gelinsky, S.C. Heilshorn, T. Jüngst, J. Malda, V.A. Mironov, K. Nakayama, A. Ovsianikov, W. Sun, S. Takeuchi, J. J. Yoo, T.B.F. Woodfield, A definition of bioinks and their distinction from biomaterial inks, Biofabrication 11 (2018), 013001, https://doi.org/10.1088/1758-5090/aaec52.
[46] M. Bauer, L. Kang, Y. Qiu, J. Wu, M. Peng, H.H. Chen, G. Camci-Unal, A. F. Bayomy, D.E. Sosnovik, A. Khademhosseini, R. Liao, Adult cardiac progenitor cell aggregates exhibit survival benefit both in vitro and in vivo, PLoS One 7 (2012), e50491, https://doi.org/10.1371/journal.pone.0050491.
[47] C.L. Rettinger, A.B. Fourcaudot, S.J. Hong, T.A. Mustoe, R.G. Hale, K.P. Leung, In vitro characterization of scaffold-free three-dimensional mesenchymal stem cell aggregates, Cell Tissue Res. 358 (2014) 395–405, https://doi.org/10.1007/s00441-014-1939-0.
[48] R.-Z. Lin, L.-F. Chou, C.-C.M. Chien, H.-Y. Chang, Dynamic analysis of hepatoma spheroid formation: roles of E-cadherin and β1-integrin, Cell Tissue Res. 324 (2006) 411–422, https://doi.org/10.1007/s00441-005-0148-2.
[49] M. Grellier, L. Bordenave, J. Amédée, Cell-to-cell communication between osteogenic and endothelial lineages: implications for tissue engineering, Trends Biotechnol. 27 (2009) 562–571, https://doi.org/10.1016/j.tibtech.2009.07.001.
[50] M.P. Stuart, R.A.M. Matsui, M.F.S. Santos, I. Côrtes, M.S. Azevedo, K.R. Silva, A. Beatrici, P.E.C. Leite, P. Falagan-Lotsch, J.M. Granjeiro, V. Mironov, L. S. Baptista, Successful low-cost scaffold-free cartilage tissue engineering using human cartilage progenitor cell spheroids formed by micromolded nonadhesive hydrogel, Stem Cell. Int. (2017) 1–11, https://doi.org/10.1155/2017/7053465, 2017.
[51] Y. Fukuda, T. Akagi, T. Asaoka, H. Eguchi, K. Sasaki, Y. Iwagami, D. Yamada, T. Noda, K. Kawamoto, K. Gotoh, S. Kobayashi, M. Mori, Y. Doki, M. Akashi, Layer-by-layer cell coating technique using extracellular matrix facilitates rapid fabrication and function of pancreatic β-cell spheroids, Biomaterials 160 (2018) 82–91, https://doi.org/10.1016/j.biomaterials.2018.01.020.
[52] Y. Sakai, S. Yamagami, K. Nakazawa, Comparative analysis of gene expression in rat liver tissue and monolayer- and spheroid-cultured hepatocytes, Cells Tissues Organs 191 (2010) 281–288, https://doi.org/10.1159/000272316.
[53] L. Polonchuk, M. Chabria, L. Badi, J.-C. Hoflack, G. Figtree, M.J. Davies, C. Gentile, Cardiac spheroids as promising in vitro models to study the human heart microenvironment, Sci. Rep. 7 (2017) 7005, https://doi.org/10.1038/s41598-017-06385-8.
[54] R. Burdis, D.J. Kelly, Biofabrication and bioprinting using cellular aggregates, microtissues and organoids for the engineering of musculoskeletal tissues, Acta Biomater. 126 (2021) 1–14, https://doi.org/10.1016/j.actbio.2021.03.016.
[55] J. Rouwkema, J. De Boer, C.A. Van Blitterswijk, Endothelial cells assemble into a 3-dimensional prevascular network in a bone tissue engineering construct, Tissue Eng. 12 (2006) 2685–2693, https://doi.org/10.1089/ten.2006.12.2685.
[56] S. Zhang, M. Zhou, Z. Ye, Y. Zhou, W.-S. Tan, Fabrication of viable and functional pre-vascularized modular bone tissues by coculturing MSCs and HUVECs on microcarriers in spinner flasks, Biotechnol. J. 12 (2017), 1700008, https://doi.org/10.1002/biot.201700008.
[57] R. Noguchi, K. Nakayama, M. Itoh, K. Kamohara, K. Furukawa, J. Oyama, K. Node, S. Morita, Development of a three-dimensional pre-vascularized scaffold-free contractile cardiac patch for treating heart disease, J. Heart Lung Transplant. 35 (2016) 137–145, https://doi.org/10.1016/j.healun.2015.06.001.
[58] V. Mironov, R.P. Visconti, V. Kasyanov, G. Forgacs, C.J. Drake, R.R. Markwald, Organ printing: tissue spheroids as building blocks, Biomaterials 30 (2009) 2164–2174, https://doi.org/10.1016/j.biomaterials.2008.12.084.
[59] C.-W. Wong, H.-W. Han, Y.-W. Tien, S. Hsu, Biomaterial substrate-derived compact cellular spheroids mimicking the behavior of pancreatic cancer and microenvironment, Biomaterials 213 (2019), 119202, https://doi.org/10.1016/j.biomaterials.2019.05.013.
[60] S.H. Lee, S. Hong, J. Song, B. Cho, E.J. Han, S. Kondapavulur, D. Kim, L.P. Lee, Microphysiological analysis platform of pancreatic islet β-cell spheroids, Adv. Healthc. Mater. 7 (2018), 1701111, https://doi.org/10.1002/adhm.201701111.
[61] C.-H. Wassmer, K. Bellofatto, L. Perez, V. Lavallard, D. Cottet-Dumoulin, S. Ljubicic, G. Parnaud, D. Bosco, E. Berishvili, F. Lebreton, Engineering of primary pancreatic islet cell spheroids for three-dimensional culture or transplantation: a methodological comparative study, Cell Transplant. 29 (2020), 096368972093729, https://doi.org/10.1177/0963689720937292.
[62] Y. Jun, J. Lee, S. Choi, J.H. Yang, M. Sander, S. Chung, S.-H. Lee, In vivo–mimicking microfluidic perfusion culture of pancreatic islet spheroids, Sci. Adv. 5 (2019) 1–13, https://doi.org/10.1126/sciadv.aax4520.
[63] A. Winter, S. Breit, D. Parsch, K. Benz, E. Steck, H. Hauner, R.M. Weber, V. Ewerbeck, W. Richter, Cartilage-like gene expression in differentiated human stem cell spheroids: a comparison of bone marrow-derived and adipose tissue-derived stromal cells, Arthritis Rheum. 48 (2003) 418–429, https://doi.org/10.1002/art.10767.

[64] D.N. Heo, M. Hospodiuk, I.T. Ozbolat, Synergistic interplay between human MSCs and HUVECs in 3D spheroids laden in collagen/fibrin hydrogels for bone tissue engineering, Acta Biomater. 95 (2019) 348–356, https://doi.org/10.1016/j.actbio.2019.02.046.

[65] B. Ayan, Y. Wu, V. Karuppagounder, F. Kamal, I.T. Ozbolat, Aspiration-assisted bioprinting of the osteochondral interface, Sci. Rep. 10 (2020), 13148, https://doi.org/10.1038/s41598-020-69960-6.

[66] L. Song, X. Yuan, Z. Jones, K. Griffin, Y. Zhou, T. Ma, Y. Li, Assembly of human stem cell-derived cortical spheroids and vascular spheroids to model 3-D brain-like tissues, Sci. Rep. 9 (2019) 5977, https://doi.org/10.1038/s41598-019-42439-9.

[67] L. Song, X. Yuan, Z. Jones, C. Vied, Y. Miao, M. Marzano, T. Hua, Q.-X.A. Sang, J. Guan, T. Ma, Y. Zhou, Y. Li, Functionalization of brain region-specific spheroids with isogenic microglia-like cells, Sci. Rep. 9 (2019), 11055, https://doi.org/10.1038/s41598-019-47444-6.

[68] S.A. Sloan, J. Andersen, A.M. Paşca, F. Birey, S.P. Paşca, Generation and assembly of human brain region–specific three-dimensional cultures, Nat. Protoc. 13 (2018) 2062–2085, https://doi.org/10.1038/s41596-018-0032-7.

[69] P. Zhuang, A.X. Sun, J. An, C.K. Chua, S.Y. Chew, 3D neural tissue models: from spheroids to bioprinting, Biomaterials 154 (2018) 113–133, https://doi.org/10.1016/j.biomaterials.2017.10.002.

[70] K.E. Samy, E.S. Levy, K. Phong, B. Demaree, A.R. Abate, T.A. Desai, Human intestinal spheroids cultured using Sacrificial Micromolding as a model system for studying drug transport, Sci. Rep. 9 (2019) 9936, https://doi.org/10.1038/s41598-019-46408-0.

[71] H. Miyoshi, T.S. Stappenbeck, In vitro expansion and genetic modification of gastrointestinal stem cells in spheroid culture, Nat. Protoc. 8 (2013) 2471–2482, https://doi.org/10.1038/nprot.2013.153.

[72] E. Buzhor, O. Harari-Steinberg, D. Omer, S. Metsuyanim, J. Jacob-Hirsch, T. Noiman, Z. Dotan, R.S. Goldstein, B. Dekel, Kidney spheroids recapitulate tubular organoids leading to enhanced tubulogenic potency of human kidney-derived cells, Tissue Eng. 17 (2011) 2305–2319, https://doi.org/10.1089/ten.tea.2010.0595.

[73] S. Lagies, M. Schlimpert, S. Neumann, A. Wäldin, B. Kammerer, C. Borner, L. Peintner, Cells grown in three-dimensional spheroids mirror in vivo metabolic response of epithelial cells, Commun, Biol. 3 (2020) 246, https://doi.org/10.1038/s42003-020-0973-6.

[74] S. Chou, C. Lee, J. Lai, Bioengineered keratocyte spheroids fabricated on chitosan coatings enhance tissue repair in a rabbit corneal stromal defect model, J. Tissue Eng. Regen. Med. 12 (2018) 316–320, https://doi.org/10.1002/term.2456.

[75] X. Gong, C. Lin, J. Cheng, J. Su, H. Zhao, T. Liu, X. Wen, P. Zhao, Generation of multicellular tumor spheroids with microwell-based agarose scaffolds for drug testing, PLoS One 10 (2015), e0130348, https://doi.org/10.1371/journal.pone.0130348.

[76] F. Wan, S. Zhang, R. Xie, B. Gao, B. Campos, C. Herold-Mende, T. Lei, The utility and limitations of neurosphere assay, CD133 immunophenotyping and side population assay in glioma stem cell research, Brain Pathol. 20 (2010) 877–889, https://doi.org/10.1111/j.1750-3639.2010.00379.x.

[77] L.P. Deleyrolle, G. Ericksson, B.J. Morrison, J.A. Lopez, K. Burrage, P. Burrage, A. Vescovi, R.L. Rietze, B.A. Reynolds, Determination of somatic and cancer stem cell self-renewing symmetric division rate using sphere assays, PLoS One 6 (2011), e15844, https://doi.org/10.1371/journal.pone.0015844.

[78] J. Fukuda, A. Khademhosseini, Y. Yeo, X. Yang, J. Yeh, G. Eng, J. Blumling, C.-F. Wang, D.S. Kohane, R. Langer, Micromolding of photocrosslinkable chitosan hydrogel for spheroid microarray and co-cultures, Biomaterials 27 (2006) 5259–5267, https://doi.org/10.1016/j.biomaterials.2006.05.044.

[79] M.A. Gionet-Gonzales, J.K. Leach, Engineering principles for guiding spheroid function in the regeneration of bone, cartilage, and skin, Biomed. Mater. 13 (2018), 034109, https://doi.org/10.1088/1748-605X/aab0b3.

[80] G. Bresciani, L.J. Hofland, F. Dogan, G. Giamas, T. Gagliano, M.C. Zatelli, Evaluation of spheroid 3D culture methods to study a pancreatic neuroendocrine neoplasm cell line, Front. Endocrinol. 10 (2019) 1–10, https://doi.org/10.3389/fendo.2019.00682.

[81] E. Fennema, N. Rivron, J. Rouwkema, C. van Blitterswijk, J. de Boer, Spheroid culture as a tool for creating 3D complex tissues, Trends Biotechnol. 31 (2013) 108–115, https://doi.org/10.1016/j.tibtech.2012.12.003.

[82] A.N. Mehesz, J. Brown, Z. Hajdu, W. Beaver, J.V.L. da Silva, R.P. Visconti, R. R. Markwald, V. Mironov, Scalable robotic biofabrication of tissue spheroids, Biofabrication 3 (2011), 025002, https://doi.org/10.1088/1758-5082/3/2/025002.

[83] J. Carlsson, J.M. Yuhas, Liquid-overlay culture of cellular spheroids, in: Recent Results Cancer Res., 1984, pp. 1–23, https://doi.org/10.1007/978-3-642-82340-4_1. Germany.

[84] Y. Tung, A.Y. Hsiao, S.G. Allen, Y. Torisawa, M. Ho, S. Takayama, High-throughput 3D spheroid culture and drug testing using a 384 hanging drop array, Analyst 136 (2011) 473–478, https://doi.org/10.1039/C0AN00609B.

[85] C. Kim, J.H. Bang, Y.E. Kim, S.H. Lee, J.Y. Kang, On-chip anticancer drug test of regular tumor spheroids formed in microwells by a distributive microchannel network, Lab Chip 12 (2012) 4135, https://doi.org/10.1039/c2lc40570a.

[86] C. Chao, L.P. Ngo, B.P. Engelward, SpheroidChip: patterned agarose microwell compartments harboring HepG2 spheroids are compatible with genotoxicity testing, ACS Biomater. Sci. Eng. 6 (2020) 2427–2439, https://doi.org/10.1021/acsbiomaterials.9b01951.

[87] L.Y. Wu, D. Di Carlo, L.P. Lee, Microfluidic self-assembly of tumor spheroids for anticancer drug discovery, Biomed, Microdevices 10 (2008) 197–202, https://doi.org/10.1007/s10544-007-9125-8.

[88] V.E. Santo, M.F. Estrada, S.P. Rebelo, S. Abreu, I. Silva, C. Pinto, S.C. Veloso, A. T. Serra, E. Boghaert, P.M. Alves, C. Brito, Adaptable stirred-tank culture strategies for large scale production of multicellular spheroid-based tumor cell models, J. Biotechnol. 221 (2016) 118–129, https://doi.org/10.1016/j.jbiotec.2016.01.031.

[89] F. Petry, D. Salzig, Large-scale production of size-adjusted β-cell spheroids in a fully controlled stirred-tank reactor, Processes 10 (2022) 861, https://doi.org/10.3390/pr10050861.

[90] E.C. Costa, D. de Melo-Diogo, A.F. Moreira, M.P. Carvalho, I.J. Correia, Spheroids formation on non-adhesive surfaces by liquid overlay technique: considerations and practical approaches, Biotechnol. J. 13 (2018), 1700417, https://doi.org/10.1002/biot.201700417.

[91] L. Zhao, J. Xiu, Y. Liu, T. Zhang, W. Pan, X. Zheng, X. Zhang, A 3D printed hanging drop dripper for tumor spheroids analysis without recovery, Sci. Rep. 9 (2019), 19717, https://doi.org/10.1038/s41598-019-56241-0.

[92] S.M. Azarin, X. Lian, E.A. Larson, H.M. Popelka, J.J. de Pablo, S.P. Palecek, Modulation of Wnt/β-catenin signaling in human embryonic stem cells using a 3-D microwell array, Biomaterials 33 (2012) 2041–2049, https://doi.org/10.1016/j.biomaterials.2011.11.070.

[93] V.N. Truskett, M.P.C. Watts, Trends in imprint lithography for biological applications, Trends Biotechnol. 24 (2006) 312–317, https://doi.org/10.1016/j.tibtech.2006.05.005.

[94] P. Mitchell, Microfluidics—downsizing large-scale biology, Nat. Biotechnol. 19 (2001) 717–721, https://doi.org/10.1038/90754.

[95] G.H. Lee, J.S. Lee, X. Wang, S. Hoon Lee, Bottom-up engineering of well-defined 3D microtissues using microplatforms and biomedical applications, Adv. Healthc. Mater. 5 (2016) 56–74, https://doi.org/10.1002/adhm.201500107.

[96] G. Lee, Y. Jun, H. Jang, J. Yoon, J. Lee, M. Hong, S. Chung, D.-H. Kim, S. Lee, Enhanced oxygen permeability in membrane-bottomed concave microwells for the formation of pancreatic islet spheroids, Acta Biomater. 65 (2018) 185–196, https://doi.org/10.1016/j.actbio.2017.10.045.

[97] G.H. Lee, J.S. Lee, G.-H. Lee, W.Y. Joung, S.H. Kim, S.H. Lee, J.Y. Park, D.-H. Kim, Networked concave microwell arrays for constructing 3D cell spheroids, Biofabrication 10 (2017), 015001, https://doi.org/10.1088/1758-5090/aa9876.

[98] A.I. Neto, P.A. Levkin, J.F. Mano, Patterned superhydrophobic surfaces to process and characterize biomaterials and 3D cell culture, Mater. Horiz. 5 (2018) 379–393, https://doi.org/10.1039/C7MH00877E.

[99] O. Frey, P.M. Misun, D.A. Fluri, J.G. Hengstler, A. Hierlemann, Reconfigurable microfluidic hanging drop network for multi-tissue interaction and analysis, Nat. Commun. 5 (2014) 4250, https://doi.org/10.1038/ncomms5250.

[100] A.P. Napolitano, P. Chai, D.M. Dean, J.R. Morgan, Dynamics of the self-assembly of complex cellular aggregates on micromolded nonadhesive hydrogels, Tissue Eng. 13 (2007) 2087–2094, https://doi.org/10.1089/ten.2006.0190.

[101] H. Fonoudi, H. Ansari, S. Abbasalizadeh, G.M. Blue, N. Aghdami, D.S. Winlaw, R. P. Harvey, A. Bosman, H. Baharvand, Large-scale production of cardiomyocytes from human pluripotent stem cells using a highly reproducible small molecule-based differentiation protocol, JoVE (2016) 1–10, https://doi.org/10.3791/54276.2016.

[102] K. Moshksayan, N. Kashaninejad, M.E. Warkiani, J.G. Lock, H. Moghadas, B. Firoozabadi, M.S. Saidi, N.-T. Nguyen, Spheroids-on-a-chip: recent advances and design considerations in microfluidic platforms for spheroid formation and culture, Sensor. Actuator. B Chem. 263 (2018) 151–176, https://doi.org/10.1016/j.snb.2018.01.223.

[103] M. Marimuthu, N. Rousset, A. St-Georges-Robillard, M.A. Lateef, M. Ferland, A.-M. Mes-Masson, T. Gervais, Multi-size spheroid formation using microfluidic funnels, Lab Chip 18 (2018) 304–314, https://doi.org/10.1039/C7LC00970D.

[104] J.M. Santos, S.P. Camões, E. Filipe, M. Cipriano, R.N. Barcia, M. Filipe, M. Teixeira, S. Simões, M. Gaspar, D. Mosqueira, D.S. Nascimento, P. Pinto-do-Ó, P. Cruz, H. Cruz, M. Castro, J.P. Miranda, Three-dimensional spheroid cell culture of umbilical cord tissue-derived mesenchymal stromal cells leads to enhanced paracrine induction of wound healing, Stem Cell Res. Ther. 6 (2015) 90, https://doi.org/10.1186/s13287-015-0082-5.

[105] M.A. Phelan, A.L. Gianforcaro, J.A. Gerstenhaber, P.I. Lelkes, An air bubble-isolating rotating wall vessel bioreactor for improved spheroid/organoid formation, Tissue Eng. C Methods 25 (2019) 479–488, https://doi.org/10.1089/ten.tec.2019.0088.

[106] W. Sun, B. Starly, A.C. Daly, J.A. Burdick, J. Groll, G. Skeldon, W. Shu, Y. Sakai, M. Shinohara, M. Nishikawa, J. Jang, D.-W. Cho, M. Nie, S. Takeuchi, S. Ostrovidov, A. Khademhosseini, R.D. Kamm, V. Mironov, L. Moroni, I. T. Ozbolat, The bioprinting roadmap, Biofabrication 12 (2020), 022002, https://doi.org/10.1088/1758-5090/ab5158.

[107] M. Dey, I.T. Ozbolat, 3D bioprinting of cells, tissues and organs, Sci. Rep. 10 (2020), 14023, https://doi.org/10.1038/s41598-020-70086-y.

[108] I.T. Ozbolat, W. Peng, V. Ozbolat, Application areas of 3D bioprinting, Drug Discov. Today 21 (2016), https://doi.org/10.1016/j.drudis.2016.04.006.

[109] I.T. Ozbolat, Bioprinting scale-up tissue and organ constructs for transplantation, Trends Biotechnol. 33 (2015) 395–400, https://doi.org/10.1016/j.tibtech.2015.04.005.

[110] I.T. Ozbolat, M. Hospodiuk, Current advances and future perspectives in extrusion-based bioprinting, Biomaterials 76 (2016) 321–343, https://doi.org/10.1016/j.biomaterials.2015.10.076.

[111] K. Jakab, C. Norotte, B. Damon, F. Marga, A. Neagu, C.L. Besch-Williford, A. Kachurin, K.H. Church, H. Park, V. Mironov, R. Markwald, G. Vunjak-Novakovic, G. Forgacs, Tissue engineering by self-assembly of cells printed into topologically defined structures, Tissue Eng. 14 (2008) 413–421, https://doi.org/10.1089/tea.2007.0173.

[112] G. Hong, J. Kim, H. Oh, S. Yun, C.M. Kim, Y. Jeong, W. Yun, J. Shim, I. Jang, C. Kim, S. Jin, Production of multiple cell-laden microtissue spheroids with a biomimetic hepatic-lobule-like structure, Adv. Mater. 33 (2021), 2102624, https://doi.org/10.1002/adma.202102624.
[113] N. V Mekhileri, K.S. Lim, G.C.J. Brown, I. Mutreja, B.S. Schon, G.J. Hooper, T.B. F. Woodfield, Automated 3D bioassembly of micro-tissues for biofabrication of hybrid tissue engineered constructs, Biofabrication 10 (2018), 024103, https://doi.org/10.1088/1758-5090/aa9ef1.
[114] E.O. Osidak, P.A. Karalkin, M.S. Osidak, V.A. Parfenov, D.E. Sivogrivov, F.D.A. S. Pereira, A.A. Gryadunova, E.V. Koudan, Y.D. Khesuani, V.A. Kasyanov, S. I. Belousov, S.V. Krasheninnikov, T.E. Grigoriev, S.N. Chvalun, E.A. Bulanova, V. A. Mironov, S.P. Domogatsky, Viscoll collagen solution as a novel bioink for direct 3D bioprinting, J. Mater. Sci. Mater. Med. 30 (2019) 31, https://doi.org/10.1007/s10856-019-6233-y.
[115] D.F. Duarte Campos, C.D. Lindsay, J.G. Roth, B.L. LeSavage, A.J. Seymour, B. A. Krajina, R. Ribeiro, P.F. Costa, A. Blaeser, S.C. Heilshorn, Bioprinting cell- and spheroid-laden protein-engineered hydrogels as tissue-on-chip platforms, Front. Bioeng. Biotechnol. 8 (2020) 1–13, https://doi.org/10.3389/fbioe.2020.00374.
[116] A. Robu, L. Stoicu, Simmmc – AN INFORMATIC APPLICATION FOR MODELING AND SIMULATING THE EVOLUTION OF MULTICELLULAR SYSTEMS IN THE VICINITY OF BIOMATERIALS that substitute or foster the regeneration of injured tissues in the human body [2]. developed a modeling and simulatio, 26 (n.d.) 145–162.
[117] J.A. Davies, E. Cachat, Synthetic biology meets tissue engineering, Biochem. Soc. Trans. 44 (2016) 696–701, https://doi.org/10.1042/BST20150289.
[118] E. Cachat, W. Liu, P. Hohenstein, J.A. Davies, A library of mammalian effector modules for synthetic morphology, J. Biol. Eng. 8 (2014) 26, https://doi.org/10.1186/1754-1611-8-26.
[119] A. Robu, V. Mironov, A. Neagu, Using sacrificial cell spheroids for the bioprinting of perfusable 3D tissue and organ constructs: a computational study, Comput. Math. Methods Med. (2019) 1–9, https://doi.org/10.1155/2019/7853586, 2019.
[120] S. Swaminathan, Q. Hamid, W. Sun, A.M. Clyne, Bioprinting of 3D breast epithelial spheroids for human cancer models, Biofabrication 11 (2019), 025003, https://doi.org/10.1088/1758-5090/aafc49.
[121] L. De Moor, S. Fernandez, C. Vercruysse, L. Tytgat, M. Asadian, N. De Geyter, S. Van Vlierberghe, P. Dubruel, H. Declercq, Hybrid bioprinting of chondrogenically induced human mesenchymal stem cell spheroids, Front. Bioeng. Biotechnol. 8 (2020) 1–20, https://doi.org/10.3389/fbioe.2020.00484.
[122] S. Han, S. Kim, Z. Chen, H.K. Shin, S.-Y. Lee, H.E. Moon, S.H. Paek, S. Park, 3D bioprinted vascularized tumour for drug testing, Int. J. Mol. Sci. 21 (2020) 2993, https://doi.org/10.3390/ijms21082993.
[123] J. Colle, P. Blondeel, A. De Bruyne, S. Bochar, L. Tytgat, C. Vercruysse, S. Van Vlierberghe, P. Dubruel, H. Declercq, Bioprinting predifferentiated adipose-derived mesenchymal stem cell spheroids with methacrylated gelatin ink for adipose tissue engineering, J. Mater. Sci. Mater. Med. 31 (2020) 36, https://doi.org/10.1007/s10856-020-06374-w.
[124] H. Gudapati, M. Dey, I. Ozbolat, A comprehensive review on droplet-based bioprinting: past, present and future, Biomaterials 102 (2016) 20–42, https://doi.org/10.1016/j.biomaterials.2016.06.012.
[125] L. Gutzweiler, S. Kartmann, K. Troendle, L. Benning, G. Finkenzeller, R. Zengerle, P. Koltay, G.B. Stark, S. Zimmermann, Large scale production and controlled deposition of single HUVEC spheroids for bioprinting applications, Biofabrication 9 (2017), 025027, https://doi.org/10.1088/1758-5090/aa7218.
[126] K. Ling, G. Huang, J. Liu, X. Zhang, Y. Ma, T. Lu, F. Xu, Bioprinting-based high-throughput fabrication of three-dimensional MCF-7 human breast cancer cellular spheroids, Engineering 1 (2015) 269–274, https://doi.org/10.15302/J-ENG-2015062.
[127] Y. Sriphutkiat, S. Kasetsirikul, Y. Zhou, formation of cell spheroids using standing surface acoustic wave (SSAW), Int. J. Bioprinting. 4 (2018) 1–12, https://doi.org/10.18063/ijb.v4i1.130.
[128] K. Chen, E. Jiang, X. Wei, Y. Xia, Z. Wu, Z. Gong, Z. Shang, S. Guo, The acoustic droplet printing of functional tumor microenvironments, Lab Chip 21 (2021) 1604–1612, https://doi.org/10.1039/D1LC00003A.
[129] H. Zhao, Y. Chen, L. Shao, M. Xie, J. Nie, J. Qiu, P. Zhao, H. Ramezani, J. Fu, H. Ouyang, Y. He, Airflow-assisted 3D bioprinting of human heterogeneous microspheroidal organoids with microfluidic nozzle, Small 14 (2018), 1802630, https://doi.org/10.1002/smll.201802630.
[130] N.I. Moldovan, N. Hibino, K. Nakayama, Principles of the kenzan method for robotic cell spheroid-based three-dimensional bioprinting, Tissue Eng. B Rev. 23 (2017) 237–244, https://doi.org/10.1089/ten.teb.2016.0322.
[131] W. LaBarge, A. Morales, D. Pretorius, A. Kahn-Krell, R. Kannappan, J. Zhang, Scaffold-free bioprinter utilizing layer-by-layer printing of cellular spheroids, Micromachines 10 (2019) 570, https://doi.org/10.3390/mi10090570.
[132] D.M. van Pel, K. Harada, D. Song, C.C. Naus, W.C. Sin, Modelling glioma invasion using 3D bioprinting and scaffold-free 3D culture, J. Cell Commun. Signal. 12 (2018) 723–730, https://doi.org/10.1007/s12079-018-0469-z.
[133] T. Imamura, M. Shimamura, T. Ogawa, T. Minagawa, T. Nagai, S. Silwal Gautam, O. Ishizuka, Biofabricated structures reconstruct functional urinary bladders in radiation-injured rat bladders, Tissue Eng. 24 (2018) 1574–1587, https://doi.org/10.1089/ten.tea.2017.0533.
[134] S. Mitsuzawa, R. Ikeguchi, T. Aoyama, H. Takeuchi, H. Yurie, H. Oda, S. Ohta, M. Ushimaru, T. Ito, M. Tanaka, Y. Kunitomi, M. Tsuji, S. Akieda, K. Nakayama, S. Matsuda, The efficacy of a scaffold-free bio 3D conduit developed from autologous dermal fibroblasts on peripheral nerve regeneration in a canine ulnar nerve injury model: a preclinical proof-of-concept study, Cell Transplant. 28 (2019) 1231–1241, https://doi.org/10.1177/0963689719855346.
[135] X.-Y. Zhang, Y. Yanagi, Z. Sheng, K. Nagata, K. Nakayama, T. Taguchi, Regeneration of diaphragm with bio-3D cellular patch, Biomaterials 167 (2018) 1–14, https://doi.org/10.1016/j.biomaterials.2018.03.012.
[136] A. Yamasaki, Y. Kunitomi, D. Murata, T. Sunaga, T. Kuramoto, T. Sogawa, K. Misumi, Osteochondral regeneration using constructs of mesenchymal stem cells made by bio three-dimensional printing in mini-pigs, J. Orthop. Res. 37 (2019) 1398–1408, https://doi.org/10.1002/jor.24206.
[137] C.S. Ong, T. Fukunishi, H. Zhang, C.Y. Huang, A. Nashed, A. Blazeski, D. DiSilvestre, L. Vricella, J. Conte, L. Tung, G.F. Tomaselli, N. Hibino, Biomaterial-free three-dimensional bioprinting of cardiac tissue using human induced pluripotent stem cell derived cardiomyocytes, Sci. Rep. 7 (2017) 4566, https://doi.org/10.1038/s41598-017-05018-4.
[138] R. Machino, K. Matsumoto, D. Taniguchi, T. Tsuchiya, Y. Takeoka, Y. Taura, M. Moriyama, T. Tetsuo, S. Oyama, K. Takagi, T. Miyazaki, G. Hatachi, R. Doi, K. Shimoyama, N. Matsuo, N. Yamasaki, K. Nakayama, T. Nagayasu, Replacement of rat tracheas by layered, trachea-like, scaffold-free structures of human cells using a bio-3D printing system, Adv. Healthc. Mater. 8 (2019), 1800983, https://doi.org/10.1002/adhm.201800983.
[139] Y. Takeoka, K. Matsumoto, D. Taniguchi, T. Tsuchiya, R. Machino, M. Moriyama, S. Oyama, T. Tetsuo, Y. Taura, K. Takagi, T. Yoshida, A. Elgalad, N. Matsuo, M. Kunizaki, S. Tobinaga, T. Nonaka, S. Hidaka, N. Yamasaki, K. Nakayama, T. Nagayasu, Regeneration of esophagus using a scaffold-free biomimetic structure created with bio-three-dimensional printing, PLoS One 14 (2019), e0211339, https://doi.org/10.1371/journal.pone.0211339.
[140] Y. Yanagi, K. Nakayama, T. Taguchi, S. Enosawa, T. Tamura, K. Yoshimaru, T. Matsuura, M. Hayashida, K. Kohashi, Y. Oda, T. Yamaza, E. Kobayashi, In vivo and ex vivo methods of growing a liver bud through tissue connection, Sci. Rep. 7 (2017), 14085, https://doi.org/10.1038/s41598-017-14542-2.
[141] H. Kizawa, E. Nagao, M. Shimamura, G. Zhang, H. Torii, Scaffold-free 3D bio-printed human liver tissue stably maintains metabolic functions useful for drug discovery, Biochem. Biophys. Reports. 10 (2017) 186–191, https://doi.org/10.1016/j.bbrep.2017.04.004.
[142] Y. Nakanishi, T. Okada, N. Takeuchi, N. Kozono, T. Senju, K. Nakayama, Y. Nakashima, Histological evaluation of tendon formation using a scaffold-free three-dimensional-bioprinted construct of human dermal fibroblasts under in vitro static tensile culture, Regen. Ther. 11 (2019) 47–55, https://doi.org/10.1016/j.reth.2019.02.002.
[143] A. Nakamura, D. Murata, R. Fujimoto, S. Tamaki, S. Nagata, M. Ikeya, J. Toguchida, K. Nakayama, Bio-3D printing iPSC-derived human chondrocytes for articular cartilage regeneration, Biofabrication 13 (2021), 044103, https://doi.org/10.1088/1758-5090/ac1c99.
[144] I.N. Aguilar, D.J. Olivos, A. Brinker, M.B. Alvarez, L.J. Smith, T.G. Chu, M. A. Kacena, D.R. Wagner, Scaffold-free bioprinting of mesenchymal stem cells using the Regenova printer: spheroid characterization and osteogenic differentiation, Bioprinting 15 (2019), e00050, https://doi.org/10.1016/j.bprint.2019.e00050.
[145] A.M. Blakely, K.L. Manning, A. Tripathi, J.R. Morgan, Bio-pick, place, and perfuse: a new instrument for three-dimensional tissue engineering, Tissue Eng. C Methods 21 (2015) 737–746, https://doi.org/10.1089/ten.tec.2014.0439.
[146] F. Mirab, Y.J. Kang, S. Majd, Preparation and characterization of size-controlled glioma spheroids using agarose hydrogel microwells, PLoS One 14 (2019), e0211078, https://doi.org/10.1371/journal.pone.0211078.
[147] N. Tejavibulya, J. Youssef, B. Bao, T.-M. Ferruccio, J.R. Morgan, Directed self-assembly of large scaffold-free multi-cellular honeycomb structures, Biofabrication 3 (2011), 34110, https://doi.org/10.1088/1758-5082/3/3/034110.
[148] C.M. Livoti, J.R. Morgan, Self-assembly and tissue fusion of toroid-shaped minimal building units, Tissue Eng. 16 (2010) 2051–2061, https://doi.org/10.1089/ten.tea.2009.0607.
[149] B.C. Ip, F. Cui, A. Tripathi, J.R. Morgan, The bio-gripper: a fluid-driven micro-manipulator of living tissue constructs for additive bio-manufacturing, Biofabrication 8 (2016), 025015, https://doi.org/10.1088/1758-5090/8/2/025015.
[150] F.R. Cui, B.C. Ip, J.R. Morgan, A. Tripathi, Hydrodynamics of the bio-gripper: a fluid-driven "claw machine" for soft microtissue translocation, SLAS Technol. Transl. Life Sci. Innov. 23 (2018) 540–549, https://doi.org/10.1177/2472630318775079.
[151] B.C. Ip, F. Cui, B.T. Wilks, J. Murphy, A. Tripathi, J.R. Morgan, Perfused organ cell-dense macrotissues assembled from prefabricated living microtissues, Adv. Biosyst. 2 (2018), 1800076, https://doi.org/10.1002/adbi.201800076.
[152] B. Ayan, D.N. Heo, Z. Zhang, M. Dey, A. Povilianskas, C. Drapaca, I.T. Ozbolat, Aspiration-assisted bioprinting for precise positioning of biologics, Sci. Adv. 6 (2020), https://doi.org/10.1126/sciadv.aaw5111 eaaw5111.
[153] M. Dey, B. Ayan, M. Yurieva, D. Unutmaz, I.T. Ozbolat, Studying tumor angiogenesis and cancer invasion in a three-dimensional vascularized breast cancer micro-environment, Adv. Biol. 5 (2021), 2100090, https://doi.org/10.1002/adbi.202100090.
[154] Y. Wu, B. Ayan, K.K. Moncal, Y. Kang, A. Dhawan, S. V Koduru, D.J. Ravnic, F. Kamal, I.T. Ozbolat, Hybrid bioprinting of zonally stratified human articular cartilage using scaffold-free tissue strands as building blocks, Adv. Healthc. Mater. 9 (2020), 2001657, https://doi.org/10.1002/adhm.202001657.
[155] B. Ayan, N. Celik, Z. Zhang, K. Zhou, M.H. Kim, D. Banerjee, Y. Wu, F. Costanzo, I. T. Ozbolat, Aspiration-assisted freeform bioprinting of pre-fabricated tissue spheroids in a yield-stress gel, Commun. Phys. 3 (2020) 183, https://doi.org/10.1038/s42005-020-00449-4.

[156] A.C. Daly, M.D. Davidson, J.A. Burdick, 3D bioprinting of high cell-density heterogeneous tissue models through spheroid fusion within self-healing hydrogels, Nat. Commun. 12 (2021) 753, https://doi.org/10.1038/s41467-021-21029-2.
[157] V.H.B. Ho, W.M. Guo, C.L. Huang, S.F. Ho, S.Y. Chaw, E.Y. Tan, K.W. Ng, J.S. C. Loo, Manipulating magnetic 3D spheroids in hanging drops for applications in tissue engineering and drug screening, Adv. Healthc. Mater. 2 (2013) 1430–1434, https://doi.org/10.1002/adhm.201200408.
[158] T.R. Olsen, B. Mattix, M. Casco, A. Herbst, C. Williams, A. Tarasidis, D. Simionescu, R.P. Visconti, F. Alexis, Manipulation of cellular spheroid composition and the effects on vascular tissue fusion, Acta Biomater. 13 (2015) 188–198, https://doi.org/10.1016/j.actbio.2014.11.024.
[159] B. Mattix, T.R. Olsen, Y. Gu, M. Casco, A. Herbst, D.T. Simionescu, R.P. Visconti, K.G. Kornev, F. Alexis, Biological magnetic cellular spheroids as building blocks for tissue engineering, Acta Biomater. 10 (2014) 623–629, https://doi.org/10.1016/j.actbio.2013.10.021.
[160] B.M. Mattix, T.R. Olsen, M. Casco, L. Reese, J.T. Poole, J. Zhang, R.P. Visconti, A. Simionescu, D.T. Simionescu, F. Alexis, Janus magnetic cellular spheroids for vascular tissue engineering, Biomaterials 35 (2014) 949–960, https://doi.org/10.1016/j.biomaterials.2013.10.036.
[161] V.H.B. Ho, K.H. Müller, A. Barcza, R. Chen, N.K.H. Slater, Generation and manipulation of magnetic multicellular spheroids, Biomaterials 31 (2010) 3095–3102, https://doi.org/10.1016/j.biomaterials.2009.12.047.
[162] A.M. Bratt-Leal, K.L. Kepple, R.L. Carpenedo, M.T. Cooke, T.C. McDevitt, Magnetic manipulation and spatial patterning of multi-cellular stem cell aggregates, Integr. Biol. 3 (2011) 1224–1232, https://doi.org/10.1039/c1ib00064k.
[163] H. Akiyama, A. Ito, Y. Kawabe, M. Kamihira, Cell-patterning using poly (ethylene glycol)-modified magnetite nanoparticles, J. Biomed. Mater. Res., Part A 9999A (2009), https://doi.org/10.1002/jbm.a.32313. NA-NA.
[164] M. Chorny, I.S. Alferiev, I. Fishbein, J.E. Tengood, Z. Folchman-Wagner, S. P. Forbes, R.J. Levy, Formulation and in vitro characterization of composite biodegradable magnetic nanoparticles for magnetically guided cell delivery, Pharm. Res. (N. Y.) 29 (2012) 1232–1241, https://doi.org/10.1007/s11095-012-0675-y.
[165] C. Tassa, S.Y. Shaw, R. Weissleder, Dextran-coated iron oxide nanoparticles: a versatile platform for targeted molecular imaging, molecular diagnostics, and therapy, Acc. Chem. Res. 44 (2011) 842–852, https://doi.org/10.1021/ar200084x.
[166] T. Kim, E. Momin, J. Choi, K. Yuan, H. Zaidi, J. Kim, M. Park, N. Lee, M. T. McMahon, A. Quinones-Hinojosa, J.W.M. Bulte, T. Hyeon, A.A. Gilad, Mesoporous silica-coated hollow manganese oxide nanoparticles as positive T1 contrast agents for labeling and MRI tracking of adipose-derived mesenchymal stem cells, J. Am. Chem. Soc. 133 (2011) 2955–2961, https://doi.org/10.1021/ja1084095.
[167] D.A. Bowser, M.J. Moore, Biofabrication of neural microphysiological systems using magnetic spheroid bioprinting, Biofabrication 12 (2019), 015002, https://doi.org/10.1088/1758-5090/ab41b4.
[168] C. Adine, K.K. Ng, S. Rungarunlert, G.R. Souza, J.N. Ferreira, Engineering innervated secretory epithelial organoids by magnetic three-dimensional bioprinting for stimulating epithelial growth in salivary glands, Biomaterials 180 (2018) 52–66, https://doi.org/10.1016/j.biomaterials.2018.06.011.
[169] H. Tseng, J.A. Gage, T. Shen, W.L. Haisler, S.K. Neeley, S. Shiao, J. Chen, P. K. Desai, A. Liao, C. Hebel, R.M. Raphael, J.L. Becker, G.R. Souza, A spheroid toxicity assay using magnetic 3D bioprinting and real-time mobile device-based imaging, Sci. Rep. 5 (2015), 13987, https://doi.org/10.1038/srep13987.
[170] M. Dey, M.H. Kim, M. Nagamine, M. Dogan, L. Kozhaya, N. Celik, D. Unutmaz, I. T. Ozbolat, Chemotherapeutics and CAR-T cell-based immunotherapeutics screening on a 3D bioprinted vascularized breast tumor model, Adv. Funct. Mater. (2022), 2203966, https://doi.org/10.1002/adfm.202203966.
[171] S.Y. Hann, H. Cui, T. Esworthy, S. Miao, X. Zhou, S. Lee, J.P. Fisher, L.G. Zhang, Recent advances in 3D printing: vascular network for tissue and organ regeneration, Transl. Res. 211 (2019) 46–63, https://doi.org/10.1016/j.trsl.2019.04.002.
[172] S. Coffey, M.J.A. Williams, B. Cox, Letter by Coffey et al Regarding Article, "Estimating Deaths From Cardiovascular Disease: a Review of Global Methodologies of Mortality Measurement, Circulation 128 (2013) 2123, https://doi.org/10.1161/CIRCULATIONAHA.113.002123.
[173] J.G. Brink, D.K.C. Cooper, Heart transplantation: the contributions of christiaan barnard and the university of cape town/groote schuur hospital, World J. Surg. 29 (2005) 953–961, https://doi.org/10.1007/s00268-005-0154-2.
[174] Z.-W. Tao, M. Mohamed, M. Hogan, B. Salazar, N.M. Patel, R.K. Birla, Establishing the framework for fabrication of a bioartificial heart, ASAIO J 61 (2015) 429–436, https://doi.org/10.1097/MAT.0000000000000233.
[175] M. Izadifar, D. Chapman, P. Babyn, X. Chen, M.E. Kelly, UV-assisted 3D bioprinting of nanoreinforced hybrid cardiac patch for myocardial tissue engineering, Tissue Eng. C Methods 24 (2018) 74–88, https://doi.org/10.1089/ten.tec.2017.0346.
[176] M.A. Mohamed, M.K. Hogan, N.M. Patel, Z.-W. Tao, L. Gutierrez, R.K. Birla, Establishing the framework for tissue engineered heart pumps, Cardiovasc. Eng. Technol. 6 (2015) 220–229, https://doi.org/10.1007/s13239-015-0211-4.
[177] F. Migneco, S.J. Hollister, R.K. Birla, Tissue-engineered heart valve prostheses: 'state of the heart, Regen. Med. 3 (2008) 399–419, https://doi.org/10.2217/17460751.3.3.399.
[178] N.M. Patel, R.K. Birla, The bioengineered cardiac left ventricle, ASAIO J 64 (2018) 56–62, https://doi.org/10.1097/MAT.0000000000000642.
[179] L. Hecker, L. Khait, M.J. Welsh, R. Birla, Bioengineering functional human aortic vascular smooth-muscle strips in vitro, Biotechnol. Appl. Biochem. 50 (2008) 155, https://doi.org/10.1042/BA20070139.
[180] O. Caspi, A. Lesman, Y. Basevitch, A. Gepstein, G. Arbel, I.H.M. Habib, L. Gepstein, S. Levenberg, Tissue engineering of vascularized cardiac muscle from human embryonic stem cells, Circ. Res. 100 (2007) 263–272, https://doi.org/10.1161/01.RES.0000257776.05673.ff.
[181] G. Vunjak-Novakovic, N. Tandon, A. Godier, R. Maidhof, A. Marsano, T. P. Martens, M. Radisic, Challenges in cardiac tissue engineering, Tissue Eng. B Rev. 16 (2010) 169–187, https://doi.org/10.1089/ten.teb.2009.0352.
[182] H. Tseng, L.R. Balaoing, B. Grigoryan, R.M. Raphael, T.C. Killian, G.R. Souza, K. J. Grande-Allen, A three-dimensional co-culture model of the aortic valve using magnetic levitation, Acta Biomater. 10 (2014) 173–182, https://doi.org/10.1016/j.actbio.2013.09.003.
[183] H. Tseng, J.A. Gage, W.L. Haisler, S.K. Neeley, T. Shen, C. Hebel, H.G. Barthlow, M. Wagoner, G.R. Souza, A high-throughput in vitro ring assay for vasoactivity using magnetic 3D bioprinting, Sci. Rep. 6 (2016), 30640, https://doi.org/10.1038/srep30640.
[184] C.S. Ong, P. Yesantharao, N. Hibino, 3D and 4D scaffold-free bioprinting, in: 3D and 4D Printing in Biomedical Applications: Process Engineering and Additive Manufacturing, Wiley-VCH, 2019. http://dnb.d-nb.de.
[185] L. Polonchuk, L. Surija, M.H. Lee, P. Sharma, C. Liu Chung Ming, F. Richter, E. Ben-Sefer, M.A. Rad, H. Mahmodi Sheikh Sarmast, W. Al Shamery, H.A. Tran, L. Vettori, F. Haeusermann, E.C. Filipe, J. Rnjak-Kovacina, T. Cox, J. Tipper, I. Kabakova, C. Gentile, Towards engineering heart tissues from bioprinted cardiac spheroids, Biofabrication 13 (2021), 045009, https://doi.org/10.1088/1758-5090/ac14ca.
[186] I. Pitaktong, C. Lui, J. Lowenthal, G. Mattson, W.-H. Jung, Y. Bai, E. Yeung, C. S. Ong, Y. Chen, S. Gerecht, N. Hibino, Early vascular cells improve microvascularization within 3D cardiac spheroids, Tissue Eng. C Methods 26 (2020) 80–90, https://doi.org/10.1089/ten.tec.2019.0228.
[187] S.K. Williams, J.S. Touroo, K.H. Church, J.B. Hoying, Encapsulation of adipose stromal vascular fraction cells in alginate hydrogel spheroids using a direct-write three-dimensional printing system, Biores. Open Access 2 (2013) 448–454, https://doi.org/10.1089/biores.2013.0046.
[188] Y. Huang, B. Malanda, R. Fernandes, S. Karuranga, N.H. Cho, IDF Diabetes Atlas estimates for the global diabetes prevalence among adults older than 60 years, in: Int. Diabetes Fed., 2017, p. 2017, 2017.
[189] R. Gates, R. Smith, M.I. Hunt, N. Lazarus, Return to normal of blood-glucose, plasma-insulin, and weight gain in New Zealand obese mice after implantation of islets of langerhans, Lancet 300 (1972) 567–570, https://doi.org/10.1016/S0140-6736(72)91960-5.
[190] D.J. Ravnic, A.N. Leberfinger, I.T. Ozbolat, Bioprinting and cellular therapies for type 1 diabetes, Trends Biotechnol. 35 (2017) 1025–1034, https://doi.org/10.1016/j.tibtech.2017.07.006.
[191] P. Augsornworawat, L. Velazco-Cruz, J. Song, J.R. Millman, Hydrogel Platform for in Vitro Three-Dimensional Assembly of Human Stem Cell-Derived β Cells and Endothelial Cells, BioRxiv, 2019, https://doi.org/10.1101/653378.
[192] M. Urbanczyk, A. Zbinden, S.L. Layland, G. Duffy, K. Schenke-Layland, Controlled heterotypic pseudo-islet assembly of human β-cells and human umbilical vein endothelial cells using magnetic levitation, Tissue Eng. 26 (2020) 387–399, https://doi.org/10.1089/ten.tea.2019.0158.
[193] M. Hospodiuk, M. Dey, B. Ayan, D. Sosnoski, K.K. Moncal, Y. Wu, I.T. Ozbolat, Sprouting angiogenesis in engineered pseudo islets, Biofabrication 10 (2018), 035003, https://doi.org/10.1088/1758-5090/aab002.
[194] J. Kim, I.K. Shim, D.G. Hwang, Y.N. Lee, M. Kim, H. Kim, S.-W. Kim, S. Lee, S. C. Kim, D.-W. Cho, J. Jang, 3D cell printing of islet-laden pancreatic tissue-derived extracellular matrix bioink constructs for enhancing pancreatic functions, J. Mater. Chem. B. 7 (2019) 1773–1781, https://doi.org/10.1039/C8TB02787K.
[195] D.G. Hwang, Y. Jo, M. Kim, U. Yong, S. Cho, Y. Choi, J. Kim, J. Jang, A 3D bioprinted hybrid encapsulation system for delivery of human pluripotent stem cell-derived pancreatic islet-like aggregates, Biofabrication 14 (2022), 014101, https://doi.org/10.1088/1758-5090/ac23ac.
[196] D. Hakobyan, C. Médina, N. Dusserre, M.-L. Stachowicz, C. Handschin, J.-C. Fricain, J. Guillermet-Guibert, H. Oliveira, Laser-assisted 3D bioprinting of exocrine pancreas spheroid models for cancer initiation study, Biofabrication 12 (2020), 035001, https://doi.org/10.1088/1758-5090/ab7cb8.
[197] R.L. Siegel, K.D. Miller, A. Jemal, Cancer statistics, Ca - Cancer J. Clin. 69 (2019) (2019) 7–34, https://doi.org/10.3322/caac.21551.
[198] J.-V. Gaustad, T.G. Simonsen, L.M.K. Andersen, E.K. Rofstad, Vascular abnormalities and development of hypoxia in microscopic melanoma xenografts, J. Transl. Med. 15 (2017) 241, https://doi.org/10.1186/s12967-017-1347-9.
[199] A. Álvarez-Varela, L. Novellasdemunt, F.M. Barriga, X. Hernando-Momblona, A. Cañellas-Socias, S. Cano-Crespo, M. Sevillano, C. Cortina, D. Stork, C. Morral, G. Turon, F. Slebe, L. Jiménez-Gracia, G. Caratù, P. Jung, G. Stassi, H. Heyn, D.V. F. Tauriello, L. Mateo, S. Tejpar, E. Sancho, C. Stephan-Otto Attolini, E. Batlle, Mex3a marks drug-tolerant persister colorectal cancer cells that mediate relapse after chemotherapy, Nat. Can. (Que.) 3 (2022) 1052–1070, https://doi.org/10.1038/s43018-022-00402-0.
[200] G. Vlachogiannis, S. Hedayat, A. Vatsiou, Y. Jamin, J. Fernández-Mateos, K. Khan, A. Lampis, K. Eason, I. Huntingford, R. Burke, M. Rata, D.-M. Koh, N. Tunariu, D. Collins, S. Hulkki-Wilson, C. Ragulan, I. Spiteri, S.Y. Moorcraft, I. Chau, S. Rao, D. Watkins, N. Fotiadis, M. Bali, M. Darvish-Damavandi, H. Lote, Z. Eltahir, E. C. Smyth, R. Begum, P.A. Clarke, J.C. Hahne, M. Dowsett, J. de Bono, P. Workman, A. Sadanandam, M. Fassan, O.J. Sansom, S. Eccles, N. Starling, C. Braconi, A. Sottoriva, S.P. Robinson, D. Cunningham, N. Valeri, Patient-derived

organoids model treatment response of metastatic gastrointestinal cancers, Science 359 (2018) 920–926, https://doi.org/10.1126/science.aao2774, 80.
[201] Z. Zhou, K. Van der Jeught, Y. Fang, T. Yu, Y. Li, Z. Ao, S. Liu, L. Zhang, Y. Yang, H. Eyvani, M.L. Cox, X. Wang, X. He, G. Ji, B.P. Schneider, F. Guo, J. Wan, X. Zhang, X. Lu, An organoid-based screen for epigenetic inhibitors that stimulate antigen presentation and potentiate T-cell-mediated cytotoxicity, Nat. Biomed. Eng. 5 (2021) 1320–1335, https://doi.org/10.1038/s41551-021-00805-x.
[202] K.C. Hribar, D. Finlay, X. Ma, X. Qu, M.G. Ondeck, P.H. Chung, F. Zanella, A. J. Engler, F. Sheikh, K. Vuori, S.C. Chen, Nonlinear 3D projection printing of concave hydrogel microstructures for long-term multicellular spheroid and embryoid body culture, Lab Chip 15 (2015) 2412–2418, https://doi.org/10.1039/C5LC00159E.
[203] M. Dey, M.H. Kim, M. Nagamine, E. Karhan, L. Kozhaya, M. Dogan, D. Unutmaz, I.T. Ozbolat, Biofabrication of 3D breast cancer models for dissecting the cytotoxic response of human T cells expressing engineered MAIT cell receptors, Biofabrication 14 (2022), 044105, https://doi.org/10.1088/1758-5090/ac925a.
[204] D.M. Kingsley, C.L. Roberge, A. Rudkouskaya, D.E. Faulkner, M. Barroso, X. Intes, D.T. Corr, Laser-based 3D bioprinting for spatial and size control of tumor spheroids and embryoid bodies, Acta Biomater. 95 (2019) 357–370, https://doi.org/10.1016/j.actbio.2019.02.014.
[205] M.J. Waring, J. Arrowsmith, A.R. Leach, P.D. Leeson, S. Mandrell, R.M. Owen, G. Pairaudeau, W.D. Pennie, S.D. Pickett, J. Wang, O. Wallace, A. Weir, An analysis of the attrition of drug candidates from four major pharmaceutical companies, Nat. Rev. Drug Discov. 14 (2015) 475–486, https://doi.org/10.1038/nrd4609.
[206] F.H. Gage, S. Temple, Neural stem cells: generating and regenerating the brain, Neuron 80 (2013) 588–601, https://doi.org/10.1016/j.neuron.2013.10.037.
[207] H.-W. Han, S. Hsu, Using 3D bioprinting to produce mini-brain, Neural Regen. Res. 12 (2017) 1595, https://doi.org/10.4103/1673-5374.217325.
[208] B. Qiu, N. Bessler, K. Figler, M. Buchholz, A.C. Rios, J. Malda, R. Levato, M. Caiazzo, Bioprinting neural systems to model central nervous system diseases, Adv. Funct. Mater. 30 (2020), 1910250, https://doi.org/10.1002/adfm.201910250.
[209] R. Thayakaran, N.J. Adderley, C. Sainsbury, B. Torlinska, K. Boelaert, D. Šumilo, M. Price, G.N. Thomas, K.A. Toulis, K. Nirantharakumar, Thyroid replacement therapy, thyroid stimulating hormone concentrations, and long term health outcomes in patients with hypothyroidism: longitudinal study, BMJ 366 (2019) l4892, https://doi.org/10.1136/bmj.l4892.
[210] A.A. Kurmann, M. Serra, F. Hawkins, S.A. Rankin, M. Mori, I. Astapova, S. Ullas, S. Lin, M. Bilodeau, J. Rossant, J.C. Jean, L. Ikonomou, R.R. Deterding, J. M. Shannon, A.M. Zorn, A.N. Hollenberg, D.N. Kotton, Regeneration of thyroid function by transplantation of differentiated pluripotent stem cells, Cell Stem Cell 17 (2015) 527–542, https://doi.org/10.1016/j.stem.2015.09.004.
[211] R. Ma, R. Latif, T.F. Davies, Human embryonic stem cells form functional thyroid follicles, Thyroid 25 (2015) 455–461, https://doi.org/10.1089/thy.2014.0537.
[212] K.K. Moncal, R.S.T. Aydin, M. Abu-Laban, D.N. Heo, E. Rizk, S.M. Tucker, G. S. Lewis, D. Hayes, I.T. Ozbolat, Collagen-infilled 3D printed scaffolds loaded with miR-148b-transfected bone marrow stem cells improve calvarial bone regeneration in rats, Mater. Sci. Eng., C 105 (2019), 110128, https://doi.org/10.1016/j.msec.2019.110128.
[213] M. Heller, H.-K. Bauer, E. Goetze, M. Gielisch, I.T. Ozbolat, K.K. Moncal, E. Rizk, H. Seitz, M. Gelinsky, H.C. Schröder, X.H. Wang, W.E.G. Müller, B. Al-Nawas, Materials and scaffolds in medical 3D printing and bioprinting in the context of bone regeneration, Int. J. Comput. Dent. 19 (2016) 301–321.
[214] F. Obregon, C. Vaquette, S. Ivanovski, D.W. Hutmacher, L.E. Bertassoni, Three-dimensional bioprinting for regenerative dentistry and craniofacial tissue engineering, J. Dent. Res. 94 (2015) 143S–152S, https://doi.org/10.1177/0022034515588885.
[215] D.P. Lennon, J.M. Edmison, A.I. Caplan, Cultivation of rat marrow-derived mesenchymal stem cells in reduced oxygen tension: effects on in vitro and in vivo osteochondrogenesis, J. Cell. Physiol. 187 (2001) 345–355, https://doi.org/10.1002/jcp.1081.
[216] P. Apelgren, M. Amoroso, K. Säljö, A. Lindahl, C. Brantsing, L. Stridh Orrhult, K. Markstedt, P. Gatenholm, L. Kölby, Long-term in vivo integrity and safety of <scp>3D</scp> -bioprinted cartilaginous constructs, J. Biomed. Mater. Res. Part B Appl. Biomater. 109 (2021) 126–136, https://doi.org/10.1002/jbm.b.34687.
[217] T. Anada, C.-C. Pan, A. Stahl, S. Mori, J. Fukuda, O. Suzuki, Y. Yang, Vascularized bone-mimetic hydrogel constructs by 3D bioprinting to promote osteogenesis and angiogenesis, Int. J. Mol. Sci. 20 (2019) 1096, https://doi.org/10.3390/ijms20051096.
[218] H. Cui, W. Zhu, M. Nowicki, X. Zhou, A. Khademhosseini, L.G. Zhang, Hierarchical fabrication of engineered vascularized bone biphasic constructs via dual 3D bioprinting: integrating regional bioactive factors into architectural design, Adv. Healthc. Mater. 5 (2016) 2174–2181, https://doi.org/10.1002/adhm.201600505.
[219] N. Celik, M.H. Kim, D.J. Hayes, I.T. Ozbolat, miRNA induced co-differentiation and cross-talk of adipose tissue-derived progenitor cells for 3D heterotypic pre-vascularized bone formation, Biofabrication 13 (2021), 044107, https://doi.org/10.1088/1758-5090/ac23ae.
[220] N. Celik, M.H. Kim, M. Yeo, F. Kamal, D.J. Hayes, I.T. Ozbolat, miRNA induced 3D bioprinted-heterotypic osteochondral interface, Biofabrication 14 (2022), 044104, https://doi.org/10.1088/1758-5090/ac7fbb.
[221] A.C. Daly, D.J. Kelly, Biofabrication of spatially organised tissues by directing the growth of cellular spheroids within 3D printed polymeric microchambers, Biomaterials 197 (2019) 194–206, https://doi.org/10.1016/j.biomaterials.2018.12.028.
[222] A. Dhawan, P.M. Kennedy, E.B. Rizk, I.T. Ozbolat, Three-dimensional bioprinting for bone and cartilage restoration in orthopaedic surgery, J. Am. Acad. Orthop. Surg. 27 (2019), https://doi.org/10.5435/JAAOS-D-17-00632 e215–e226.
[223] J. Farr, B. Cole, A. Dhawan, J. Kercher, S. Sherman, Clinical cartilage restoration: evolution and overview, Clin. Orthop. Relat. Res. 469 (2011) 2696–2705, https://doi.org/10.1007/s11999-010-1764-z.
[224] E.A. Makris, A.H. Gomoll, K.N. Malizos, J.C. Hu, K.A. Athanasiou, Repair and tissue engineering techniques for articular cartilage, Nat. Rev. Rheumatol. 11 (2015) 21–34, https://doi.org/10.1038/nrrheum.2014.157.
[225] S. Nehrer, M. Spector, T. Minas, Histologic analysis of tissue after failed cartilage repair procedures, Clin. Orthop. Relat. Res. 365 (1999) 149–162. https://linkinghub.elsevier.com/retrieve/pii/S0167779917301853.
[226] B.J. Cole, C. Pascual-Garrido, R.C. Grumet, Surgical management of articular cartilage defects in the knee, J. Bone Jt. Surg. 7 (1991) 1778–1790.
[227] D.G. Nguyen, J. Funk, J.B. Robbins, C. Crogan-Grundy, S.C. Presnell, T. Singer, A. B. Roth, Bioprinted 3D primary liver tissues allow assessment of organ-level response to clinical drug induced toxicity in vitro, PLoS One 11 (2016), e0158674, https://doi.org/10.1371/journal.pone.0158674.
[228] G.H. Underhill, S.R. Khetani, Bioengineered liver models for drug testing and cell differentiation studies, Cell. Mol. Gastroenterol. Hepatol. 5 (2018) 426–439, https://doi.org/10.1016/j.jcmgh.2017.11.012, e1.
[229] C.C. Bell, D.F.G. Hendriks, S.M.L. Moro, E. Ellis, J. Walsh, A. Renblom, L. Fredriksson Puigvert, A.C.A. Dankers, F. Jacobs, J. Snoeys, R.L. Sison-Young, R. E. Jenkins, Å. Nordling, S. Mkrtchian, B.K. Park, N.R. Kitteringham, C.E. P. Goldring, V.M. Lauschke, M. Ingelman-Sundberg, Characterization of primary human hepatocyte spheroids as a model system for drug-induced liver injury, liver function and disease, Sci. Rep. 6 (2016), 25187, https://doi.org/10.1038/srep25187.
[230] A. Skardal, M. Devarasetty, H.-W. Kang, I. Mead, C. Bishop, T. Shupe, S.J. Lee, J. Jackson, J. Yoo, S. Soker, A. Atala, A hydrogel bioink toolkit for mimicking native tissue biochemical and mechanical properties in bioprinted tissue constructs, Acta Biomater. 25 (2015) 24–34, https://doi.org/10.1016/j.actbio.2015.07.030.
[231] N.S. Bhise, V. Manoharan, S. Massa, A. Tamayol, M. Ghaderi, M. Miscuglio, Q. Lang, Y. Shrike Zhang, S.R. Shin, G. Calzone, N. Annabi, T.D. Shupe, C. E. Bishop, A. Atala, M.R. Dokmeci, A. Khademhosseini, A liver-on-a-chip platform with bioprinted hepatic spheroids, Biofabrication 8 (2016), 014101, https://doi.org/10.1088/1758-5090/8/1/014101.
[232] E. Goulart, L.C. de Caires-Junior, K.A. Telles-Silva, B.H.S. Araujo, S.A. Rocco, M. Sforca, I.L. de Sousa, G.S. Kobayashi, C.M. Musso, A.F. Assoni, D. Oliveira, E. Caldini, S. Raia, P.I. Lelkes, M. Zatz, 3D bioprinting of liver spheroids derived from human induced pluripotent stem cells sustain liver function and viability in vitro, Biofabrication 12 (2019), 015010, https://doi.org/10.1088/1758-5090/ab4a30.
[233] S.R. Khetani, S.N. Bhatia, Microscale culture of human liver cells for drug development, Nat. Biotechnol. 26 (2008) 120–126, https://doi.org/10.1038/nbt1361.
[234] S.N. Bhatia, U.J. Balis, M.L. Yarmush, M. Toner, Effect of cell–cell interactions in preservation of cellular phenotype: cocultivation of hepatocytes and nonparenchymal cells, Faseb. J. 13 (1999) 1883–1900, https://doi.org/10.1096/fasebj.13.14.1883.
[235] E.L. LeCluyse, R.P. Witek, M.E. Andersen, M.J. Powers, Organotypic liver culture models: meeting current challenges in toxicity testing, Crit. Rev. Toxicol. 42 (2012) 501–548, https://doi.org/10.3109/10408444.2012.682115.
[236] P.M. van Midwoud, M.T. Merema, E. Verpoorte, G.M.M. Groothuis, A microfluidic approach for in vitro assessment of interorgan interactions in drug metabolism using intestinal and liver slices, Lab Chip 10 (2010) 2778, https://doi.org/10.1039/c0lc00043d.
[237] J. Shan, R.E. Schwartz, N.T. Ross, D.J. Logan, D. Thomas, S.A. Duncan, T. E. North, W. Goessling, A.E. Carpenter, S.N. Bhatia, Identification of small molecules for human hepatocyte expansion and iPS differentiation, Nat. Chem. Biol. 9 (2013) 514–520, https://doi.org/10.1038/nchembio.1270.
[238] M.W. Laschke, M.D. Menger, Spheroids as vascularization units: from angiogenesis research to tissue engineering applications, Biotechnol, Adv 35 (2017) 782–791, https://doi.org/10.1016/j.biotechadv.2017.07.002.
[239] L. De Moor, I. Merovci, S. Baetens, J. Verstraeten, P. Kowalska, D. V Krysko, W. H. De Vos, H. Declercq, High-throughput fabrication of vascularized spheroids for bioprinting, Biofabrication 10 (2018), 035009, https://doi.org/10.1088/1758-5090/aac7e6.
[240] Y. Tan, D.J. Richards, T.C. Trusk, R.P. Visconti, M.J. Yost, M.S. Kindy, C.J. Drake, W.S. Argraves, R.R. Markwald, Y. Mei, 3D printing facilitated scaffold-free tissue unit fabrication, Biofabrication 6 (2014), 024111, https://doi.org/10.1088/1758-5082/6/2/024111.
[241] L.A. Kunz-Schughart, J.A. Schroeder, M. Wondrak, F. van Rey, K. Lehle, F. Hofstaedter, D.N. Wheatley, Potential of fibroblasts to regulate the formation of three-dimensional vessel-like structures from endothelial cells in vitro, Am. J. Physiol. Physiol. 290 (2006) C1385, https://doi.org/10.1152/ajpcell.00248.2005. –C1398.
[242] F. Berthod, L. Germain, N. Tremblay, F.A. Auger, Extracellular matrix deposition by fibroblasts is necessary to promote capillary-like tube formation in vitro, J. Cell. Physiol. 207 (2006) 491–498, https://doi.org/10.1002/jcp.20584.
[243] A.P. Rago, D.M. Dean, J.R. Morgan, Controlling cell position in complex heterotypic 3D microtissues by tissue fusion, Biotechnol. Bioeng. 102 (2009) 1231–1241, https://doi.org/10.1002/bit.22162.
[244] A. Shahin-Shamsabadi, P.R. Selvaganapathy, A rapid biofabrication technique for self-assembled collagen-based multicellular and heterogeneous 3D tissue

constructs, Acta Biomater. 92 (2019) 172–183, https://doi.org/10.1016/j.actbio.2019.05.024.
[245] A. Shahin-Shamsabadi, P.R. Selvaganapathy, A 3D self-assembled in vitro model to simulate direct and indirect interactions between adipocytes and skeletal muscle cells, Adv. Biosyst. 4 (2020), 2000034, https://doi.org/10.1002/adbi.202000034.
[246] J. Frenkel, Viscous flow of crystalline bodies under the action of surface tension, J. Phys. 9 (1945) 385–391.
[247] E. Flenner, F. Marga, A. Neagu, I. Kosztin, G. Forgacs, Relating biophysical properties across scales, in: S. Schnell, P.K. Maini, S.A. Newman, T.J.B.T.-C.T. in, D.B. Newman (Eds.), Multiscale Model. Dev. Syst., Academic Press, 2008, pp. 461–483, https://doi.org/10.1016/S0070-2153(07)81016-7.
[248] J.G. Amar, The Monte Carlo method in science and engineering, Comput. Sci. Eng. 8 (2006) 9–19.
[249] F. Graner, J.A. Glazier, Simulation of biological cell sorting using a two-dimensional extended Potts model, Phys. Rev. Lett. 69 (1992) (2016) 2013, https://doi.org/10.1103/PhysRevLett.69.2013.
[250] J.A. Glazier, F. Graner, Simulation of the differential adhesion driven rearrangement of biological cells, Phys. Rev. E. 47 (1993) 2128–2154, https://doi.org/10.1103/PhysRevE.47.2128.
[251] P.A. Fleming, W.S. Argraves, C. Gentile, A. Neagu, G. Forgacs, C.J. Drake, Fusion of uniluminal vascular spheroids: a model for assembly of blood vessels, Dev. Dynam. 239 (2010) 398–406, https://doi.org/10.1002/dvdy.22161.
[252] A. Mondal, A. Gebeyehu, M. Miranda, D. Bahadur, N. Patel, S. Ramakrishnan, A. K. Rishi, M. Singh, Characterization and printability of Sodium alginate -Gelatin hydrogel for bioprinting NSCLC co-culture, Sci. Rep. 9 (2019), 19914, https://doi.org/10.1038/s41598-019-55034-9.
[253] J. He, J. Shao, X. Li, Q. Huang, T. Xu, Bioprinting of coaxial multicellular structures for a 3D co-culture model, Bioprinting 11 (2018), e00036, https://doi.org/10.1016/j.bprint.2018.e00036.
[254] S. Giovannini, J. Diaz-Romero, T. Aigner, P. Heini, P. Mainil-Varlet, D. Nesic, Micromass co-culture of human articular chondrocytes and human bone marrow mesenchymal stem cells to investigate stable neocartilage tissue formation in vitro, Eur. Cell. Mater. 20 (2010) 245–259, https://doi.org/10.22203/eCM.v020a20.
[255] P. Beauchamp, C.B. Jackson, L.C. Ozhathil, I. Agarkova, C.L. Galindo, D. B. Sawyer, T.M. Suter, C. Zuppinger, 3D Co-culture of hiPSC-derived cardiomyocytes with cardiac fibroblasts improves tissue-like features of cardiac spheroids, Front. Mol. Biosci. 7 (2020) 1–17, https://doi.org/10.3389/fmolb.2020.00014.
[256] R.N.B. Bhandari, L.A. Riccalton, A.L. Lewis, J.R. Fry, A.H. Hammond, S.J. B. Tendler, K.M. Shakesheff, Liver tissue engineering: a role for Co-culture systems in modifying hepatocyte function and viability, Tissue Eng. 7 (2001) 345–357, https://doi.org/10.1089/10763270152044206.
[257] I.N. Aguilar, L.J. Smith, D.J. Olivos, T.-M.G. Chu, M.A. Kacena, D.R. Wagner, Scaffold-free bioprinting of mesenchymal stem cells with the regenova printer: optimization of printing parameters, Bioprinting 15 (2019), e00048, https://doi.org/10.1016/j.bprint.2019.e00048.
[258] L.-S. Fan, C. Zhu, Principles of Gas-Solid Flows, Cambridge University Press, 2005.
[259] S.-H. Kim, G.H. Lee, J.Y. Park, Microwell fabrication methods and applications for cellular studies, Biomed. Eng. Lett. 3 (2013) 131–137, https://doi.org/10.1007/s13534-013-0105-z.
[260] J.M. Lee, D.Y. Park, L. Yang, E.-J. Kim, C.D. Ahrberg, K.-B. Lee, B.G. Chung, Generation of uniform-sized multicellular tumor spheroids using hydrogel microwells for advanced drug screening, Sci. Rep. 8 (2018), 17145, https://doi.org/10.1038/s41598-018-35216-7.
[261] D.W. Hutmacher, M. Sittinger, M. V Risbud, Scaffold-based tissue engineering: rationale for computer-aided design and solid free-form fabrication systems, Trends Biotechnol. 22 (2004) 354–362, https://doi.org/10.1016/j.tibtech.2004.05.005.
[262] G. Chen, T. Ushida, T. Tateishi, Scaffold design for tissue engineering, Macromol. Biosci. 2 (2002) 67–77.
[263] C.M. Agrawal, R.B. Ray, Biodegradable Polymeric Scaffolds for Musculoskeletal Tissue Engineering, 2000, https://doi.org/10.1002/1097-4636(200105)55:23.0.CO;2-J.
[264] A.E. Efimov, O.I. Agapova, L.A. Safonova, M.M. Bobrova, V.A. Parfenov, E. V. Koudan, F.D.A.S. Pereira, E.A. Bulanova, V.A. Mironov, I.I. Agapov, 3D scanning probe nanotomography of tissue spheroid fibroblasts interacting with electrospun polyurethane scaffold, Express Polym. Lett. 13 (2019) 632–641, https://doi.org/10.3144/expresspolymlett.2019.53.
[265] L. Baptista, G. Kronemberger, I. Côrtes, L. Charelli, R. Matsui, T. Palhares, J. Sohier, A. Rossi, J. Granjeiro, Adult stem cells spheroids to optimize cell colonization in scaffolds for cartilage and bone tissue engineering, Int. J. Mol. Sci. 19 (2018) 1285, https://doi.org/10.3390/ijms19051285.
[266] J. Kundu, J. Shim, J. Jang, S. Kim, D. Cho, An additive manufacturing-based PCL-alginate-chondrocyte bioprinted scaffold for cartilage tissue engineering, J. Tissue Eng. Regen. Med. 9 (2015) 1286–1297, https://doi.org/10.1002/term.1682.
[267] N.I. Moldovan, Progress in scaffold-free bioprinting for cardiovascular medicine, J. Cell Mol. Med. 22 (2018) 2964–2969, https://doi.org/10.1111/jcmm.13598.
[268] I. Guggenmoos-Holzmann, B. Engel, V. Henke, G.O. Naumann, Cell density of human lens epithelium in women higher than in men, Invest. Ophthalmol. Vis. Sci. 30 (1989) 330–332.
[269] R.E. McClelland, R. Dennis, L.M. Reid, J.P. Stegemann, B. Palsson, J. M. Macdonald, in: Third E. Bronzino (Ed.), Tissue Engineering, Introd. To Biomed. Eng., Elsevier, Boston, 2012, pp. 273–357, https://doi.org/10.1016/B978-0-12-374979-6.00006-X. J.D. Enderle, J.D.B.T.-I. to B.E.
[270] H. Yurie, R. Ikeguchi, T. Aoyama, Y. Kaizawa, J. Tajino, A. Ito, S. Ohta, H. Oda, H. Takeuchi, S. Akieda, M. Tsuji, K. Nakayama, S. Matsuda, The efficacy of a scaffold-free Bio 3D conduit developed from human fibroblasts on peripheral nerve regeneration in a rat sciatic nerve model, PLoS One 12 (2017), e0171448, https://doi.org/10.1371/journal.pone.0171448.
[271] M. Ando, R. Ikeguchi, T. Aoyama, M. Tanaka, T. Noguchi, Y. Miyazaki, S. Akieda, K. Nakayama, S. Matsuda, Long-term outcome of sciatic nerve regeneration using Bio3D conduit fabricated from human fibroblasts in a rat sciatic nerve model, Cell Transplant. 30 (2021), 096368972110213, https://doi.org/10.1177/09636897211021357.
[272] P. Datta, L.Y. Cabrera, I.T. Ozbolat, Ethical challenges with 3D bioprinted tissues and organs, Trends Biotechnol. (2022), https://doi.org/10.1016/j.tibtech.2022.08.012.
[273] P. Datta, A. Barui, Y. Wu, V. Ozbolat, K.K. Moncal, I.T. Ozbolat, Essential steps in bioprinting: from pre- to post-bioprinting, Biotechnol. Adv. 36 (2018), https://doi.org/10.1016/j.biotechadv.2018.06.003.
[274] P. Rawal, D.M. Tripathi, S. Ramakrishna, S. Kaur, Prospects for 3D bioprinting of organoids, Bio-Design Manuf. 4 (2021) 627–640, https://doi.org/10.1007/s42242-020-00124-1.
[275] S.J. Nass, M.L. Rothenberg, R. Pentz, H. Hricak, A. Abernethy, K. Anderson, A. W. Gee, R.D. Harvey, S. Piantadosi, M.M. Bertagnolli, D. Schrag, R.L. Schilsky, Accelerating anticancer drug development — opportunities and trade-offs, Nat. Rev. Clin. Oncol. 15 (2018) 777–786, https://doi.org/10.1038/s41571-018-0102-3.
[276] H. Clevers, Modeling development and disease with organoids, Cell 165 (2016) 1586–1597, https://doi.org/10.1016/j.cell.2016.05.082.
[277] V. Dao, K. Yuki, Y.-H. Lo, M. Nakano, C.J. Kuo, Immune organoids: from tumor modeling to precision oncology, Trends in Cancer 8 (2022) 870–880, https://doi.org/10.1016/j.trecan.2022.06.001.
[278] P. Datta, B. Ayan, I.T. Ozbolat, Bioprinting for vascular and vascularized tissue biofabrication, Acta Biomater. 51 (2017) 1–20, https://doi.org/10.1016/j.actbio.2017.01.035.
[279] O. Guillaume, O. Kopinski-Grünwald, G. Weisgrab, T. Baumgartner, A. Arslan, K. Whitmore, S. Van Vlierberghe, A. Ovsianikov, Hybrid spheroid microscaffolds as modular tissue units to build macro-tissue assemblies for tissue engineering, Acta Biomater. (2022), https://doi.org/10.1016/j.actbio.2022.03.010.
[280] F. Schutgens, M.B. Rookmaaker, T. Margaritis, A. Rios, C. Ammerlaan, J. Jansen, L. Gijzen, M. Vormann, A. Vonk, M. Viveen, F.Y. Yengej, S. Derakhshan, K.M. de Winter-de Groot, B. Artegiani, R. van Boxtel, E. Cuppen, A.P.A. Hendrickx, M. M. van den Heuvel-Eibrink, E. Heitzer, H. Lanz, J. Beekman, J.-L. Murk, R. Masereeuw, F. Holstege, J. Drost, M.C. Verhaar, H. Clevers, Tubuloids derived from human adult kidney and urine for personalized disease modeling, Nat. Biotechnol. 37 (2019) 303–313, https://doi.org/10.1038/s41587-019-0048-8.
[281] R.A. Wimmer, A. Leopoldi, M. Aichinger, D. Kerjaschki, J.M. Penninger, Generation of blood vessel organoids from human pluripotent stem cells, Nat. Protoc. 14 (2019) 3082–3100, https://doi.org/10.1038/s41596-019-0213-z.